UCSF

UC San Francisco Electronic Theses and Dissertations

Title

Design of a glucose oxidase sensor for a mechanochemical insulin pump

Permalink

https://escholarship.org/uc/item/9847s0mw

Author

De Moor, Colette Pamela

Publication Date

1995

Peer reviewed|Thesis/dissertation

DESIGN OF A GLUCOSE OXIDASE SENSOR FOR A

MECHANOCHEMICAL INSULIN PUMP

by

COLETTE PAMELA DE MOOR

DISSERTATION

Submitted in partial satisfaction of the requirements for the degree of
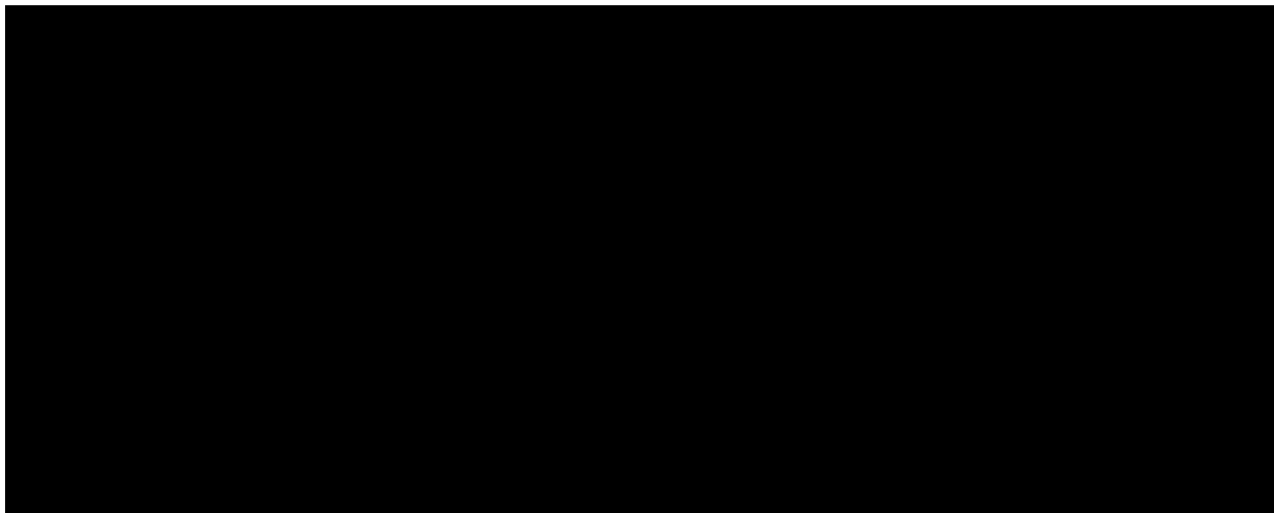
DOCTOR OF PHILOSOPHY

in

BIOENGINEERING

in the

GRADUATE DIVISION

of the

UNIVERSITY OF CALIFORNIA

San Francisco

. . . .

Date   **University Librarian**

Degree Conferred: . . . .

To my two families
who have always believed in me.
Mama, Papa, and Karen,
Dagmar, Uwe, Barbara, Harold and Cordilla

Acknowledgements

This dissertation represents the end of many years of effort and hard work. I would not have made it this far without the undying support and help of many people. I would like to express my sincere thanks and appreciation to the following people:

My main professor and thesis advisor, Dr. Ron Siegel for his support and continued interest in my success.

Dr. C. Anthony Hunt for his support and belief in my thesis project, as well as for his aid in getting me the internship at Biotrack and his support from the NIH Biotechnology Training Grant.

Dr. Edward Keller for recommending me to receive the ARCS Foundation Scholarship in 1988.

Dr. Tom Ferrin for aiding me to obtain a computer account on the San Diego Supercomputer.

My thesis committee of Drs. Siegel, Lehman and Graves for guidance and helping me finish this project.

I am especially grateful to Dr. Stan Glantz for getting me going again when I needed it most, and Dr. Steve Lehman for his continual interest and encouragement.

I would also like to thank my fellow lab mates and students at UCSF. In particular Jim Uchizono and Garrett Stanley for their encouragement and unfailing support; Bob Stull and Seaung Oh for their commradery; and in the early days, Bommi Bommannan for his friendship. I would also like to thank Mark Shattuck for not allowing me to give up , for his encouragement and support since day one, and for introducing me to Lew.

Additional thanks and gratitude goes to all those friends and family who have stuck with me through this ordeal. I would specifically like to acknowledge and thank:

All my friends and patrons at Noc Noc who have put up with me and dealt with my stress fits in the last year;

the O'Keefe family for sharing their home with me from 1989 through 1993;

Design of a Glucose Oxidase Sensor for a Mechanochemical Insulin Pump
by
C. Pamela De Moor

Abstract

A glucose sensitive membrane coupled to a pH-sensitive polymer hydrogel is being investigated for use as a sensor in an implantable mechanochemical insulin pump. The glucose sensitive membrane contains the immobilized enzymes glucose oxidase and catalase which convert glucose and oxygen into gluconate and free protons. The free protons generated by the reaction in the membrane diffuse into and ionize the hydrogel, causing the latter to swell. The design of the glucose sensitive membrane coupled to the hydrogel is crucial to the operation of the pump.

This thesis project is concerned with the diffusion/reaction modeling of the glucose sensitive membrane. The diffusion/reaction calculations for the enzyme membrane coupled to the polymer hydrogel are carried out in order to determine the rate of delivery of protons to the hydrogel as a function of the enzyme loading and the geometric properties of the membrane. The design problem is complicated by the fact that the oxygen will be depleted before the sensor detects appreciable amounts of glucose. This is because the molecular oxygen concentration in plasma is on the order of ten times less than the glucose concentration. This problem can be mitigated by providing preferential transport pathways for oxygen relative to glucose and by optimizing the geometry of the enzyme membrane. The calculations enable us to determine the design which allows for enhanced oxygen transfer and efficient proton transfer as a function of the external mass transfer limitations and the external glucose concentration. A finite element model is used to solve the diffusion/reaction equations. Results of the finite element analysis are analyzed.

Ronald A. Siegel

Table of Contents

List of Tables

List of Figures

Chapter 1.

Introduction

1.1 The Problem: Diabetes Mellitus

Insulin dependent diabetes results from the breakdown of a physiologic feedback system where insulin is no longer secreted from the pancreas in response to elevated blood glucose levels. Current treatments of insulin dependent diabetes do prevent the acute manifestations of the disease. They do not however, provide good control of blood glucose concentrations. The ultimate goal of insulin therapy is to mimic pancreatic function as closely as possible and in this way control glycemia. This can best be accomplished by implementing a closed loop, self-regulating delivery device which responds to blood glucose levels in a similar fashion to the pancreas.

1.1.1 Overview of Diabetes

In a nondiabetic, a rise in glucose level due to a meal is accompanied by an increase in the secretion rate of insulin from the pancreas. The principal function of insulin is to lower blood glucose concentration and to maintain its level within a very narrow range, about 3.5 - 6.5 mM in human blood (60 - 120 mg%).[1-4] The secretion of insulin brings the glucose level back down to normal by enhancing its uptake into cells and the liver. In this manner nondiabetics are able to maintain their blood sugar levels while providing their

bodies with nourishment. This glucose homeostasis in a healthy person is maintained by a push-pull closed loop system that controls the glucose flux into and out of extracellular space. This control system is regulated mainly by the liver and pancreas and by cells that utilize glucose.

Diabetes is the result of the inability of the body to use insulin effectively, either due to insulin resistance by tissues or the inability of the pancreas to secrete sufficient amounts of insulin to maintain normal blood glucose levels. There are two main types of diabetes, insulin dependent diabetes mellitus (IDDM) or Type I diabetes and non-insulin dependent diabetes mellitus (NIDDM) or Type II diabetes. IDDM is defined as a lack or shortage of insulin. This is usually due to beta-cell damage, and little or no insulin is secreted. NIDDM is characterized by only a "relative" lack of insulin. In this case the body can produce insulin, but the need for insulin is so increased that production cannot keep up. In NIDDM, beta cells are present and may function normally but it is the insulin receptors that are defective. Often there is also increased insulin resistance by tissues, which is the inability of the insulin to tell the cells to use glucose.

Without the external administration of insulin, an insulin dependent diabetic can no longer efficiently use glucose as an energy source. For type I diabetics, insulin must be supplied. Type II diabetics can often get by with minimal insulin requirements. In either case, if sufficient insulin is not supplied, ketoacidosis results from the breakdown of fat cells for energy. Eventually coma

and death result when no treatment is given to a diabetic. Before the discovery of insulin, diabetics would die within four years of onset of the disease.

Due to the inability of diabetics to generate or effectively use insulin, diabetics frequently have high blood glucose levels or hyperglycemia. The irony of the situation is that diabetics have increased circulating levels of glucose but little intracellular glucose for ATP production. Cellular famine results in the midst of plenty because there is not sufficient insulin to enhance cellular uptake of glucose. On a short term basis, mild hyperglycemia results in frequent urination which in turn leads to excessive thirst and dehydration. The long term affects of hyperglycemia however, are more detrimental. Long term hyperglycemia results in premature artherosclerosis and microvascular disease of the eyes and kidneys, such as blindness, neuropathy and nephropathy.

1.2 Existing treatments

There are several different treatment options currently available to insulin dependent diabetics: intensive conventional therapy, transplantation of beta cells which produce insulin, or use of mechanical and/or chemical devices. A brief description of each is given below.

The most commonly used treatment is a regimen of daily subcutaneous insulin injections, and dietary restrictions. Although this type of treatment greatly prolongs the life of a diabetic, the

patient is often far removed from a normal physiologic state and exhibits high blood sugar levels. The amount of insulin in the body for this type of treatment is determined by the rate of insulin transport across the anatomical barriers separating the subcutaneous space from the bloodstream. This treatment is considered open-loop in the sense that the amount of insulin in the circulation is controlled by the user and not by the blood sugar level.

Another treatment option has been to try to transplant healthy beta cells which produce insulin into a diabetic. This method has met with success in diabetic rats.[5] Islet cell transplants in larger mammals have not been as successful due to graft rejection problems. Current research involves encapsulating the beta cells in microspheres, hollow fibers or in macroporous hydrophilic membranes. These chambers are separated from the immune system and would resist rejection. Glucose and insulin would diffuse into and out of these chambers. The problems with this system have been development of scar tissue around the chamber which limits diffusion, long term cell viability, and scaling up the system to human dimensions.[6,7]

In order to improve on the conventional treatment, Albisser and coworkers developed the electromechanical "artificial beta cell", which is like an attached artificial mechanical pancreas.[8] This electromechanical system continuously samples the patient's blood by a catheter. The sampled blood is then analyzed for glucose, and the glucose levels are fed into the computer which determines the insulin delivery rate. The correct amount of insulin is then

infused in from another catheter driven by a peristaltic pump. This system is a bedside system which provides excellent control over the glucose levels but is too large for practical use.

In an effort to develop more efficient treatments which could better control glycemia in diabetics, several open-loop systems have been developed in the past fifteen years. These systems include wearable implantable pumps.[9,10] These pumps are all electromechanical in nature and require a reliable and long-lasting power supply. In these systems the insulin is pumped into the body in response to an externally programmed delivery rate activated by the wearer. The patient must still measure their own glucose concentration using the usual methods. These devices require intense patient participation and responsibility. These pumps do provide better control over glycemia than injections, but have proved to be cumbersome to wear due to the external power supplies. In addition power failures and infections surrounding the percutaneaous junctions have also been large problems. Therefore there is still a need for a reliable implantable self-regulating device which is convenient and accurate, and which operates in direct response to blood glucose concentrations.

1.3 New Devices for Treatment of Diabetes

As mentioned previously, the ultimate solution to control diabetes would be a 'closed-loop' system where blood glucose levels are continuously and automatically monitored and insulin is released

in direct response to the blood glucose level. [One of the major difficulties with these systems has been the lack of a reliable and sensitive glucose sensor.] Many authors have worked on this problem. Developing devices that use biochemical and chemical means to release insulin in response to glucose concentrations has been an active area of research over the last few years. A few of the experimental devices are listed below.

Kim and colleagues have developed a self-regulating implantable insulin delivery system by utilizing the competitive binding affinity of glucose and glycosylated insulin (G-insulin) to plant lectin Concanavalin A (ConA).[11] A solution of the G-insulin protein bound to ConA is surrounded by a macroporous, hydrophilic membrane. The membrane allows diffusion of glucose and insulin but not blood proteins. The glycoslylated insulin is displaced by glucose, and diffuses out of the matrix. In this manner the insulin release is proportional to glucose concentration. This system has been tested in pancreatectomized dogs and shown to be fairly effective in maintaining the blood glucose concentration close to that observed for nondiabetic dogs for a period of 36 hours.[14] The performance of this device was hampered by inadequate permeability of glucose and G-insulin. Other problems with this system included immunogenic response to the ConA and the glycosylated insulin, and hindered diffusion due to scar tissue development.

A second approach to developing a self-regulating insulin delivery system couples a glucose sensing system with pH sensitive

hydrogels. These systems rely on glucose-induced chemical reactions coupled to the swelling of polymers to actuate insulin release. Several groups have researched and developed cross-linked hydrogel membranes which are pH sensitive and contain insulin.[15-17] These membranes swell when the pH is reduced thus releasing insulin which is stored either directly in the membrane or in a reservoir which is surrounded by the pH sensitive hydrogel.

In order to make these systems closed-loop, the swelling mechanism must be triggered by glucose. This is done by including the enzymes glucose oxidase, gluconolactonase and catalase in the membrane. Glucose oxidase converts glucose to gluconic acid through the reactions:

$$\text{glucose} + O_2 \xrightarrow{\text{GluOx}} \text{glucono-}\delta\text{-lactone} + H_2O_2 \quad (1a)$$

$$H_2O_2 \xrightarrow{\text{Cat}} H_2O + 1/2\, O_2 \quad (1b)$$

$$\text{glucono-}\delta\text{-lactone} + H_2O \xrightarrow{\text{Gluconolactonase}} \text{gluconate} + H^+ \quad (1c).$$
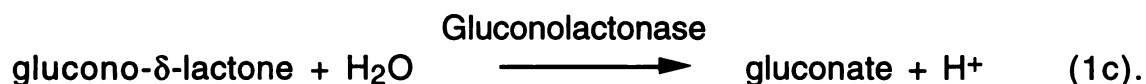
The catalase (Cat) reaction is included to prevent the accumulation of peroxide and to partially regenerate the oxygen. The important product of this reaction is the free proton which lowers the local pH, and causes a change in the membrane permeability, thus releasing insulin.

These crosslinked hydrogel membranes include tertiary amine groups which are easily ionized by the gluconic acid or the free proton. The charge repulsion between the ionized tertiary amine groups creates a positive osmotic pressure and thus causes the membrane to swell. The swelling stretches the mesh of the polymer network, enabling the insulin to permeate.

Ishihara and coworkers fabricated a glucose sensitive composite membrane by immobilizing glucose oxidase in a polyacrylamide membrane and laminating it with a pH sensitive polyamine membrane. In their device, the membrane surrounds an insulin reservoir. A rise in blood glucose is converted to a decrease in the local pH in the membrane through reactions (1a-c). The tertiary amines are protonated and repel each other, causing the membrane to swell, increasing its permeability to insulin.[18]

Horbett et. al. immobilized the glucose oxidase and catalase enzymes directly into the hydrogel containing ionizable tertiary amine groups. The membrane surrounds a saturated reservoir containing insulin. Klumb and Horbett have further utilized the above ideas and designed devices in which the enzymes and the insulin are incorporated into one gel.[19,20] In these designs as the glucose level rises, the pH decreases through reactions (1a-c). The protonated amines again cause the membrane to swell and the insulin diffuses out.

The above systems are closed loop, self-regulating systems to deliver insulin. Practical implementation of the above devices

would involve keeping insulin in an aqueous reservoir for extended time periods. Problems arise with the packaging of the insulin, however, because insulin is not stable for extended periods of time in an aqueous environment. In addition, aggregation of insulin should be considered. Aggregation, aside from reducing the activity of insulin, could lead to the possible clogging of the size-selective gel by the insulin clots.

Other gel applications which utilize the glucose oxidase/catalase mechanism include bioerodible polymers coupled to glucose oxidase membranes, and pH sensitive membranes which open and close pores through which insulin diffuses.[21,22] Fischel-Ghodsian et. al. have taken advantage of the pH sensitivity of the solubility of trilysine-insulin to design a matrix-based dissolution/diffusion system that utilizes the glucose oxidase mechanism to produce sensitivity to blood glucose levels.[23]

Some of the devices discussed above can be put into a category termed "mechanochemical". These devices are mechanochemical because they convert changes in the chemical activity (i.e. concentration) of glucose into a mechanical change, which subsequently controls the insulin release.

1.4 Scope of Thesis

This thesis project is concerned with investigating the theoretical development of a novel mechanochemical device which would mimic the endocrine action of a normal pancreas in order to minimize or possibly prevent the long-term complications of

diabetes. This device would deliver insulin in response to blood glucose changes. Since the device responds directly to blood sugar levels it is inherently a closed-loop system.

The proposed device utilizes the biochemical idea described above of coupling a glucose oxidase membrane to an osmotically active polymer gel or polyelectrolyte. Instead of using the expansion of the gels described above in order to control the diffusion of drug out of the device, however, the proposed pump uses the expansion and contraction properties of the polymer gels or liquid polyelectrolyte to expel drug out of the pump. In this way the gels act as a "piston" of a chemical engine, where the expansion and contraction cycles are powered by changes in pH produced by the glucose oxidase enzyme. These systems can be designed to swell or generate pressure at a particular pH and used in a mechanochemical pump in such a way as to make the system self-regulating or closed-loop.

The long term goal of the project is to develop a working prototype of the mechanochemical pump. This thesis will focus on the analytical modeling of the pump to determine the theoretical feasibility of this system and to determine the design parameters required to build a stable, accurate, and reliable system. The project can be divided into three inter-related areas of analytical modeling: the control dynamics of the pump, the diffusion/reaction analysis of the coupled enzyme membrane and polymer system, and the pressure calculations of the polymer/diaphragm system. The main focus of this thesis is to model the diffusion/reaction of the

coupled enzyme membrane and polymer system. The goal is to determine a sensor design which will maximize the pump performance.

In Chapter 2 the proposed mechanochemical pump is described in more detail. The pump is has many components which require investigation. Details are given on the size and volume requirements of the proposed design followed by some discussion of polymer systems studied to date. The main focus of the thesis is on the sensor portion of the pump. A background of the pump design is given for completeness.

Chapters 3 through 7 describe the theoretical sensor design for the pump. Chapter 3 compares various glucose sensors and the problems associated with utilizing these sensors. A novel design for a glucose sensor, using the enzymes glucose oxidase and catalase is proposed. This sensor can be easily coupled to a titratable polymer system. The theoretical modeling of the proposed sensor design is presented in Chapter 4. The finite element modeling is discussed in Chapter 5. The modeling was done to determine the sensor designs that could generate a maximum pH difference due to a rise in blood glucose levels. Chapter 6 compares the results of the program with known analytical results and other current designs. Results for various geometries and several different enzyme loading patterns are presented and discussed in Chapter 7.

Chapter 8 gives a summary of the analytical modeling completed on the pump to date. Conclusions and recommendations for fabricating the device and future work are also presented here.

References

1. Turner, A. P. F., Pickup JC Diabetes mellitus: biosensors for research and management. *Biosensors*; **1** (1985) 85-115.

2. Krall, L. P. and Beaser, R. S., Joslin Diabetes Manual, twelfth edition, Lea and Febiger, Philadelphia (1989).

3. Howorka, K. Functional Insulin Treatment- Principles, Teaching Approach and Practice, Springer-Verlag, Berlin (1991).

4. Bradley, C., Home, P. and Christie, M. The Technology of Diabetes Care Converging Medical and Psychosocial Perspectives, Harwood Academic Publishers, Berkshire, United Kingdom, (1991).

5. Santiago, J. White, N. Status of pancreatic transplants and mechanical devices for blood glucose control. *Ann Biomed Engr.* ; **8** (1980) 525-38.

6. Sutherland D.E.R., Ryanasiewicz J.J., Najarian J.S. Current status of pancreas and islet transplantation. In: Brownlee M.,ed. Chichester: John Wiley, *Handbook of Diabetes Mellitus*, **5** (1981) 273-416.

7. Sefton, M.V. , Broughton, R.L., Sugamori, M.E.,and Mallabone, C.L., Hydrophilic polyacrylates for the microencapsulation of fibroblasts or pancreatic islets. *J. Controlled Release* ; **6** (1987) 177-187.

8. Albisser, A.M. Devises for the control of diabetes mellitus. *Proc IEEE* ; **67**, (1979) 1308-1320.

9. Sefton,.M.V., Implantable pumps, *CRC Crit. Rev. Biomed. Eng.*, **14**, (1986) 201-240.

10. Austenat, E., Stahl, T. Insulin Pump Therapy Indication-Method - Technology, Walter de Gruyter, Berlin, New York, (1990).

11. Jeong, S.Y., Kim, S.Y., Eenik, M.J.D. and Feijen, J. Self-regulating Insulin Delivery Systems. I. Synthesis and Characterization of Glycosylated Insulin, *J. Controlled Rel.*, **1** (1984) 57-66.

12. Sato, S., Jeong, S.Y., McRea, J.C. and Kim, S.W. Self-regulating Insulin Systems. II *In Vitro* Studies, *J. Controlled Rel.*, **1** (1980) 67-77.

13. Jeong, S.Y., Kim, S.W., Holmberg, D.L.and McRea, J.C. Self-regulating Insulin Delivery Systems. III *In Vivo* Studies, *J. Contr. Rel.*, **2** (1985) 143-152.

14. Kim, S.W., Pai, C.M., Makino, K., Seminoff, L., Brown, D., Gleeson, J., Holmberg, D. and Wilson,D. "Self-Regulated Glycosylated Insulin Delivery", *J. Controlled Rel.*, **11**, (1989) 193-201.

15. Ishihara, K.; Kobayashi, M.; Ishimara, N.; Shinohara,I. Glucose Induced Permeation through a Complex membrane Consisting of Immobilized Glucose Oxidase and a Poly(Amine), *Polymer Journal* , **16** (1984) 625-631.

16. Kost,J.; Horbett, T. A.; Ratner, B. D.; Singh, M. Glucose-Sensitive Membranes Containing Glucose Oxidase: Activity, Swelling and Permeability Studies, *Journal of Biomedical Materials Research*, **19** (1985) 1117-1133.

17. Horbett, T. A.; Ratner, B. D.; Kost, J.; Singh, M. A bioresponsive membrane for insulin delivery. In: Anderson JM, Kim, SW, eds.

Recent Advances in Drug Delivery Systems , Plenum Publishing Corporation, New York (1984) 209-220

18.   Ishihara, K. and Matsui, K.   Glucose-Responsive Insulin Release from Polymer Capsule, *J. Polym. Sci., Polym. Lett. Ed.,* **2 4** (1986)   413-417.

19.   Klumb,L.A. and Horbett,T.A. The effect of hydronium ion transport on the transient behavior of glucose sensitive membranes, *J. Contr. Rel.,* **27** (1993) 95-114.

20.   Klumb,L.A. and Horbett,T.A. Design of insulin delivery devices based on glucose sensitive membranes, *J. Controlled Rel.,* **1 8** (1992) 52-80

21.   Heller, J.   Chemically self-regulated drug delivery systems, *J. Controlled Release ,* **8** (1988) 111-125.

22.   Iwata, H. and Matsuda, T. Preparation and properties of novel environment-sensitive membranes prepared by graft polymerization onto a porous membrane, *J. Membr. Sci.,* **3 8** (1988) 185-199.

23.   Fischel-Ghodsian, F., Brown, L., Mathiowitz, E., Brandenburg, D. and Langer, R.   Enzymatically controlled drug delivery, *Proc. Natl. Acad. Sci.,* **85** (1988) 2403.

24.   Wilkins, E.S., Toward Implantable Glucose Sensors: A Review, *J. Biomed. Eng.,* **11** (1989) 354-361.

Chapter 2.

Pump Design

2.1 Characteristics of Ideal Pumps

As described in the Introduction, the goal of this investigation is to determine the feasibility of using implantable pumps containing pH-sensitive hydrogels for insulin delivery. Before discussing the actual design to be studied some background on the development of this design is given.

Several considerations must first be given to the development of implantable systems. Sefton has documented a few guidelines to use to determine the characteristics of the ideal implantable pump.[1] These guidelines are summarized in Table 2-1.

First and foremost, from Table 2-1, the implantable pump must be able to deliver the drug reliably at the prescribed rate for extended periods of time. This should include a capability of the pump to achieve a wide range of delivery rates in case the patients' drug need changes with time. This is especially important in designing a device for diabetics, many of whom require variable amounts of insulin at different times. The pump should be designed to give accurate, precise and stable drug delivery at the appropriate times. This implicitly implies that the pump have reliable mechanical and/or electrical components. The movable parts of the pump should be simple and stick-free. (Many peristaltic pumps have

rotors which get stuck.) In addition possible clogging of the device by the drug or by tissue encapsulation should be avoided. This involves designing devices with as few moving parts as possible, and choosing the correct materials for the pump.

Table 2-1: Characteristics of the Ideal Implantable Pump
[From Sefton, M. CRC Critical Reviews in Biomedical Engineering, Volume 14, Issue 3, 1986]

1. Must deliver drug reliably.
    (i) Wide range of delivery rates.
    (ii) Accurate, precise and stable delivery.
    (iii) Reliable pump and electrical components.

2. Must be safe.
    (i) Biocompatible exterior.
    (ii) Overdose protection.
    (iii) No leakage.

3. Drug must be stable both chemically and biologically.
    (i) Compatible with pump internals.

4. Convenient to use.
    (i) Long reservoir life.
    (ii) Long battery life.
    (iii) Easy programmability.
    (iv) Implantable under local anesthesia.
    (v) Simple method to monitor status.

5. Sterilizable.

Safety and longevity of the pump are other major factors of concern with implants, as is biocompatibility. The device must be capable of residing in the body for a period of years to make the surgery worthwhile. More importantly any implantable device must

be capable of remaining in the patient without creating discomfort or having any toxic effects. This implies choosing the pump materials and design very carefully such that the device causes the minimum amount of distress to the body.

The requirement that the pump be able to remain in the body for extended time periods is another major consideration in the design of an implantable device. In order to accomplish this, the drug must be compatible with the pump materials and must remain chemically, physically and biologically stable for a long period of time and/or for the life of the implant. If refilling is necessary, the pump must be placed in a convenient location. In addition, any leakage or dumping of the drug must be prevented, especially with insulin systems. Fail-safe mechanisms to prevent overdose of insulin are especially important.

In designing the present device concept, as many of the above characteristics were taken into account as possible. Special consideration was given to size and power source. It was desired to design a system which would require no external power source and which could operate for up to a year in the body. It was also considered important to avoid any percutaneous junctions. External biocompatibility issues were not considered as important at this stage, since only the physical aspects of the device concept were considered.

In the present work the normal functioning pancreas is taken as the performance standard for the design of an insulin pump. In

the nondiabetic body a rise in blood glucose level triggers a biphasic increase in the insulin secretion rate where a pulse or spike in secretion rate followed by a return to steady-state secretion rate which is slightly higher than the basal secretion rate. Thus the insulin secretion rate is determined by both the current value and by the rate of change of glucose concentration.

To mimic the pancreas we desire a device which will exhibit proportional-derivative control, i.e. that will simply release, in response to a step increase in glucose concentration, a "burst" of insulin followed by a secondary slower release phase. The main focus of the present pump design is to try to deliver a burst of insulin in response to glucose levels. It is proposed that another method be used to deliver the basal amount of insulin. Also we prefer a device that delivers insulin directly to liver. Device designs which can implanted in peritoneal cavity, which feeds into the hepatic portal vein, are therefore of interest.

2.2 Hydrogels, Liquid Polyelectrolyte Systems

The idea of using pH-sensitive hydrogels to power drug delivery from a pump arose from the phase transition/swelling properties of the lightly crosslinked copolymer gels being studied in our laboratory. These gels contain amine groups which become protonated at low pH. This reaction causes the gel to have charged sites in close proximity to each other. Electrostatic repulsion between the charged sites occurs and causes the polymer network to expand.

It was thought that a device containing hydrogels which respond to chemical rather than mechanical or electrical stimuli would be more reliable. Some of the hydrogels studied in the laboratory exhibit the ability to swell and shrink in response to pH changes reproducibly and unfatigued for long time periods. In addition, the expansion and contraction of the hydrogels are powered by a chemical reaction which will be present in the device as long as the glucose oxidase enzyme remains active. This fact figured greatly in the design, since the pump would be self-powered, and there would be no need for an external power source.

Several types of hydrogels were considered for use in the pump.[2-5] Swelling equilibria and kinetics were measured as a function of solution pH for several lightly crosslinked copolymer gels. The gels which were studied were fairly hydrophobic gels containing combinations of the hydrophobic comonomer methyl methacrylate and a tertiary amine-bearing comonomer; either N,N-dimethylaminoethyl methacrylate (DMA) or N,N-dimethylaminoethyl methacrylamide (DMAA). The hydrogels are loosely crosslinked with divinylbenzene (DVB). What we wanted to create were hydrogels which at high pH, i.e. low blood glucose levels, were unswollen and collapsed. This meant that the DMA or DMAA monomer be neutral and the hydrophobic MMA monomer dominates keeping the gel collapsed. At low pH, (high blood glucose levels) the amine group in the gel ionizes, causing the membrane to swell due to electrostatic and osmotic forces.

Using two of these gels, we were able to generate equilibrium swelling isotherms with swelling transitions around pH 6.6 and 7.6, respectively. The gels containing DMAA are more hydrophilic and have a higher degree of swelling near neutral pH. At pH 7.4 the water fraction for the gels containing DMAA is 0.617 versus a water fraction of less than 0.1 for the gels containing DMA. This implies that at pH 7.4 the gels containing DMA are in a collapsed and unswollen state and will not turn "on" until the pH is decreased to below 6.6. The gels containing DMAA, however, are already swollen at pH 7.4, and thus will change from one swollen state to another as the pH is decreased. (The reader is referred to references 2-5 for more detail.)

Another feature of the pump is that it must be able to respond quickly to changes in blood glucose levels, thus it is imperative that the "engine" be able to respond quickly. This requires that the polyelectrolyte gels be able to change volumes quickly in response to changes in pH. A comparison of the dynamics of swelling changes for both the DMA and the DMAA gels considered shows that the DMA gels respond much faster than the DMAA gels. In both cases the gels took longer to swell than to deswell. The exact relaxation dynamics for these gels have not been worked out. In both cases, however, significant volume changes are obtained within an hour.

Before we continue with the proposed design of the pump, we discuss briefly another polymer system that was considered for use. For any polyelectrolyte, in order to transfer a pH change into a change in volume it is necessary to have 1) a change in the degree of

protonation of the gel or polymer, or 2) a change in the ionization state of various counterions. These two conditions produce changes in the electrostatic and Donnan osmotic forces within the gel or polymer. These forces can also be present with liquid polyelectrolyte systems, where the advantage of a liquid system is the lack of crosslinks. The crosslinks in the hydrogel actually oppose expansion and may lead to slower swelling/deswelling kinetics, reducing the efficiency of the polyelectrolyte in converting chemical changes into a mechanical force. The major design problems with liquid systems is their containment. An advantage however is that a soluble system is not confined to a particular shape.

Several different liquid polyelectrolyte systems were studied in our laboratory with intent for use in the pump.[6] These liquid polymers contained hydrophobic polybasic chain molecules. Titration experiments and kinetic studies of colloid osmotic pressure development and release were performed for several precipitating and non-precipitating linear polyelectrolytes. These experiments showed that copolymers of the hydrophobic p(N,N-diethylaminoethyl methacrylate•HCl) [p(DEA•HCl)] and methacryloxyethyl trimethyl ammonium chloride (MTAC), are capable of generating a Donnan pressure change of around 0.1 atm in about an hour. The drop in colloid osmotic pressure upon neutralization is again slower than the increase, as for the hydrogels. Nevertheless, these polyelectrolytes were shown to be capable of producing changes in osmotic pressures of 0.1 atm. These pressure

fluctuations could be switched on and off by changing the pH of the reference solution.

The two gels which were studied for use in the pump each had individual problems. The MMA/DMAA gels exhibited long term stability problems.[5] Whether the MMA/DMA gels can be utilized in the pump depends on whether the sensor can operate at the low pH values required to swell and shrink this gel. As will be seen later, it is difficult to move the pH down to these values. The liquid polymers appear to be very promising and more research is needed to determine a correct combination of nontoxic monomers.

There are probably many other combinations of monomers which could be used to obtain the desired response. Therefore instead of developing several different combinations, this thesis concerns itself with determining the required responses we wish to obtain in order to have a feasible working pump. This is done in the remaining chapters. An estimation of kinetic constants is required for a stable insulin delivery system. The polymers or hydrogels could then be "designed" to fit these requirements. At this point the design of a particular polymer system becomes dependent on the parameters determined by the glucose/insulin dynamics, and the glucose sensing system. This section simply gives ideas of the range of polymer systems available to power an implantable pump. The exact system will depend on the desired kinetic response of the pump, the exact design of the pump and the pump type.

2.3 Mechanochemical Pump

The current device bears some relationship to osmotic pumps in that both exploit pressure changes. Osmotic pumps act by utilizing osmotic activity changes between an outside water compartment and a highly concentrated osmotic agent compartment. The change in osmotic activity between these two separate compartments causes water to flow into the highly concentrated salt compartment, and this excess volume flow, in turn can be used to expel drug out of a device.[8] In order for an osmotic pump to turn on and off as would be required for an insulin pump, the pH-sensitive gel would need to be an on/off device. This requirement is very stringent and thus the idea of using an osmotic pump was shelved in favor of the concept of the mechanochemical insulin pump.

In order to circumvent the difficulties of obtaining a polymer system which is entirely an on/off device, it was decided to try to design a pump which turns itself on and off by utilizing the change in swelling or pressure generating properties of the polyelectrolyte systems. The goal became to design a device which exploits the volume changes in a gel, instead of permeability changes. In doing this one can take advantage of the faster kinetics of going from one swollen state to another swollen state. If liquid polyelectrolytes are used instead of gels, the pump will be designed to go from one partially osmotically active state to another more osmotically pressurized state.

The proposed device or pump functions by converting chemical energy in the form of changes in blood glucose activity, into a mechanical hydraulic force which pumps insulin out of the device. The pump is powered by the osmotic swelling action of a pH-sensitive hydrogel or liquid polyelectrolyte. The polymer system is coupled to a glucose sensitive membrane which contains the enzymes that convert glucose into an acid. The polymer gel swells in response to a decrease in local pH (high glucose levels) and contracts in response to an increase in local pH (basal glucose levels). This device would be intended for use as a long-term implantable pump.

This pump is a three compartment system: one compartment contains the hydrogel membranes placed in series, the second is an incompressible fluid chamber which allows the pump to be reset, and the third is the drug chamber containing insulin (see figure 2-1 below). The hydrogel membranes are adjacent to a diaphragm. As the pH-sensitive gel swells in response to gluconic acid, it applies pressure to the diaphragm. The diaphragm conducts the pressure to the second and third compartments. When enough pressure is applied a valve opens and releases the insulin. The second and third chambers are separated by a movable/flexible partition which when expanded acts to force the insulin out of the pump. When glucose is present in the blood stream this process is set in motion.

The device concept is illustrated in Figure 2-1 below. This proposed design for the pump contains three compartments, two valves and a flexible elastomeric diaphragm. Chamber I contains the

glucose sensitive swellable polymer system. For the present purposes, Chamber I will be modeled as a composite membrane where one component is the immobilized glucose oxidase enzyme membrane and the other is a polybasic hydrogel which expands when the blood glucose concentration rises. Chamber II contains an incompressible aqueous fluid, such as saline solution, and Chamber III contains the drug formulation. Chamber III is separated from the environment by a one way valve which opens when the internal pressure of the pump exceeds the external surrounding pressure allowing insulin to flow out of the pump. Chamber II also contains a one way valve which opens when the surrounding pressure is greater than the internal pressure. Chambers II and III are separated by a movable partition which collapses as drug is released. Chamber I communicates with the body fluids through a rigid porous membrane which allows the influx of small molecules but excludes the large molecules such as plasma proteins. Chambers I and II are separated by the diaphragm. The diaphragm separates the polymer gel from the inside of the pump and in this way serves as a pressure transmitter. It deforms in response to the increase in osmotic pressure from the swelling gel and in this way, transfers the pressure from the gel to Chamber II. The diaphragm also acts by elastic recoil to push fluid out of the polymer gel when the gel contracts.

Figure 2-1: **Schematic of proposed Mechanochemical Insulin Pump**
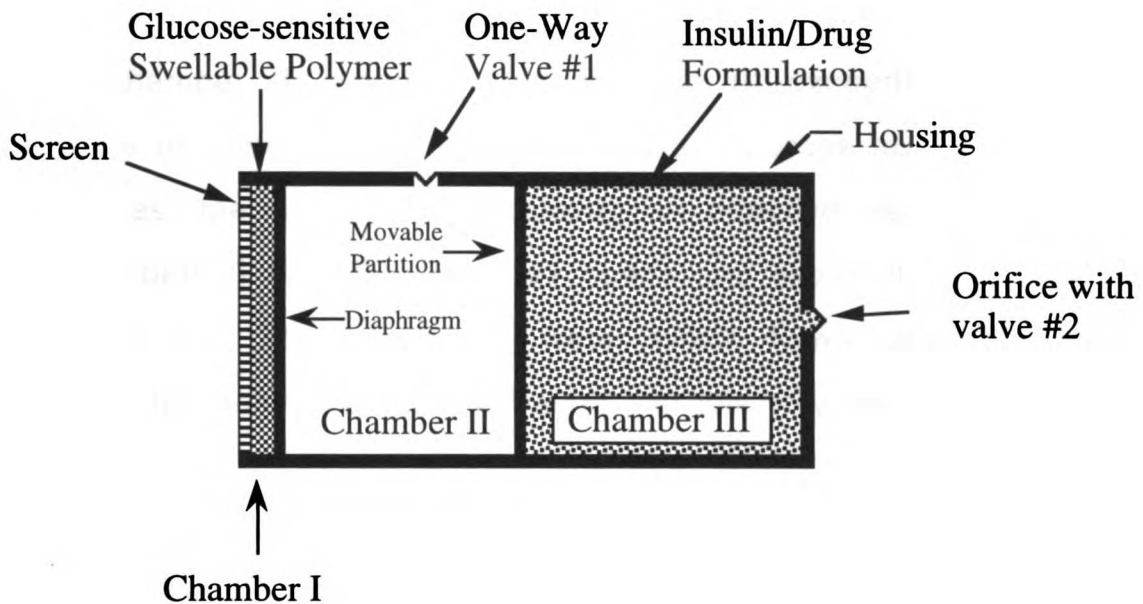
Chamber I - Polymer System, Glucose oxidase
                  membrane (sensor)

Chamber II - Aqueous Fluid Compartment

Chamber III - Drug Compartment

A schematic of the pump operation is shown in Figure 2-2. When the blood glucose concentration is high, the glucose oxidase membrane in Chamber I catalyzes the conversion of glucose into gluconate and protons. The protons then diffuse into the polybasic gel also contained in Chamber I. The polybasic gel contains amine groups which bind the protons. This leads to an osmotic pressure due the fixed charges on the gel and the excess of mobile counterions present to maintain electroneutrality within the polymer. The polymer gel then swells as a result of the increase in osmotic force. The swelling action of the polymer causes the

diaphragm to expand and to exert a pressure on the fluid in Chamber II. The increased pressure in II closes valve #1 and is transferred to Chamber III by the incompressible fluid in II. The drug is expelled from Chamber III when the pressure in III exceeds the cracking pressure of valve #2. Conversely when the glucose level in the blood decreases, the gel contracts causing an effective negative pressure in Chambers II and III. Valve #1 opens and allows fluid to flow into Chamber II. The volume of water which flows into Chamber II replaces the volume of drug released. In this way the pump is reset.

Figure 2-2:   Workings of Proposed Pump

pH down
or
Blood
Glucose
Up

I   II   III

pH up
or
Blood
Glucose
Down
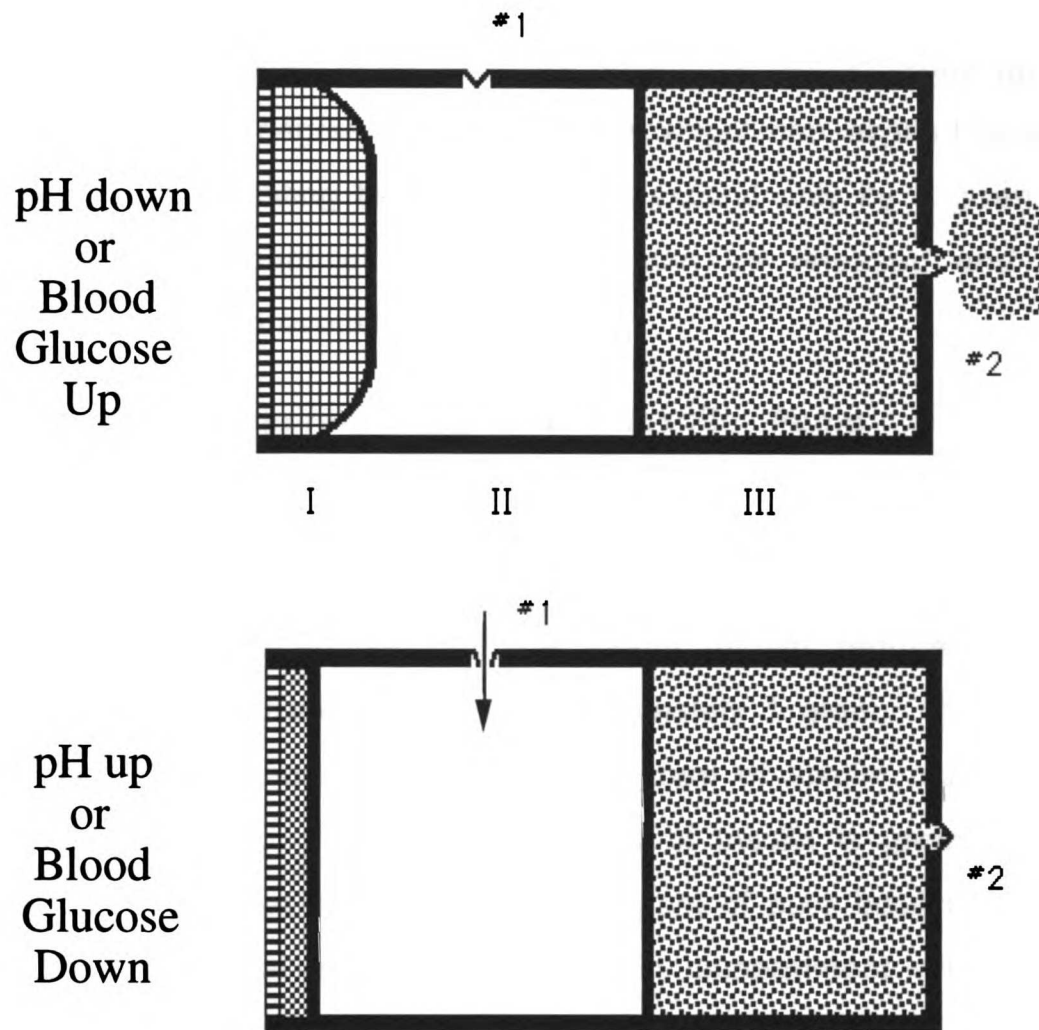
The model proposed in Figure 2-1 became the basis for the theoretical design of the mechanochemical pump.   The appealing features of this pump is that it operates by the direct conversion of chemical energy, manifested by changes in glucose levels, to a mechanical pumping of insulin.   This eliminates the need for an external power source.   Second, as in the osmotic pump, the insulin can be formulated in any method, since it is kept completely separate from the rest of the device.   This may aid in solving some

of the long-term stability and aggregation problems associated with insulin. The fail-safe device in this design is associated with the diaphragm. Insulin release in response to a rise in blood glucose is limited by the degree by which the hydrogel can expand against the diaphragm. Limiting the diaphragm to expand only by a given volume limits the amount of insulin which can be released and thereby automatically prevents overdosing.

2.4 Size Requirements for the Insulin Pump

The overall size of the pump is largely determined by the amount of insulin required to store within the pump for the intended duration of the implant. The yearly insulin requirement for an average sized diabetic male is approximately 1 gram. If the pump is to be refilled once a year, then this gram of insulin must be stored within the pump. The specific gravity of insulin is greater than one which means that the volume of one gram of pure insulin is less than 1 ml. The total volume of the insulin compartment will depend on the type of formulation used. If the insulin is formulated as a finely divided powder in a semi-solid suspension, one gram of insulin can be stored in this form in a volume of 10 ml by using a concentration of 100 mg/ml. This volume may change of course depending on the insulin formulation.

A volume of 10 ml for Chamber III can easily be accomodated. Chamber II is initially empty and engrossed by Chamber III, therefore it does not require much extra space. Since the mechanochemical pump has no rotor or other electrical or

mechanical parts, the remainder of the pump can easily be encased in a volume of under 20 ml. This compares favorably to other implantable pumps currently available, which have insulin reservoirs of 10 - 50 ml and an overall average volume of 200 - 300 ml.[1]

It should be noted that the overall size of Chamber I of the pump outlined in Figure 2-1 can be made very small by incorporating very thin membranes. One advantage of using very thin membranes is that the kinetics of diffusion become faster allowing for a quicker response time. The diaphragm, as will be shown, can be made as thick or thin as required. The valves in this design must be designed to meet size specifications.

2.5 Amount of Insulin Delivery

The proposed mechanochemical pump shown in Figure 2-1 is designed for insulin delivery at peak glucose levels right after meals. This design does not take into account basal insulin delivery which must be provided by some other means. In order to design the pump correctly it is required to know the actual amount of insulin delivered after each meal.

The amount of insulin to be delivered after each meal can be estimated as follows. A normal individual of average size needs approximately 50 units of insulin per day, with a basal rate of 1 unit/hr and a peak rate of 5 units/hr. This corresponds to 24

units/day required for basal secretion rate and 26 units/day after meals. If it is assumed that one has three meals per day, this corresponds to approximately 9 units of insulin required per meal or 9 units per dose. Depending on the site of insulin delivery, this amount may need to be increased. It has been documented that if the insulin is delivered subcutaneously, the same amount is delivered as if the insulin were delivered intravenously. It simply takes much longer to reach the plasma if delivered subcutaneously. If, however the insulin is delivered intraperitoneally, only about half the amount of insulin could be accounted for in the plasma.[9] This implies that the pump should be able to deliver a dose of 9 - 20 units each meal, depending of course on the individual. This dosage corresponds to 360 - 800 μg/dose or delivering 3.6 - 8 μl per dose if the insulin concentration in the drug compartment is 100 mg/ml.

Another method to generate a rough estimate of how much insulin needs to be delivered per dose is to assume that an average person needs 1000 bursts of insulin per year. (This corresponds to one dose per meal, three boosts per day times 365 days per year.) To accomodate the 1000 doses per year with a volume of 10 ml in the insulin reservoir, each dose would be required to be approximately 10 μl. Given an approximate concentration of insulin in the drug compartment as 100 mg/ml, 10 μl/dose corresponds to 1000 μg/dose or 25 units/dose. This value is higher than that estimated above. It can easily be altered by changing the concentration of insulin in the drug reservoir or designing the pump to only release a lower volume.

For the purposes of obtaining a generic design for the pump, it was assumed that a dose of 10 µl is required.

2.6 Conclusions

This chapter describes the proposed mechanochemical insulin pump. Due to unknowns in the design and problems with the experiments, it was decided to pursue a more theoretical approach. It was decided to design the initial portion of the pump, or the sensor in more detail. The theoretical approach is used to determine a range of parameters which will facilitate the design of a better, more feasible pump.

References

1. Sefton,.M.V., Implantable pumps, *CRC Crit. Rev. Biomed. Eng.*, **14**, Issue 3, (1986) 201-240.

2. Firestone, B. A., Ph. D. Dissertation, University of California, San Francisco, 1990

3. Firestone, B. A. and Siegel R. A., Dynamic pH-Dependent Swelling Properties of a Hydrophobic Polyelectrolyte Gel, *Polym. Commun.*, **29**, (1988) 204-208.

4. Siegel, R. A. and Firestone, B.A., pH-Dependent Equilibrium Swelling Properties of Hydrophobic Polyelectrolyte Copolymer Gels, *Macromolecules*, **21** (1988) 3254-3259.

5. De Moor, C. P., Doh, L., and Siegel, R. A., Long Term Structural Changes in pH Sensitive Hydrogels, *Biomaterials*, **12**, (1991) 836-840.

6. Cornejo, J., Ph. D. Dissertation, University of California, San Francisco, 1992

7. Siegel, R. A., pH-Sensiitve Gels: Swelling Equilibria, Kinetics, and Applications for Drug Delivery, in <u>Pulsed and Self-Regulated Drug Delivery</u> (J. Kost, ed.), CRC Press,

8. Theeuwes, F. and Yum, S. I., Principles of the Design and Operation of Generic Osmotic Pumps for The Delivery of Semisolid or Liquid Drug Formulations, *Annals of Biomedical Engineering*, **4,** (1976) 343-353.

9. Schade, D. S., Eaton, R. P., Friedman, N. and Spencer, W., "The Intravenous, Intraperitioneal, and Subcutaneous Routes of

Insulin Delivery in Diabetic Man", *Diabetes*, Vol. **28**, (1979) 1069-1072.

10. Siegel, R. A. and Firestone, B. A., Mechanochemcial Approaches to Self-Regulating Insulin Pump Design, *J. of Controlled Release*, **11**, (1990) 181-192.

11. Siegel, R.A., Grant Proposal to NIH, Implantable, Self-Regulating Mechanochemical Insulin Pump, (1990)

Chapter 3.

Sensor Design

3.1 Introduction

In a normal individual the beta cells of a healthy pancreas continually measure blood glucose and release insulin accordingly. In a diabetic this process is either no longer functioning or greatly reduced. Therefore, one of most important requirements in order to obtain a working closed-loop device for insulin dependent diabetics (IDD) is a reliable, *in vivo* glucose sensor. This chapter reviews current glucose sensor technology and the problems associated with utilizing these sensors. A novel design for a glucose sensor, using the enzymes glucose oxidase and catalase is proposed. This sensor can be easily coupled to a titratable polymer system which is used in the proposed implantable device.

Many of the difficulties encountered in the treatment of diabetes are concerned with the accurate measurement of blood glucose levels in order to obtain the correct amount of insulin required. Diabetics currently need to measure their blood glucose level at least three times a day; once in the morning, at bedtime and at least one time before a meal. Six to eight blood glucose measurements a day are considered optimal to obtain good glycemic control according to the Functional Insulin Treatment Program.[1] Self-monitoring of blood glucose (SMBG) involves drawing blood

using finger-pricking devices and measuring the blood glucose level using blood glucose test strips, which can be evaluated either on the basis of color or inserted into a glucose meter. The development of a reliable, sensitive and long lasting (*in vivo*) biosensor which can monitor the blood glucose level is therefore imperative to the advancement of diabetic treatments.

3.2 Glucose Sensors: What is available.

Glucose sensor technology has been active for more than 25 years.[2] The final goal of glucose sensor development is to obtain a biosensor which can monitor glucose level for effective feedback control. Some of the desirable characteristics for an implantable glucose sensor include reliablity, reproduciblity, biocompatiblity, and an *in vivo* lifetime of several years. In addition a reliable sensor must be specific only or primarily towards glucose and must not have any inhibitory or poisoning effects towards the body. Ease of fabrication and cost effectiveness are also important factors to consider. These "wishes" are by no means simple to achieve. A durable *in vivo* glucose sensor is still needed in order to close the loop in diabetic treatment.

Several papers have documented advances and current research in glucose sensor development.[3-6] Most of the research has been concentrated on enzyme electrodes, or other enzyme-catalysed sensors which utilize immobilized enzymes to detect glucose. Other potential sensors which do not use enzymes have been studied

with some success.   These include metal catalysed glucose sensors using an activated   platinum electrode and affinity sensors using lectin concanavalin A as described in the Introduction of this thesis. Another sensor, termed the coated wire sensor, has been developed by Wilkins.[7]   This sensor converts glucose to an ionic substance using the association-dissociation mechanism of glucose salts.   The glucose concentration is measured by an electrode either polarographically, potentiometrically or amperometrically due to the dissociation or the association of the glucose salt in equilibrium with a glucose solution.

Some of the major problems encountered with development of these glucose sensors have been the interaction of the implanted sensors with body tissues or biocompatibility, the need for *in vivo* calibration since sensors often give lower values when implanted than would be anticipated from prior *in vitro* calibration, and unpredictable drift of sensors *in vitro* and *in vivo*.   Specificity problems are encountered with the non-enzymatic sensors such as the metal catalyzed glucose sensors.   In addition, many of the electrode sensors have had stability problems *in vivo*. The enzymatic sensors have the general problem of short lifetimes, depending on the life of the particular enzyme.

To date the enzyme-catalyzed sensors have been the most successful in measuring glucose levels.   The main advantage of these sensors is that they are specific to glucose, thereby making the the signal due only to glucose and not to other chemicals in the body. These sensors are also biocompatible and do not have the

immunological problems which the affinity sensors do, because the enzymes used, such as glucose oxidase, exist in the body.

The purpose in this project is to develop a sensor which will interact with the rest of the pump described in Chapters 1and 2 in a closed loop fashion. Most of the above devices are simply sensors and not an entire delivery system. Our goal is to use the above research and adapt some of the above ideas to design a sensor which will function in the pump. We have chosen the enzyme-catalyzed sensor using glucose oxidase.

3.3 Glucose Oxidase Sensor

The majority of the enzyme sensors to date use glucose oxidase to detect glucose.   Glucose oxidase has been used extensively in commercial products. It is used to remove glucose or oxygen from food products, in the production of gluconic acid, for quantitative determination of glucose in blood (YSI instruments), and more recently has been implemented in glucose biosensors.[8-11] Due to its importance in commercial applications and its current use in biosensors, glucose oxidase has been studied extensively. Glucose oxidase has been referred to as an ideal enzyme to use in a biosensor by Wilson and Turner.[12]

The enzyme was first detected in the extracts of *Aspergillus niger* .[13]   It has since been purified and characterized.[14,15] Its amino acid sequence and most recently its crystal structure have been determined.[16-18]

Glucose oxidase (β-D-glucose:oxygen oxidoreductase, EC 1.1.3.4) catalyzes the oxidation of β-D-glucose to glucono-δ-lactone and hydrogen peroxide by reducing molecular oxygen. This enzyme is highly specific for β-D-glucose which makes it extremely valuable in detecting the glucose concentrations. The flavoprotein glucose oxidase is a dimer of identical monomer units with a molecular weight of 150,000. It contains two tightly non-covalently bound FAD cofactors and 2 moles of covalently bound phosphate groups per dimer.[18,19] Glucose oxidase is also a glycoprotein containing 11-16% carbohydrates.[20,21] It is thought that the carbohydrate shell around the enzyme contributes to its unique solubility and stability properties. The enzyme is very soluble in water and resistant to many proteases.

The mechanism of the glucose oxidase reaction, the kinetics and the pH dependence of the GO reaction are well documented[22,23], as are the stability and activity of the enzyme.[20,24-27] Glucose oxidase is inactivated by hydrogen peroxide[8,28] and by putrescine.[26] Inactivation also results with the loss of the FAD coenzyme, and when the dimer becomes disassociated.[27] Deglycosylation does not inactivate the enzyme although it does affect the kinetics of the reaction.[20,29] The flavoprotein chemistry and the possible reaction intermediates have also been investigated.[30]

Due to its high degree of substrate specificity, glucose oxidase has been investigated for use in a number of enzyme electrodes.[8,10,24,31-34] When glucose oxidase is used to detect glucose in this fashion, glucose oxidase is often immobilized in a

polymer matrix. There are several, well-documented methods one can use to immobilize enzymes. The soluble enzyme can be sandwiched between two polymer membrane layers.[33,34] Other more effective methods have been used. Trapping the enzyme in a gel matrix is what is most commonly done.[8-11,31,35-39] The gel matrix can be poly-acrylamide or glutaraldehyde. Initially the above two methods result in some loss of sensitivity due to loss of free glucose oxidase. In addition, in time such membranes may lose their activity to due a slow leakage of the enzyme. This problem can be countered by covalent attachment of the enzyme to the membrane.[40] It has also been suggested to cover the enzyme layer with cellulose acetate. The purpose of this is to restrict access of interfering substances such as ascorbate, uric acid and bilirubin. The covering can also act as a diffusional barrier for glucose, and can reduce the effects of variation in temperature and pH on enzyme kinetics, as well as forming an interface between the body and the device and ensure biocompatibility.

The major disadvantage in using glucose oxidase as a glucose sensor is its sensitivity to oxygen. Glucose oxidase requires oxygen to reoxidize it. Thus many of the sensors experience variations of output with alterations in oxygen levels at the sensing site. In addition, the molecular oxygen concentration in plasma is much lower than the glucose concentration. This implies that oxygen will be depleted before the sensor detects appreciable amounts of glucose. In order to mitigate this problem, the sensor must be

designed to enhance the transport of oxygen relative to that of glucose.

3.4 Current Designs

There are two current designs that are of interest to us in that each design uses glucose oxidase and combats the oxygen deficiency problem. These sensors attempt to increase oxygen concentration with respect to glucose concentration by either providing excess oxygen or by providing preferential oxygen transport. Increasing the oxygen concentration within the glucose oxidase/catalase membrane can be accomplished by entirely or partially covering the immobilized enzyme gel with a hydrophobic membrane. The hydrophobic membrane is very permeable to oxygen and virtually impermeable to glucose or other hydrophilic substances.

Enzyme electrodes are chemical-specific sensors in which immobilized enzymes are coupled to electrodes that measure the potential difference caused by a difference in the concentration of an analyte. These sensors utilize immobilized glucose oxidase to measure the glucose level by monitoring either oxygen consumption[8-11,41] or hydrogen peroxide production[33,34,42] at a platinum base electrode. Gough et. al. developed a two dimensional glucose sensor which eliminated the oxygen deficit problem. The sensor consists of a thin cylindrical electrode, surrounded by a gel containing immobilized glucose oxidase and catalase. This gel is surrounded in turn by a hydrophobic, oxygen permeable membrane. Thus the glucose can enter the gel in the axial direction only, but

oxygen can enter by both the axial and the radial directions. This sensor has been tested both in vitro and in vivo with good results.

Abel et al. used a perforated hydrophobic membrane to modify a Clark-type glucose electrode to decrease the electrodes' sensitivity to oxygen concentrations.[33,34] Their design consists of a membrane-covered polarographic electrode which measures the production of hydrogen peroxide. The membrane consists of a hydrophilic membrane of cellulose acetae next to the elecrode, covered by a layer of immobilized glucose oxidase in sepharose, which is covered by a hydrophobic membrane. The hydrophobic membrane is perforated directly above the anode. The hole in the hydrophobic membrane allows glucose to enter the sensor. Without the hydrophobic membrane, the studies showed that the sensor could only detect glucose levels up to 3 mmol. Addition of the hydrophobic membrane allowed this range to be extended to 40 mmol.

3.5 Proposed sensor

The electrode sensors mentioned above are not entirely feasible for the proposed pump. The sensor for the proposed device is required to detect glucose by converting it into gluconate and hydrogen ions, and by delivering the hydrogen ions to the polymer gel. This sensor must therefore be adjacent to the polymer gel, which in turn must be allowed to swell without damaging the sensor. In addition this sensor requires entry and exit paths for the acid during the discharge or shrinking phase of the pump. For these

reasons, the design used by Gough cannot be accomodated. Instead it was decided to adapt the design used by Abel et. al.

The idea is to cover a planar glucose oxidase/catalase membrane with a thin hydrophobic membrane that is periodically punctured. The holes allow the diffusion of glucose, oxygen, protons, gluconate, buffers and ions. Only oxygen can diffuse through the hydrophobic layer. This system couples the advantages of the membrane covering to enhance the oxygen concentration and the holes in the hydrophobic membrane the effectively generate a two dimensional sensor. Figure 3-1 below illustrates the proposed sensor.

Figure 3-1: Schematic of proposed glucose sensor
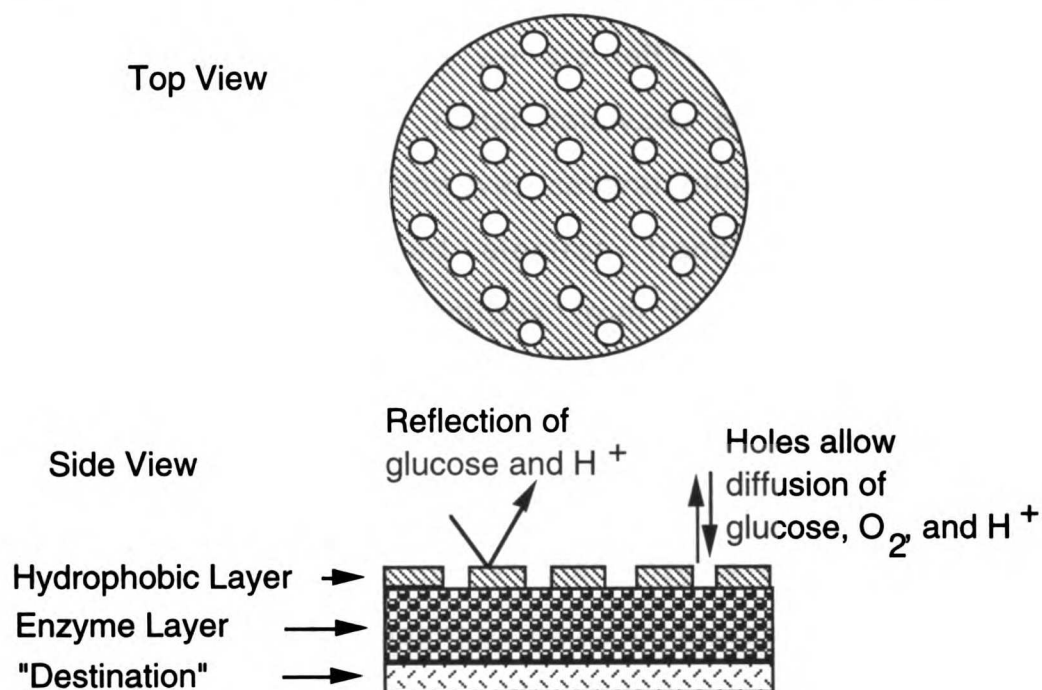
The goal of this system will be to design the sensor in such a fashion as to maximize delivery of the protons from the glucose oxidase/catalase reaction to the destination layer when glucose is high and minimize it when glucose is low, regardless of the oxygen concentrations. By optimizing the geometry of the enzyme membrane, the location and amount of enzyme within the membrane, and the location and size of the perforations in the hydrophobic membrane, the afore mentioned goal can be attained. The next chapter describes the mathematical modeling undertaken to determine the dimensions of the sensor.

3.6 Other possible solutions.

In choosing to use the enzyme system glucose oxidase and catalase we have chosen enzyme which employs oxygen as the final charge acceptor, and thus we are left with the problem of oxygen sensitivities. The other metal catalyzed electrodes have specificity problems. There are however several other possibities. A sensor which uses a mediated electron transfer substance such as ferrocene to transfer electrons from the reduced enzyme to an underlying electrode has been studied with some success.[43] In this case oxygen is no longer the final electron acceptor in the glucose oxidase-catalyzed reaction and the sensor is oxygen insenitive. Another possibility is to use another enzyme to oxidize glucose to an acid. Glucose dehydrogenase oxidizes glucose to gluconolactone as well. This enzyme requires the enzyme co-factors FAD and NAD. Chung et al. have developed an insulin releasing membrane by immobilizing this enzyme with these co-factors.[40]

Much more research is needed in the area of enzyme sensors, specifically glucose sensors. Preliminary successes have occured with the enzyme glucose oxidase. The major difficulty with the glucose oxidase sensor is the oxygen sensitivity problem which occurs *in vivo*. The remaining chapters show a theoretical solution to this problem.

References

1. Howorka, K. Functional Insulin Treatment- Principles, Teaching Approach and Practice, Springer-Verlag, Berlin, (1990)

2. Clark,LC and Lyons, C., Electrode system for continuous monitoring in cardiovascular surgery. *Ann NY Acad Sci*, **102**: (1962) 29-45

3. Wilkins ES, Towards implantable glucose sensors: a review, *J. Biomed. Eng.* ,**11**, (1989) 354-361

4. Pickup JC, Biosensors: a clinical perspective. *Lancet* ; **2**: (1985) 817-20

5. Soeldner JS, ed. Symposium on potentially implantable glucose sensors, *Diabetes Care*; **5**: (1982)147-217

6. Turner APF and Pickup JC. Diabetes mellitus: biosensors for research and management. *Biosensors* ; **1**: (1985) 85-115

7. Wilkins, E., Wilkins, M. Implantable glucose sensor. *J. Biomed Eng*, **5**: (1983) 309-315

8. Gough,D.A., *Proceed. Intern. Symp. Comntol. Rel. Bioact. Mater.*, **17**, (1990) 85-86

9. Leypoldt,J.K. and Gough, D.A., Model of a Two-Substrate Enzyme Electrode for Glucose, *Anal. Chem.* ; **56**: (1984) 2896-2904

10. Lucisano, J.Y., Armour, J.C. and Gough,D.A., In Vitro Stability of an Oxygen Sensor. *Anal Chem.* ; **59**: (1987) 736-739

11. Gough DA, Lucisano JY, Tse PHS. Two-dimensional enzyme electrode sensor for glucose. *Anal Chem* ; **57**: (1985) 2351-7

12. Wilson, R. and Turner, APF. Glucose oxidase: an ideal enzyme. *Biosensors & Bioelectronics*, **7**: (1992) 165-185

13. Muller,D. (1928) *Biochem. Z.* **199**, 136-170, Elsevier, Amsterdam

14. Pazur,J.H., Kleppe,K. The oxidation of glucose and related compounds by glucose oxidase from *Aspergillus niger* . *Biochemistry* **3**: (1964) 578-583

15. Swoboda, B.E.P., and Massey, V. Purification and properties of glucose oxidase from *Aspergillus niger. J. Biol. Chem.* **240**: (1965) 2209-15

16. Frederick, K.R., Tung,J., Emnerick,R.S., Masiarz,F.R., Chamberlain, S.H., Vasavada, A., Rosenberg,S., Chakraborty,S., Schopter,L.M., Massay,V. Glucose oxidase from *Aspergillus niger. J. Biol. Chem.*, **265**: (1990) 3793-3802

17. Kriechbaum,M.,Heilmann,H.J., Wientjes, F.J.,Hahn, M.,Jany, K., Gassen, H.G.,Sharif,F., and Alaeddinoglu,G. Cloning and DNA sequence analysis of the glucose oxidase gene from *Aspergillus niger* NRL-3. *FEBS Letters*, **255**: (1989) 63-66

18. Hecht, H.J., Kalisz, H. M., Hendle, J., Schmid, R.D. and Schomburg, D., Crystal Structure of Glucose Oxidase from *Aspergillus niger* Refined at 2.3 A Resolution, *J. Mol. Biol.*, **229**: (1993) 153-179

19. James,T.L., Edmondson,D.E., and Husain,M. Glucose oxidase contains a disubstituted phosphorus residue: phosphorus-31 nuclear magnetic resonance studies on the flavin and non-flavin phosphate residues. *Biochemistry* **20**: (1981) 617-621

20. Nakamura,S., Hayashi,S. and Hasumi,H. <u>Flavins and Flavoproteins</u>, ed. T.P. Sanger, Elsevier, Amsterdam: (1976) 691-707

21. Nakamura, S., Hayashi, S. and Koga, K. Effect of periodate on the structure and properties of glucose oxidase. *Biochem. Biophys. Acta*, **445**, (1976) 294-308

22. Gibson, Q.H., Swoboda,B.E. P., and Massey, V. Kinetics and mechanism of action of glucose oxidase. *J. Biol. Chem.* **239**: (1964) 3927-3934

23. Weibel, M. K. and Bright, H.J., The glucose oxidase mechanism: interpretation of the pH dependence. *J. Biol. Chem.*, **246**: (1971) 2734-2744

24. Thevenot,D.R., Sternberg,R. and Coulet,P. A glucose electrode using high-stability glucose-oxidase collagen membranes. *Diabetes Care* **5**: (1982) 203-206

25. Voet, J.G., Coe,J., Epstein, J.,Matossian,V. and Shipley, T. Electrostatic Control of Enzyme Reactions: Effect of Ionic Strength on the pKa of an Essential Acidic Group on Glucose Oxidase *Biochemistry* , **20**: (1981) 7182-7185

26. Voet ,J. G., and Andersen, E.C. Electrostatic control of enzyme reactions: mechanism of inhibition of glucose oxidase by putrescine. *Arch. Biochem. Biophys.* **233**: (1984) 88-92

27. Ye, W. and Combes, D. The relationship between the glucose oxidase subunit structure and its thermostability. *Biochimica et Biophysica Acta*, **999**: (1989) 86-93

28. Kleppe, K. The effect of hydrogen peroxide on glucose oxidase from *Aspergillus niger. Biochemistry*, **5**: (1966) 139

29. Kalisz, H.M., Hecht, H., Schomburg,D. and Schmid, R.D. Crystallization and Preliminary X-ray Diffraction Studies of a Deglycosylated Glucose Oxidase from *Aspergillus niger. J. Mol. Biol.,* **213**: (1990) 207-209

30. Hemmerich,P., Nagelschneider,G. and Veeger,C., Chemistry and Molecular Biology of Flavins and Flavoproteins *FEBS Letters,* **8**, (1970) 69-83

31. Tse,P.H.S. and Gough, D.A. Time dependent inactivation of immobilized glucose oxidase and catalase. *Biotechnology and Bioeng.,* **29**: (1987) 705-713

32. Clark LA, and Duggan CA, Implantable Electroenzymatic Glucose Sensors, *Diabetes Care,* **5**: (1982) 174-180

33. Abel P, Fischer U, Muller A, Freyse EJ. *J Eur Soc Artif Organs* ; **1**: (1983) 45-8

34. Abel P, Muller A, Fischer U. Experience with an implantable glucose sensor as a prerequisite of an artificial beta cell. *Biomed Biochem Acta* ; **43**: (1984) 577-84

35. Horbett T, Ratner B, Kost J, Singh M. A bioresponsive membrane for insulin delivery. In: Anderson JM, Kim SW, eds, *Recent Advances in Drug Delivery Systems, Proc. Int. Symp.* 1983. New York: Plenum Press, 1984: 209-20.

36. Kost J, Horbett TA, Ratner, BD and Singh, M. Glucose-sensitive Membranes Containing Glucose Oxidase: Activity, Swelling and Permeability Studies, *J. Biomed. Mater. Res.,* **19**: (1985) 1117-1133

37. Albin G, Horbett TA, Miller SR and Ricker NL, Theoretical and experimental studies of glucose sensitive membranes, *J. Controlled Release* , **6**: (1987) 267-91

38. Klumb LA and Horbett TA, Design of insulin delivery devices based on glucose sensitvie memebranes, *J. Controlled Release*, **18:** (1992) 59-80

39. Klumb LA and Horbett TA, The effect of hydronium ion transport on the transient behavior of glucose sensitive membranes, *J. of Controlled Release*, **27:** (1993) 95-114

40. Chung, D., Ito, Y. and Imanishi, Y. An insulin-releasing membrane system on the basis of oxidation reaction of glucose, *J. of Controlled Release*, **18:** (1992), 45-54

41. Updike S and Hicks G, Glucose based on an oxygen probe. *Nature*; **214:** (1967) 986

42. Shichiri M, Kawamari R, Goriya Y, Yamasaki Y, Nomura M, Hakui N, Abe H. Glycaemic control in pancreatectomized dogs with a wearable artificial endocrine pancreas. *Diabetologia* ; **24:** (1983) 179-84.

43. Cass, AEG, et al., Ferrocene-mediated enzyme electrode for amperometric determination of glucose. *Anal Chem* ; **56:** (1984) 667-771

Chapter 4.

Mathematical Modeling of Glucose Sensor

4.1 Introduction

In this chapter the modeling aspects of the glucose sensor are considered. As described in Chapter 3, the sensor is a glucose sensitive membrane containing the immobilized enzymes glucose oxidase, gluconolactonase and catalase. These enzymes convert glucose and oxygen into gluconate and free protons. The free protons generated by the reaction in the membrane diffuse into and ionize the hydrogel, causing the latter to swell. A major goal in the membrane design is to control the mass transfer of protons within and from the polymer hydrogel; this mass transfer is in turn controlled by the mass transfer and subsequent reaction of both glucose and oxygen into and within the enzyme membrane.

This problem poses some complex modeling issues. Therefore the diffusion/reaction calculations for the enzyme membrane coupled to the polymer hydrogel are being carried out in order to determine the rate of delivery of protons to the hydrogel as a function of the enzyme loading and the geometric properties of the membrane. The design problem is complicated by the fact that the molecular oxygen concentration in plasma is much lower than the glucose concentration, so oxygen may be depleted before the sensor detects appreciable amounts of glucose. This problem has been documented by a variety of authors: Gough and Lucisano (1985),

Fischer and Abel (1982), Albin et.al. (1987), Klumb and Horbett (1992), and Wilson and Turner (1992) to mention a few.[1-7] As mentioned in the last chapter, this problem can be mitigated by providing preferential transport pathways for oxygen relative to glucose and by optimizing the geometry of the enzyme membrane. These calculations will enable us to determine the design which allows for enhanced oxygen transfer and efficient proton transfer as a function of the external mass transfer limitations and the external glucose concentration.

This chapter describes the mathematical modeling undertaken for the proposed glucose sensor. A simplified model for the sensor is described, and the assumptions involved in deriving the mass transfer equations are made explicit. The diffusion/reaction equations are then derived for the model. The boundary conditions used in this model are also discussed.

4.2 Assumptions and Simplification of the Model

As described in Chapter 3, the transport pathways for oxygen are provided by means of a thin hydrophobic perforated membrane which covers the enzyme membrane, and which is permeable to oxygen but impermeable to glucose and hydrogen ions. The glucose and protons can only diffuse into and out of the perforations in the membrane while the oxygen can diffuse through the whole sensor area.

Figure 4-1 shows a schematic of the proposed enzyme sensor along with the polymer layer or the destination layer into and out of which the protons diffuse. The enzyme membrane is a composite membrane in which the enzyme layer is sandwiched between the destination layer and the hydrophobic layer. Diffusion of the species from the bulk solution into the enzyme layer is assumed to occur only in the axial direction with only the top side exposed to the environment. The rest of the sensor or enzyme membrane is assumed to be contained in a cylindrical casing which does not permit radial diffusion into the sensor This assumption greatly simplifies the model and the boundary conditions as will be seen.

Figure 4-1. Schematic of Glucose Sensor
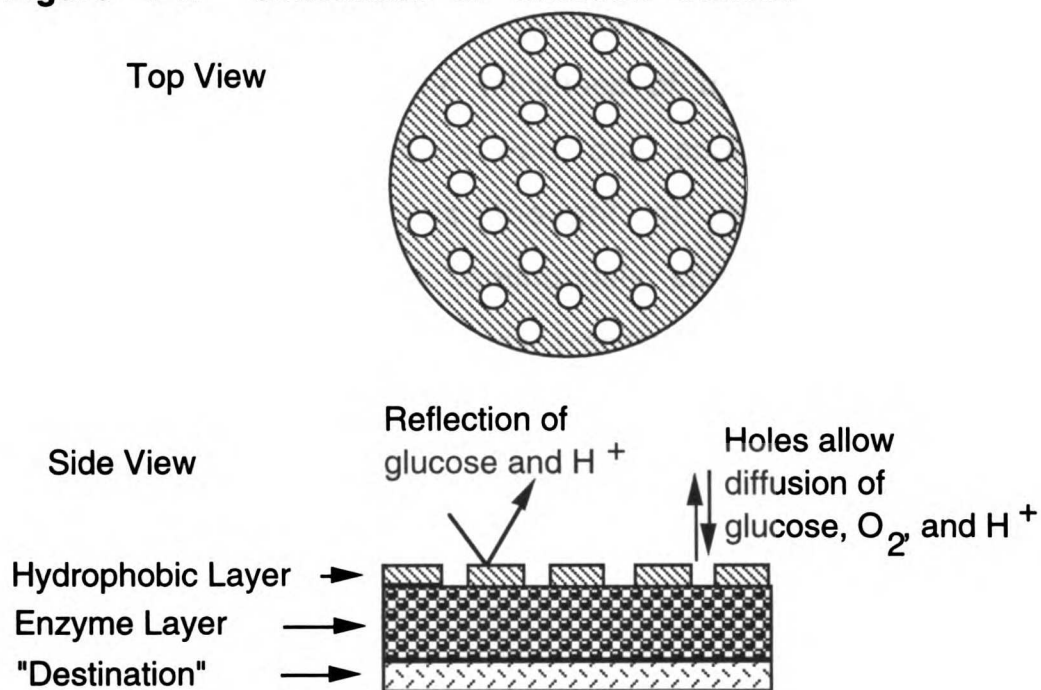
The thin hydrophobic layer is perforated in a uniform pattern with the center of each hole at the vertices of equilateral triangles with sides of length 2R, as shown in Figure 4-2a. In this way the center of each hole is equidistant from the center of all adjacent holes. It is assumed that the hydrophobic layer will completely exclude transport of the glucose, protons and any buffer present in the system, into or out of the enzyme layer. The transport of protons, buffers and glucose will take place only through the holes in the hydrophobic layer. In this design the size of the holes, the distance between the holes, and the sensor membrane thickness control the enhancement of the oxygen transport relative to that of glucose.

The thickness of the hydrophobic layer is assumed to be minimal compared with the thickness of the enzyme layer and thus the mass transfer equations were only applied to the enzyme layer. The destination layer is thought of as an area of uniform concentration such as a continuously stirred reactor, and was not included in deriving the mass transfer equations. The boundary conditions at the destination layer/enzyme reactor interface will be discussed in more detail in a later section.

Figure 4-2: Perforation Pattern of Hydrophobic Membrane

Figure 4-2a: Placement of Perforations in Hydrophobic Membrane
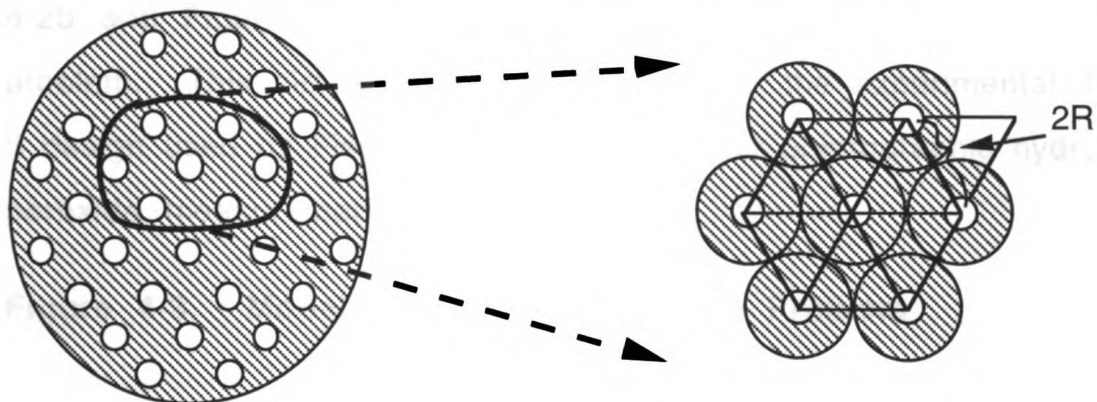
Figure 4-2b: Modeling the problem using Unit Cells
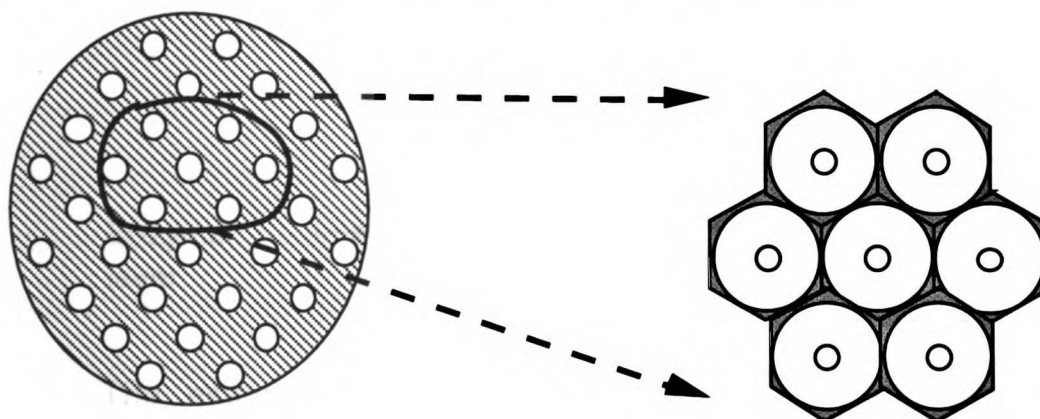
The problem to be solved is to calculate the concentration and flux profiles of each species in the membrane as a function of the external glucose concentration. In order to solve this a number of assumptions are implemented and a simplified model of Figure 4-1 is utilized. Due to the equidistance of the holes and because

diffusion from the bulk solution only occurs in the axial direction, the approximation of radial symmetry can be made. This implies that a "unit cell" can be used to model the entire membrane. Figure 4-2b and Figure 4-3 show the "unit cell" utilized in modeling this problem. This simplified model is similar to the experimental Type II design used by Fischer and Abel (1982) for polarographic hydrogen peroxide measurements.[2,3]

Figure 4-3. Model used to Analyze the Problem
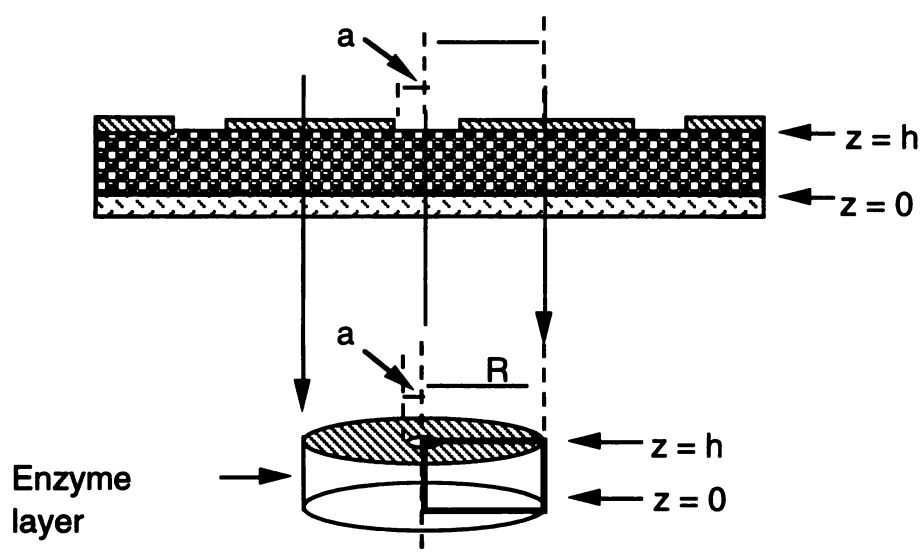
The assumption of a cylindrical "unit cell" surrounding each hole is not altogether correct however, and excludes a small portion of the gel. This can be seen in Figure 4-2b, which shows an expanded version of the top view of Figure 4-1. For complete accuracy, the "unit cell" should be a hexagonal prism with sides of length $\left(\dfrac{R}{\sin 60}\right)$. This however, would be extremely complicated to model and due to the other assumptions involved, we determined that it would be more feasible to model the cylindrical unit cell as shown in Figure

4-3. In making this assumption, we are underestimating the total area for oxygen diffusion by approximately 10%. This unaccounted for area is depicted by the shaded areas of the hexagons in Figure 4-2b, and is given by the ratio:

$$\frac{\text{area hexagon - area circle}}{\text{area hexagon}} = \frac{\frac{3R^2}{\sin 60} - \pi R^2}{\frac{3R^2}{\sin 60}} \approx 0.093.$$

Since we are using the smaller of the two areas, we are using a conservative estimate for the area of oxygen diffusion and we would expect to see slightly higher oxygen concentrations in the membrane experiments as a result.

Due to the angular symmetry involved, the diffusion/reaction equations need to be solved only on a cross-section of the unit cell shown with bold lines in Figure 4-3. Thus the diffusion/reaction equations need to be solved in cylindrical coordinates over a rectangular cross-section of height h, the enzyme layer thickness, and length R, half the distance between the center of the holes. In making these assumptions the complicated three dimensional problem has been reduced to a two-dimensional problem which can be solved using numerical techniques.

The regular techniques for solving diffusion/reaction problems are used to solve this problem.[8-10,12] The general set up of a diffusion/reaction problem is to equate the accumulation of species i with the flux of species i into and out of a particular control volume added to the generation or loss of species i due to reaction

terms. In this case the control volume is the cross-section of the unit cell shown in Figure 4-3. Using the above explanation, the diffusion/reaction continuity equation for species i is given by:

$$\frac{\partial c_i}{\partial t} = - \nabla \cdot J_i + \sum \nu_{ij} \, r_j \qquad (1)$$

The model we are using assumes steady state conditions. This means that there is no net accumulation of species i within the control volume, or $\frac{\partial c_i}{\partial t} = 0$. Therefore, in this model we are balancing the flux and the reaction terms.

Several other assumptions were made in analyzing this problem. The most significant of these is the assumption that the ionic strength of the medium is high enough to screen any electric potential effects. This assumption translates to simplifying the Nernst-Planck equation to Fick's law of diffusion. The Nernst-Planck equation for a flux of species i within a membrane is given by Equation (2), where c_i, D_i, μ_i are the concentration, diffusivity and mobility, respectively, of the species i within the membrane.

$$J_i = - D_i \, \nabla c_i + \mu_i \, z_i \, c_i \, E + c_i \, v_f$$
$$= - D_i \, \nabla c_i - \mu_i \, z_i \, c_i \, F \nabla \Psi + c_i \, v_f \qquad (2)$$

The right hand side of (2) includes contributions from diffusion, electrical migration with ψ as the local electrical potential, and convection with v_f as the mass centered fluid velocity. The assumption of high ionic strength implies that the electrical potential effects become negligible with respect to the diffusion

effects. In addition it is assumed that the convection fluxes are negligible compared with the diffusion flux. These assumptions allow equation (2) to be simplified to Fick's law of diffusion given by equation (3) for each species i,

$$J_i = -D_i \nabla c_i \qquad (3).$$

Several authors have also made this assumption (Albin , Gough, Varanassi, Grodzinsky).[1,4-6,11-14] In addition it has been experimentally shown that the migration and convection fluxes are minimal compared to the diffusional fluxes.[11-14]

Another approximation used in the development of this analysis is that there is no selective partitioning of the species in the membrane. This implicitly implies that there are no charges on the membrane so that no Donnan effects are present. This assumption may not be completely valid since the enzyme glucose oxidase is very anionic and carries a charge of -80 at physiologic pH.[15,16] Other authors have been able to use this assumption with qualitative success, however.[1,4-6] It should be noted that this assumption will be valid in a situation of high ionic strength and low enzyme loading. [The mathematical model can allow for different amounts of partitioning within the membrane by assuming different equilibrium partition coefficients, α_i, for each species i, but as of yet the coefficients are all considered to be equal to one.]

It is also assumed that the diffusivity of each species is independent of concentration and the best estimate of the

intramembrane diffusion coefficients are used when possible. This is discussed in more detail in the section on parameter estimation.

4.3 Reaction Term Modeling

The reactions catalyzed by the enzymes glucose oxidase, catalase in excess, and gluconolactonase, respectively, are shown below,

$$\text{glucose} + O_2 \xrightarrow{\text{GluOx}} \text{glucono-}\delta\text{-lactone} + H_2O_2 \qquad (4a)$$

$$H_2O_2 \xrightarrow{\text{Cat}} H_2O + 1/2\ O_2 \qquad (4b)$$

$$\text{glucono-}\delta\text{-lactone} + H_2O \xrightarrow{\text{Gluconolactonase}} \text{gluconate} + H^+ \qquad (4c).$$
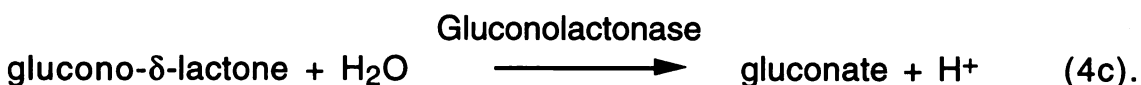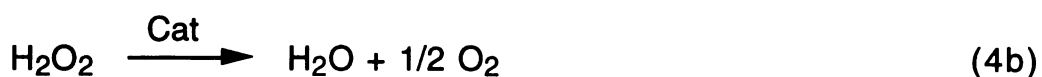
Summing 4a-c the net reaction becomes:

$$\textbf{glucose} + \textbf{1/2}\ O_2 \longrightarrow \textbf{gluconate} + H^+ \qquad (4d).$$

This reaction has been modeled by a two substrate Michaelis-Menten model, known as the ping-pong mechanism. The model was originally developed by Nakamura and Ogura in 1967 and since then has been used by numerous authors (Weibel and Bright, Horbett et al., Klumb, Gough).[1,4-6,17-19] This three parameter model given below, was shown to fit the overall reaction kinetics to within 1% for a given pH.

$$\frac{E_t}{v} = \frac{1}{k_{red}c_g} + \frac{1}{k_{ox}c_o} + \frac{1}{k_{cat}}$$

(5)

where c_g = glucose concentration in moles/liter (M)

c_o = oxygen concentration in moles/liter (M)

E_t = total enzyme concentration in moles/liter (M)

v = rate of reaction in moles/liters-seconds (M/sec).

This equation can be rewritten to express explicitly the rate of reaction, v, as a function of the glucose and oxygen concentrations. In writing equation (6) shown below, K_g and K_o are Michaelis-Menten constants for glucose and oxygen, respectively, k_{cat} represents the irreversible decomposition of the enzyme-substrate complex and E_t is the total enzyme concentration.

$$v = \frac{k_{cat} E_t}{1 + k_{cat}/(k_{red} c_g) + k_{cat}/(k_{ox} c_o)}$$

$$= \frac{k_{cat} E_t}{1 + K_g/c_g + K_o/c_o}$$

$$= \frac{V^*}{1 + K_g/c_g + K_o/c_o}$$

(6)

The above equation was used to model the glucose oxidase reaction. The performance of glucose oxidase is dependent on pH and has an optimum performance at pH 5.5. More discussion of this will

be given in Chapter 7 where the values of the parameters used in the simulations are determined.

4.4 Derivation of Mass Transfer Equations

The model uses conservation of mass and Fick's second law to describe the diffusion and reaction in the glucose sensitive membrane. As was discussed in the assumptions section, equation (3) is valid for the six species involved in the problem. Using the conservation of mass principle given by equation (1) with the steady state assumption, and applying Fick's second law to equation (3), the species conservation equations become:

$$\nabla \bullet (-D_i \, \nabla c_i) = \sum_j v_{i,j} \, r_j \qquad (7)$$

In equation (7) the index j represents a particular reaction, r_j is the rate of the j'th reaction, and $v_{i,j}$ is the stoichiometric coefficient of the i'th species in the j'th reaction. The diffusion coefficient and concentration of species i are denoted by D_i, and c_i, respectively. The divergence operator, $\nabla \bullet$, and the gradient operator, ∇, are represented in cylindrical coordinates.

The six species involved in the glucose sensor are glucose (denoted by subscript "g"), oxygen (o), hydronium ion (h), unprotonated buffer (b), protonated buffer (bh) and gluconate (a). Two reactions were considered in this model: one is the glucose

oxidase/catalase reaction denoted by reaction rate v given by equation (6); and the acid/base reaction with the buffer whose reaction rate is denoted by r_b. For completeness both reactions are initially included. Below all the species conservation terms are written out:

$$\nabla \bullet (-D_g \nabla c_g) = -v \qquad (7a)$$

$$\nabla \bullet (-D_o \nabla c_o) = -\frac{1}{2} v \qquad (7b)$$

$$\nabla \bullet (-D_h \nabla c_h) = v + r_b \qquad (7c)$$

$$\nabla \bullet (-D_{b\text{-}} \nabla c_{b\text{-}}) = r_b \qquad (7d)$$

$$\nabla \bullet (-D_{bh} \nabla c_{bh}) = -r_b \qquad (7e)$$

$$\nabla \bullet (-D_a \nabla c_a) = v \qquad (7f)$$

In equations (7a-f),

$$\nabla \bullet (-D_i \nabla c_i) = \frac{1}{r}\frac{\partial}{\partial r}\left(r\left(-D_i\frac{\partial c_i}{\partial r}\right)\right) + \frac{\partial}{\partial z}\left(-D_i\frac{\partial c_i}{\partial z}\right) .$$

These six equations can be simplified by assuming that (i) the diffusivity of the unprotonated buffer is equal to the diffusivity of the protonated buffer, and (ii) that the system is "closed" within the device. The second assumption implies that there is no generation of buffer species within the enzyme membrane or the destination layer. Then adding equations (7d) and (7e) and using the above assumptions, it can be shown that inside the device:

$$D_b \nabla^2 c_{tb} = 0 \qquad \text{where} \qquad c_{tb} = c_{bh} + c_{b-}. \qquad (7d)+(7e)$$

This eliminates one of the six equations above. If in addition it is assumed that the buffer is in acid/base equilibrium at all locations in the membrane, then equations (7d) and (7e) can be replaced by equation (8) shown below.

$$c_{bh} = \frac{c_{tb} c_h}{K_b + c_h} \; ; \quad K_b = \frac{c_{b-} c_h}{c_{bh}} \qquad (8)$$

where K_b is the equilibrium constant for the buffer.

Adding equations (7e) and (7c), equation (9) is obtained:

$$\nabla \bullet (-D_h \nabla c_h) + \nabla \bullet (-D_b \nabla c_{bh}) = v \qquad (9)$$

Equations (7a), (7b), (8) and (9) completely describe the problem at hand. (Equation (7f) does not need to be solved explicitly because once the other five concentrations and fluxes are known the gluconate concentration can be determined.)

Since c_{tb} and K_b are constants, and c_{bh} depends only on c_h, this problem can be simplified further. Substituting equation (8) into equation (9) and taking the derivative of the protonated buffer concentration using the chain rule, equation (10) is obtained.

$$\nabla c_{bh} = \frac{\partial c_{bh}}{\partial c_h} \nabla c_h = \frac{c_{tb} K_b}{(K_b + c_h)^2} \nabla c_h \qquad (10)$$

Substituting equation (10) into (9) and collecting like terms, the final equations (11) and (12) are obtained to solve for the hydrogen ion concentration.

$$\nabla \bullet (-D_{app,h} \nabla c_h) = v \tag{11}$$

where;

$$D_{app,h} = D_h + D_b \frac{c_{tb} K_b}{(K_b + c_h)^2} \tag{12}$$

Equations (7a), (7b) and (11) now represent the diffusion/reaction equations which need to be solved. Equations (6) and (12) are used implicitly in solving for the concentrations c_g, c_o and c_h. This set of equations represents a highly nonlinear problem and an iterative numerical procedure is used to solve this problem with the geometry given in figure 4-2. These equations are listed together below.

<u>Diffusion/Reaction Equations</u>

$$\nabla \bullet (-D_g \nabla c_g) = -v \tag{7a}$$

$$\nabla \bullet (-D_o \nabla c_o) = -\frac{1}{2} v \tag{7b}$$

$$\nabla \bullet (-D_{app,h} \nabla c_h) = v \tag{11}$$

where,

$$\nabla \bullet (-D_i \nabla c_i) = \frac{1}{r} \frac{\partial}{\partial r} (r(-D_i \frac{\partial c_i}{\partial r})) + \frac{\partial}{\partial z} (-D_i \frac{\partial c_i}{\partial z})$$

and,

$$v = \frac{k_{cat}\,E_t}{1 + \dfrac{K_g}{c_g} + \dfrac{K_o}{c_o}} \qquad (6)$$

$$D_{app,h} = D_h + D_b \frac{c_{tb}\,K_b}{(K_b + c_h)^2} \qquad (12)$$

It should be noted that Albin and Horbett[4] have used a slightly different method to solve for the hydrogen ion concentration. This involves solving equations (7a,b) for the reaction rate using equation (5), and then solving for gluconic acid using equation (7f). The pH was solved once the gluconic acid concentration had been determined. This method was not used in this analysis.

4.5 Boundary Conditions

Thus far we have written down the necessary transport field equations for the problem at hand. However, the complete mathematical description requires that boundary conditions also be specified. Figure 4-4 summarizes the boundary conditions placed over the rectangular area. No flux boundary conditions are assigned to side 1 and side 3, as shown in equations (13) and (14).

$$\text{Side 1:} \quad r = 0 \; ; \; 0 \leq z \leq h : \qquad \frac{\partial c_i}{\partial r} = 0 \qquad i = g, o, H^+ \qquad (13)$$

$$\text{Side 3:} \quad r = R \; ; \; 0 \leq z \leq h : \qquad \frac{\partial c_i}{\partial r} = 0 \qquad i = g, o, H^+ \qquad (14)$$

At $r = 0$, the center of the unit cell, all the concentrations must be finite and the fluxes must therefore equal zero. At $r = R$ at the outer edge of the unit cell, it is assumed that the fluxes are zero because of symmetry. It is assumed that beyond the boundary at any point where $r = R$, there is another cell which is a mirror image of the cell being considered. This may not be completely valid since in the actual design the "unit" cell is a hexagonal prism not a cylinder. Given all the other assumptions made however this will probably only contribute a minor error in the calculations. It should be noted that this has been tested by varying R and determining if the fluxes are zero along this edge.

The boundary conditions along side 2 are given by matching the mass transfer rate from the bulk solution to the gel to the diffusion rate within the gel for a given species. In applying these boundary conditions we assume no forced convection is occuring into the device and only free convection from the bulk solution to the device is occuring. This assumption is valid for Reynold numbers below 20,000, where it is assumed that the flow into the device is very slow. If the device is placed in a region of no blood flow, this assumption is valid.

The mass transfer coefficient for species i into the enzyme membrane are given by the symbol k_i. These mass transfer parameters from the bulk solution to the device have been estimated by Gough et. al. using a membrane-covered, rotated disc electrode system simulating passive diffusion from the bulk solution to a membrane (Reynold numbers less than 5000).[20-22] The determination of these parameters will be discussed in more detail in Chapter 7.

Since there is a hydrophobic membrane which excludes the transfer of some species, the boundary conditions for side 2 are not straightforward and must be broken up into two sections; the area of the hydrophobic membrane and the area of no membrane. Along the region of no membrane (the hole), mass transfer of all species is allowed, and the boundary conditions are given by equation (15a) for glucose and oxygen.

Side 2: z = h; 0 ≤ r ≤ a

$$D_i \frac{\partial c_i}{\partial z} = k_i \left(c_{iB} - \frac{c_i}{\alpha_i} \right)$$

$$i = g, o \qquad (15a)$$

The boundary condition for hydrogen is slightly more complicated due to the fact that we need to take into account the flux of the free hydrogen ions as well as the flux of the hydrogen ions bound to buffer. Thus the boundary condition along the hole for hydrogen becomes:

Side 2: z = h; 0 ≤ r ≤ a

$$D_{app,h} \frac{\partial c_h}{\partial z} = D_h \frac{\partial c_h}{\partial z} + D_b \frac{\partial c_{bh}}{\partial z}$$

$$= k_h \left(c_{hB} - \frac{c_h}{\alpha_h} \right) + k_b \left(c_{bhB} - \frac{c_{bh}}{\alpha_b} \right) \qquad (15b\text{-}1)$$

This equation can be simplified and written only in terms of the hydrogen concentration by substituting equation (8) in for c_{bh} and c_{bhB} .

Side 2: z = h; 0 ≤ r ≤ a

$$D_{app,h} \frac{\partial c_h}{\partial z} = \left[k_h + \frac{k_b c_{tb}}{K_b + c_{hB}} \right] c_{hB} - \left[k_h + \frac{k_b c_{tb}}{K_b + c_h} \frac{\alpha_h}{\alpha_b} \right] \frac{c_h}{\alpha_h}$$

$$= k_{h1} c_{hB} - k_{h2}(c_h) \frac{c_h}{\alpha_h} \qquad (15b\text{-}2)$$

The first term in this equation is a constant, whereas the second term is a nonlinear function of the hydrogen concentration. Equation (15b-2) is in a similar form as (15a) with unequal mass transfer coefficients used for the bulk and the actual concentrations.

Along the area of the membrane, due to the characteristics of the membrane, only mass transfer of oxygen is permitted and the boundary conditions are given by equations (16a,b).

Side 2: z = h; a ≤ r ≤ R

$$D_o \frac{\partial c_o}{\partial z} = k_o \left(c_{oB} - \frac{c_o}{\alpha_o} \right)$$

(16a)

$$\frac{\partial c_i}{\partial z} = 0; \quad i = g, H^+$$

(16b)

In equations (15) and (16), k_i is the mass transfer coefficient for species i, c_{iB} is the bulk concentration of species i and α_i is the partition coefficient of species i in the enzyme membrane. (For the computations involved, all the partition coefficients, α_i, were set to one.) Equation (16b) represents the no flux condition for glucose and hydrogen along the area of the hydrophobic membrane, whereas equation (16a) represents the mass transfer of oxygen all along the membrane. [It should be noted that if the membrane were to allow passage of buffer as well as oxygen, then the boundary condition given by (16b) is incorrect for hydrogen. To correct it, one needs to set $k_h = 0$ and $k_b \neq 0$ in equation (15b).]

The boundary conditions for the destination layer, side 4, are more complicated than for the other sides. This boundary condition is essentially unknown for this particular problem because the destination layer is an unknown polymer system of unknown size. The goal of this project was to determine the pH at the destination layer boundary for a given sensor design, without regard for the polymer system. In order to do this the polymer system was not considered in this analysis. However this still made it difficult in determining the exact nature of the boundary conditions to use at this interface.

Boundary conditions can be of two forms: setting the concentration, or setting the flux conditions. At the edge of the destination layer, the realistic boundary condition is to set the flux conditions; that is the fluxes from the enzyme gel to the destination layer should be set equal to the fluxes in the destination layer at this boundary. Implementing this boundary condition would imply solving the transport equations within the destination area. This in itself is not difficult, for a known system.

The exact polymer system, however is unknown. At the time of this analysis, liquid polymer systems which buffered the system at pH 7.2 were being studied. Other liquid polymer systems studied exhibited buffer-like behavior and their acid/amino group interactions followed a titration curve.[23] The gel polymer systems studied exhibit highly complex behavior and cannot be described easily by a simple acid/base equilibrium. Due to these conditions, several different boundary conditions were tried. First we briefly

discuss the various boundary conditions which were tried for glucose and oxygen, followed by the hydrogen boundary conditions.

No flux conditions were initially tried for glucose and oxygen. This condition corresponds to having the destination layer be a barrier which allows no transport of any species accross it. In reality this is not the case for any of the species. Both glucose and oxygen will diffuse into and out of the destination layer, but no reaction will be occuring in this region. This would imply that using a boundary condition of constant concentrations would be more accurate. The problem in this condition is what value to use for both glucose and oxygen.

Sink conditions, where either the glucose and oxygen concentrations are set to zero, are unrealistic for this problem. The goal of this design is to enhance the oxygen concentration at the destination layer so it is undesireable to have zero oxygen concentrations in this region. There is ample glucose in the system so that having zero glucose concentrations at the enzyme/polymer interface is also unrealistic. The exact boundary conditions used are discussed below.

It is desirable to allow hydrogen to flow into this region so the initial boundary condition corresponded to setting the pH. The value that the pH was set at was determined by the buffering power of a liquid polymer system that was under investigation in our lab at the time. Initially this value was pH = 7.2, and the fluxes into and out of the destination layer were looked at. Other polymer systems

however either buffered the layer at a different pH or had much more complex titration behavior, so this value was not used in all the analysis. Instead the condition shown below was used once the glucose and oxygen profiles had been determined.

At steady state we might normally expect the destination layer to be an area of uniform concentration with no flux into or out of this area. However, applying a boundary condition of no flux generally leads to a nonuniform concentration distribution along the bottom edge. Since it is not very realistic to have a nonuniform concentration distribution along the bottom edge, we applied a constant concentration boundary condition along side 4 for each of the species. The final boundary condition concentrations were determined as the concentration at which the integrated flux along the destination layer was zero. Equation (17) show the boundary condition for the destination layer.

Side 4: $z = 0$; $0 \leq r \leq R$

$c_i = c_{ibottom}$ such that

$$\int_{\substack{r=0 \\ bottom}}^{r=R} D_i \frac{\partial c_i}{\partial z} r \partial r = 0 \qquad i = g, o, H^+ \qquad (17)$$

for H^+: $D_i \Rightarrow D_{app,h}$

It is noted that for hydrogen, the diffusion coefficient in (17) is the apparent diffusivity which includes the contribution of the protonated buffer. The exact procedure used in applying this boundary condition is discussed in Chapter 5.

In the boundary conditions given by equations (13)-(17), the selective partitioning is included for completeness of the formulation. Selective partitioning of species into the enzyme membrane is represented by the partition coefficient for each species. The equilibrium partition coefficient is given by $\alpha_i = c_i/c_{iB}$, where the subscript iB refers to the concentration of species i in the bulk solution, and the subscript i refers to the concentration of species i in the membrane. These two concentrations are assumed to be in equilibrium.

Figure 4-4 : Summary of boundary conditions
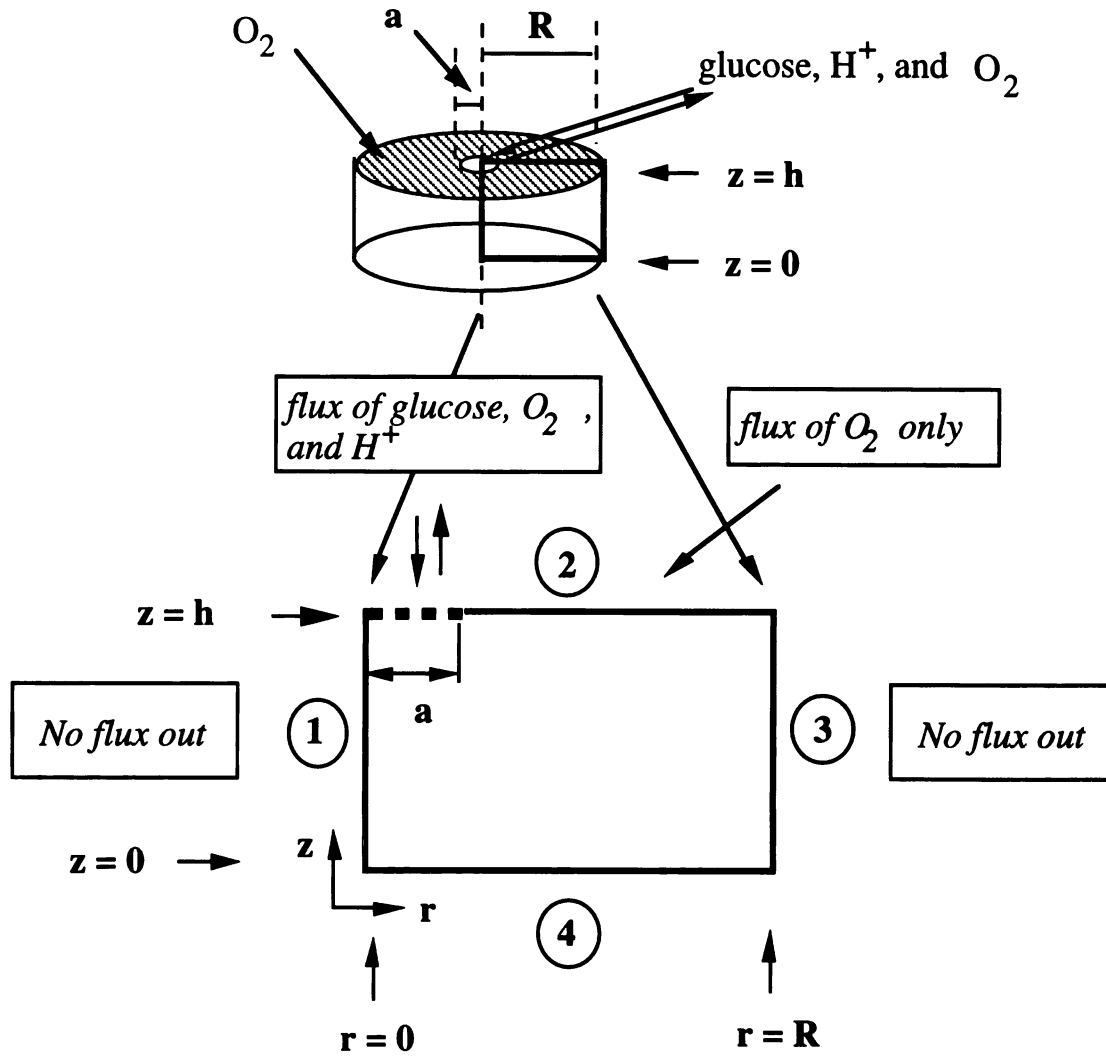
4.6 Nondimensionalization of Equations

The transport/reaction equations and boundary conditions were nondimensionalized to facilitate solving this problem and to generalize the method of solution. The nondimensional quantities used are given in Table 4-1.

Table 4-1: Nondimensional Quantities

Distances	Concentrations	Glucose Oxidase Reaction constants
$\rho = \dfrac{r}{R}$	$\overline{c_0} = \dfrac{c_0}{\alpha_0\, c_{oB}}$	$\kappa_0 = \dfrac{K_0}{\alpha_0\, c_{oB}}$
$\zeta = \dfrac{z}{h}$	$\overline{c_i} = \dfrac{D_i\, c_i}{\alpha_0\, D_0\, c_{oB}}$, $i = g,\ H^+,\ tb,\ a$	$\kappa_g = \dfrac{D_g\, K_g}{\alpha_0\, D_0\, c_{oB}}$
$\varepsilon = \dfrac{R}{h}$		$\phi^2 = \dfrac{R^2\, V^*}{\alpha_0\, D_0\, c_{oB}}$, Thiele modulus; $V^* = k_{cat}\, E_t$

In addition, the nondimensional buffer equilibrium constant is given by $\kappa_H = \dfrac{D_H K_b}{\alpha_o D_o c_{oB}}$.

In the above equations, c_{oB} is the concentration of oxygen in the bulk solution. We chose to nondimensionalize the concentrations and the reaction constants by the quantity $\alpha_o D_o c_{oB}$ because oxygen is the limiting concentration. In the body the oxygen level varies from 0.01 mM in venous blood to 0.15 mM in arterial blood, whereas glucose levels vary from 3 - 8 mM. In addition, the maximum saturation level of oxygen in water at atmospheric pressure is only 0.274 mM. It was desired that the nondimensional oxygen concentration vary from 0 to 1, thus letting the nondimensional glucose concentrations be greater than 1. By nondimensionalizing by the product of the bulk oxygen concentration, the diffusivity of oxygen in the membrane and the partition coefficient within the membrane, the diffusion and partition coefficients are taken care of, and the problem focuses on the oxygen concentrations.

Substituting the nondimensional reaction constants from Table 4-1 into equation (6), the nondimensional enzyme reaction rate becomes:

$$\overline{V} = v\left[\frac{R^2}{\alpha_o D_o c_{oB}}\right] = \frac{\phi^2}{1 + \kappa_g/(c_g) + \kappa_o/(c_o)} \qquad (18)$$

Substituting the nondimensional concentrations and dimensions, and the nondimensional reaction rate into equations

(7a), (7b), (11) and (12), the final nondimensional equations are obtained and are shown below in equations (19a-c) and (20).

$$\frac{1}{\rho^m} \frac{\partial}{\partial \rho} \left\{ \rho^m \frac{\partial \overline{c_g}}{\partial \rho} \right\} + \varepsilon^2 \frac{\partial^2 \overline{c_g}}{\partial \zeta^2} - \overline{V} \ (\ \overline{c_g} , \overline{c_o} \ ) = 0 \qquad (19a)$$

$$\frac{1}{\rho^m} \frac{\partial}{\partial \rho} \left\{ \rho^m \frac{\partial \overline{c_o}}{\partial \rho} \right\} + \varepsilon^2 \frac{\partial^2 \overline{c_o}}{\partial \zeta^2} - \frac{1}{2} \overline{V} \ (\ \overline{c_g} , \overline{c_o} \ ) = 0 \qquad (19b)$$

$$\frac{1}{\rho^m} \frac{\partial}{\partial \rho} \left\{ \rho^m \ D_{app} \ \frac{\partial \overline{c_h}}{\partial \rho} \right\} + \varepsilon^2 \frac{\partial}{\partial \zeta} \left\{ D_{app} \ (\frac{\partial \overline{c_h}}{\partial \zeta}) \right\} + \overline{V} \ (\ \overline{c_g} , \overline{c_o} \ ) = 0 \qquad (19c)$$

where:

$$D_{app} = \frac{(D_{app,h})}{D_H} = 1 + \frac{(\frac{\overline{c_{tb}}}{\kappa_H})}{(1 + \frac{\overline{c_h}}{\kappa_H})^2} \qquad (20).$$

The "m" in equations (19a-c) gives the user the flexibility to use planar (m=0) or cylindrical (m=1) coordinates. The problem was formulated in this fashion to allow the user to change geometries if necessary. In addition, equation (18) is used for the reaction rate in equations (19).

It was noted earlier that the glucose oxidase reaction is dependent on pH. Equation (18) can be altered to incorporate the pH dependence, however this reaction rate was initially used in order to start with a slightly simpler problem. It was later determined that the pH change within the membrane is small enough to warrant the use of (18) rather than a more complicated form, which incorporates the hydronium ion concentration.

Equations (18), (19a-c) and (20) represent the nondimensional equations which solve the diffusion/reaction problem posed here for glucose, oxygen and hydrogen. The boundary conditions must also be nondimensionalized. The nondimensional forms of equations (13)-(17) are given in Table 4-2, equations (21) - (25).

In Table 4-2, equations (22) and (23) are the nondimensional mass transfer boundary conditions. The quantities, Bi_i and Bi_o are the Biot numbers for species i (either glucose, hydrogen or buffer) and oxygen respectively. These quantities represent ratios of the external mass transfer rate to the internal rate of diffusion and are given by $Bi_i = \dfrac{k_i \, h}{D_i \, \alpha_i}$. The effective substrate concentration ratio within the gel for species i is $\overline{c_i^*}$ and is given by $\overline{c_i^*} = \dfrac{\alpha_i \, D_i \, c_{iB}}{\alpha_o \, D_o \, c_{oB}}$. The quantity $\overline{c_i^*}$ relates the rates of diffusion of species i within the membrane to that of the limiting species oxygen.

Table 4-2: Nondimensional Boundary conditions

Side	ρ	ζ	Boundary Condition
1	$\rho = 0$	$0 \leq \zeta \leq 1$	$\dfrac{\partial \overline{c_i}}{\partial \rho} = 0 \quad i = g, o, H^+ \qquad (13) \Rightarrow (21)$
2 - in area of no membrane	$0 \leq \rho \leq \dfrac{a}{R}$	$\zeta = 1$	$\dfrac{\partial \overline{c_i}}{\partial \zeta} = Bi_i(\overline{c_i^*} - \overline{c_i}); i = g, b$ $\dfrac{\partial \overline{c_o}}{\partial \zeta} = Bi_o(1 - \overline{c_o}) \quad (15a) \Rightarrow (22a)$ Please see text for $(15b) \Rightarrow (22b)$
2 - in area of membrane	$\dfrac{a}{R} < \rho \leq 1$	$\zeta = 1$	$\dfrac{\partial \overline{c_i}}{\partial \zeta} = 0 \quad i = g, H^+, b$ $\qquad\qquad\qquad (16b) \Rightarrow (23b)$ $\dfrac{\partial \overline{c_o}}{\partial \zeta} = Bi_o(1 - \overline{c_o})$ $\qquad\qquad\qquad (16a) \Rightarrow (23a)$
3	$\rho = 0$	$0 \leq \zeta \leq 1$	$\dfrac{\partial \overline{c_i}}{\partial \rho} = 0 \quad i = g, o, H^+ \qquad (14) \Rightarrow (24)$

4	$0 \leq \rho \leq 1$	$\zeta = 0$	$c_i = c_{i\text{bottom}}$; s.t. $\displaystyle\int_{\rho=0}^{1} \overline{\frac{\partial c_i}{\partial \zeta}} \rho^m \partial\rho = 0$ $i = g, o$; and $c_h = c_{h\text{bottom}}$; s.t. $\displaystyle\int_{\rho=0}^{1} D_{app} \overline{\frac{\partial c_h}{\partial \zeta}} \rho^m \partial\rho = 0$ $(17) \Rightarrow (25)$

The hydrogen boundary conditions for sides 2 and 4 are slightly different than those of the other species. The apparent diffusivity is included in the hydrogen flux terms because we desired to take into account the total flux of hydrogen into and out of the enzyme membrane. By including the nondimensional apparent diffusivity, the flux calculated includes free hydrogen ions and those bound to buffer. Equation (15b) is slightly more complicated to nondimensionalize. The nondimensional form is given below:

$$D_{app} \frac{\partial \overline{c_h}}{\partial \zeta} = \left[Bi_h + Bi_b \frac{\alpha_b \overline{c_{tb}}}{\alpha_h \kappa_h + \overline{c_h^*}} \right] \overline{c_h^*}$$

$$- \left[Bi_h + Bi_b \frac{\overline{c_{tb}}}{\kappa_h + \overline{c_h}} \right] \overline{c_h}$$

$$= Bi_{h^*}^{eff} \overline{c_h^*} - Bi_h^{eff}(\overline{c_h}) \overline{c_h} \qquad (22b)$$

In (22b), $Bi_{h^*}^{eff}$ and $Bi_h^{eff}(\overline{c_h})$ are effective Biot numbers for the total hydrogen ion concentration and are functions of the nondimensional free hydrogen concentration, $\overline{c_h}$ or the effective hydrogen concentration in the membrane, $\overline{c_h^*}$.

References

1. Gough DA, Lucisano JY, Tse PHS. Two-dimensional enzyme electrode sensor for glucose. *Anal Chem* ; **57**: (1985) 2351-7

2. Fischer U, Abel P, Muller A, Freyse EJ. *J Eur Soc Artif Organs*; **1**: (1983) 45-8

3. Abel P, Muller A, Fischer U. Experience with an implantable glucose sensor as a prerequisite of an artificial beta cell. *Biomed Biochem Acta* ; **43**: (1984) 577-84

4. Albin G, Horbett TA, Miller SR and Ricker NL, Theoretical and experimental studies of glucose sensitive membranes, *J. Controlled Release* , **6**: (1987) 267-91

5. Klumb LA and Horbett TA, Design of insulin delivery devices based on glucose sensitvie memebranes, *J. Controlled Release*, **18**: (1992) 59-80

6. Klumb LA and Horbett TA, The effect of hydronium ion transport on the transient behavior of glucose sensitive membranes, *J. of Controlled Release*, **27**: (1993) 95-114

7. Wilson, R. and Turner, APF. Glucose oxidase: an ideal enzyme. *Biosensors & Bioelectronics*, **7**: (1992) 165-185

8. Crank, J. Mathematics of Diffusion. Clarendon Press: Oxford. (1975)

9. Cussler, E. L. Diffusion, Mass Transfer in Fluid Systems. Cambridge University Press: New York. (1984)

10. Aris, R. The Mathematical Theory of Diffusion and Reaction in Permeable Catalysts. Clarendon Press: Oxford (1975)

11. Ruckenstein, E. and Varanasi, S. Transient Behaviour of Facilitated Transport Through Liquid Membranes, *J. Membr. Sci.*, **12**; (1982), 27-50

12. Varanasi, S., Stevens, R. L., and Ruckenstein, E. Design of Enzyme-pH Electrodes. *AIChE Journal*, Vol. **33**, No. 4; (1987), 558-572

13. Nussbaum, J. H. and Grodzinsky, A.J. Proton Diffusion Reaction in a Protein Polyelectrolyte Membrane and the Kinetics of Electromechanical Forces. *J. Membr. Sci.*, **8**; (1981), 193-219

14. Grimshaw, P.E., Nussbaum, J. H., and Grodzinsky, A. J. Kinetics of electrically and chemically induced swelling in polyelectrolyte gels. *J. Chem. Phys.*, **93**(6), (1990) 4462-4472

15. Voet, J.G., Coe, J., Epstein, J., Matossian,V. and Shipley, T. Electrostatic Control of Enzyme Reactions: Effect of Ionic Strength on the pKa of an Essential Acidic Group on Glucose Oxidase *Biochemistry* , **20**, (1981) 7182-7185

16. Voet, J. G., and Andersen, E.C. Electrostatic control of enzyme reactions: mechanism of inhibition of glucose oxidase by putrescine. *Arch. Biochem. Biophys.* **233**; (1984) 88-92

17. Nakamura, S. and Ogura Y. Action Mechanism of Glucose Oxidase of *Aspergillus niger. J. of Biochemistry*, **63**(3); (1968) 308-316

18. Weibel, M. K. and Bright, H.J., The glucose oxidase mechanism: interpretation of the pH dependence. *J. Biol. Chem.*, **246**: (1971) 2734-2744

19. Gibson, Q.H., Swoboda,B.E. P., and Massey, V. Kinetics and mechanism of action of glucose oxidase. *J. Biol. Chem.*, **239**: (1964) 3927-3934

20. Gough, D.A. and Leypoldt, J. K. Membrane-Covered, Rotated Disc Electrode. *Anal. Chem.*, **51**(3); (1979) 439-444

21. Gough, D.A. and Leypoldt, J. K. Rotated, Membrane-Covered Oxygen Electrode. *Anal. Chem.*, **52**; (1980) 1126-1130

22. Gough, D.A. and Leypoldt, J. K. A Novel Rotated Disc Electrode and Time Lag Method for Characterizing Mass Transport in Liquid-Membrane Systems. *AIChE Journal*, **26**(6); (1980) 1013-1019

23. Cornejo, J., Ph. D. Dissertation, University of California, San Francisco, 1992

24. Bird RB, Stewart WE and Lightfoot EN, Transport Phenomena, John Wiley and Sons, New York, 1960.

25. Al Baldawi NF and Abercrombie RF, Cytoplasmic hydrogen ion diffusion coefficient, *J. Biophysical Society*, **61**,(1992) 1470-1479

Appendix 4-1.

List of Variables

R   Radius between preforations in the hydrophobic membrane; radius of a unit cell. (cm)

a   Radius of a preforation in the hyrdophobic membrane (cm)

h   Thickness of sensor (cm)

r   radial coordinate in unit cell

z   axial coordinate in unit cell

J_i flux of species i $(\frac{mmole}{cm^2\text{-}sec})$

D_i diffusion coefficient of species i within the enzyme membrane $(\frac{cm^2}{sec})$

c_i concentration of species i $(\frac{mole}{liter} = M = \frac{mmole}{cm^3})$

μ_i mobility of species i $(\frac{cm^2\ mole}{Joules\ sec})$

z_i charge on species i

E   electric field $(\frac{volt}{cm})$

$E = - F \nabla \Psi$

F : farraday's constant, 96,500 $\frac{coulomb}{mole}$

Ψ: local electric potential (volt)

[Note: 1 coulomb-volt = 1 Joule]

v_f mass centered fluid velocity $(\frac{cm}{sec})$

k_i mass transfer coefficient $(\frac{cm}{sec})$

α_i partition coefficient

Reaction Variables

r_i rate of i'th reaction $(\frac{M}{sec})$

$v_{j,i}$ stoichiometric coefficient of the j'th species in the i'th reaction

r_b acid/base reaction with buffer $(\frac{M}{sec})$

v rate of glucose oxidase reaction $(\frac{M}{sec})$

k_{red} rate constant for reduction of glucose oxidase by glucose $(\frac{sec}{M})$

k_{ox} rate constant for oxidation of glucose oxidase by oxygen $(\frac{sec}{M})$

k_{cat} rate constant for irreversible decomposition of enzyme-substrate complex (sec)

K_g Michaelis-Menton constant for glucose in the glucose oxidase reaction (M) $[= \frac{k_{cat}}{k_{red}}]$.

K_o Michaelis-Menton constant for oxygen in the glucose oxidase reaction (M) $[= \frac{k_{cat}}{k_{ox}}]$.

E_t total enzyme concentration in moles/liter (M; mmole/cm^3)

V^* maximum rate of glucose oxidase reaction $(\frac{M}{sec})$ [= $k_{cat}\ E_t$]

K_b equilibrium coefficient for acid/base reaction (M)

Subscripts

g   glucose

o   oxygen

h   hydrogen

b   buffer, assumed to be bicarbonate

a   gluconate

bh   protonated buffer

tb   total buffer

iB   bulk concentration of species i

i   species i

Nondimensional Variables

ρ nondimensional radial coordinate [= $\frac{r}{R}$]

ζ nondimensional axial coordinate [= $\frac{z}{h}$]

ε aspect ratio [= $\frac{R}{h}$]

$\overline{c_i}$ nondimensional concentrations $[= \dfrac{D_i\, c_i}{\alpha_o\, D_o\, c_{oB}}$, $i = g, o, H^+, tb, a$]; over bar carried only in Chapter 4, dropped for simplicity in Chapter 5.

κ_o nondimensional Michaelis Menton constant for oxygen in the glucose oxidase reaction $[= \dfrac{K_o}{\alpha_o\, c_{oB}}]$

κ_g nondimensional Michealis Menton constant for glucose in the glucose oxidase reaction $[= \dfrac{D_g\, K_g}{\alpha_o\, D_o\, c_{oB}}]$

ϕ^2 Thiele modulus $[= \dfrac{R^2\, V^*}{\alpha_o\, D_o\, c_{oB}}]$

κ_H the nondimensional buffer equilibrium constant $[= \dfrac{D_H\, K_b}{\alpha_o\, D_o\, c_{oB}}]$

$\overline{V}$ nondimensional reaction rate $[= v \left[\dfrac{R^2}{\alpha_o\, D_o\, c_{oB}}\right]]$

D_{app} nondimensional diffusion coefficient for hydrodium ion $[= \dfrac{(D_{app,h})}{D_H}]$

Bi_i Biot number, ratio of mass transfer rate to diffusion rate $[= \dfrac{k_i\, h}{D_i\, \alpha_i}]$

$\overline{c_i^*}$ effective substrate concentration ratio within the gel $[= \dfrac{\alpha_i\, D_i\, c_{iB}}{\alpha_o\, D_o\, c_{oB}}]$

Mathematical Symbols

$$\nabla = \left(\frac{\partial}{\partial \rho} , \frac{\partial}{\partial \zeta} \right)$$ gradient operator

$\nabla \bullet a$ divergence operator

$$= \left(\frac{1}{\rho^m} \frac{\partial}{\partial \rho} (\rho^m\ a)\ n_\rho + \frac{\partial a}{\partial \zeta}\ n_\zeta \right),$$

m = 0   rectangular coordinates

m = 1   cylindrical coordinates

Chapter 5.

Method of Solution - Finite Element Modeling

5.1 Introduction

As derived in Chapter 4, equations (19a), (19b) and (19c) represent the nondimensional diffusion/reaction equations which need to be solved along with the nondimensional boundary conditions given in equations (21) - (25) (see Table 4-2). In addition equations (18) and (20) are used implicitly in solving for the nondimensional concentrations c_g, c_o and c_h. (For the rest of this section and the remainder of this chapter, the bar over the concentrations will be dropped and it is understood that the concentrations are nondimensional unless indicated otherwise.) This set of equations represents a highly nonlinear problem and it is necessary to use an iterative numerical procedure to solve it. Several different numerical methods were considered to solve this set of coupled nonlinear partial differential equations.

The finite difference method relies on approximating the derivatives in the equations by difference formulas obtained from the Taylor series. The difference formulas represent differences between values of the solution at discrete mesh points. Although this is the most straightforward method of solving this problem, it was rejected due to the difficulty in incorporating the nonlinear

hydrogen diffusivity, and due to the method's inability to refine mesh sizes easily.

The method of weighted residuals is a general method which can be applied to boundary-value problems. It is a generalization of the variational method in which the solution is chosen to minimize a functional such as an energy integral for the system. In using the method of weighted residuals the first step involves approximating the solution as a combination ($\Sigma c_j \phi_j$) of known polynomial trial functions (ϕ_j) and unknown parameters (c_j). A residual is formed by substituting this approximation into the differential equation. The unknown parameters are determined by setting the integral (over the domain) of the weighted residual of the approximation to zero. For different choices of the weight functions, ψ_i, the method is known by different names. The method of collocation, for example, uses Dirac delta functions as the weight functions, ψ_i [$\psi_i = \delta(x - x_i)$]. In doing this, the solution is required to satisfy the differential equation exactly at the collocation points, x_i, which need to be chosen over the domain. The Galerkin method is another example of the method of weighted residuals where the weighting functions are identical to the known polynomial trial functions, $\psi_i = \phi_i$. In the Galerkin method, the unknown coefficients, c_j are solved for over the whole domain and the solution at any point, (x_j, y_j) is a linear combination of these coefficients, c_j and the trial functions at that point, $\phi_j(x_j, y_j)$.

The method of weighted residuals is usually performed over the entire domain of the problem and the polynomial trial functions

must be chosen to satisfy all the boundary conditions. The difficulty with this comes in choosing the polynomial trial functions, and in choosing the points at which the residual will be evaluated. An improvement on the collocation method is to use orthogonal polynomials as the trial functions. Then the collocation points are taken as the roots to one of the polynomials and the dependent variables are the solution values at the collocation points rather than the coefficients of expansion. This method, known as the method of orthogonal collocation, has been used to solve diffusion/reaction problems.[3,4] The method of orthogonal collocation was used to solve equations (4-7a-f) by Gough et. al.[5-7], and Klumb et.al.[8,9]. Each author used different geometries than the one we are considering and furthermore, all of their models had uniform boundary conditions along each side.

The difficulty with using orthogonal collocation or any of the variational methods in solving the problem posed here arises in applying boundary conditions at the membrane/bulk solution interface, given by equations (4-15) and (4-16). Due to the membrane properties, this boundary condition is non-uniform along that side for two of the three species, glucose and hydrogen. Furthermore, it was desired to be able to vary the hole radius easily. In order to do this easily it was decided to use the method of Galerkin finite elements.

The method of finite elements is simply a piecewise application of the variational methods over elements. In the method of finite elements the domain of the problem is first discretized

into a collection of geometrically simple subdomains, or finite elements. Then over each finite element the weighted-residual method is applied, and continuity of the solution and its derivatives is assumed at the edges of the elements. The type of weighting function that is chosen will dictate the method of solution for the rest of the problem. Orthogonal collocation on finite elements can be used to solve diffusion/reaction problems using Legendre polynomials as the trial functions. [4]

As mentioned before the Galerkin method on finite elements has the advantage over the collocation method in cases of non-uniform boundary conditions. In addition the power of the Galerkin method is that the mesh can be easily refined where needed without having to refine the mesh over the entire domain. This was considered a great advantage for our problem and thus the Galerkin method of finite elements was chosen.

In using the Galerkin method of finite elements, the Galerkin method of weighted residuals is applied to the differential equations to be solved over each element with the weight functions equal to the polynomial trial functions. The differential equations are first put into variational form over a typical element, and the solution is assumed to be a combination ($\Sigma c_j \phi_j$) of the given approximation functions ϕ_j and the nodal solutions c_j. The trial functions, ϕ_j, and the weight functions, $\psi_i = \phi_i$, are polynomials that are derived using interpolation theory, and are called interpolation functions. The assumed solution is then substituted into the variational form of the differential equation. This form of the

equation is rearranged to obtain the element equations $[K^e]\{u^e\} = \{F^e\}$, where "e" represents the element in consideration, and the vector $\{u\}$ represents the unknown nodal values. The element stiffness matrix $[K]$ and the force vector $\{F\}$ depend on the interpolation functions. The element equations are then assembled to obtain the global equations, assuming interelement continuity conditions. At this point the boundary conditions are imposed and the global equations are solved by inverting the global matrix $[K_{gl}]$.

Due to the nonlinear reaction term and also the nature of the boundary conditions in this problem, solving the assembled global equations is not as straightforward as simply inverting the global stiffness matrix. This is because the reaction rate involves the concentrations of both glucose and oxygen as shown in equation (4-18). There are two ways to approach this problem: one is to incorporate the nonlinear reaction term into the global stiffness matrix and use the Newton-Raphson iterative method to solve the problem. The other method is to approximate the reaction term as a combination, $V = \Sigma V_i \psi_i$, of a constant reaction term V_i calculated at the nodes using old values of c_g and c_o, and the polynomial trial functions $\phi_i = \psi_i$. Using this method the global stiffness matrix becomes only a function of the known polynomial trial functions and can be easily inverted. Picard's method of iteration is used to obtain an accurate reaction term at the nodes, V_i. Both of these methods are discussed in more detail in Appendix 2: Handling the Nonlinear Reaction Term.

Solving for the hydrogen ion concentration involves other nonlinear terms, the apparent diffusivity and the effective Biot numbers. These terms can be handled in a similar manner as the reaction term, and will be discussed in more detail in the Numerical Solution section.

5.2 Galerkin Finite Element Method

5.2.1 Setting up the Equations - Variational Formulation

In this section the variational formulation of the problem is derived to obtain the equations in the appropriate form for the finite element method. The variational formulation (synonomous with the method of weighted residuals) involves three basic steps: (i) multiplying the equation (with all of the terms on one side of the equality) by a test function or weighting function and integrating the product over the domain of the problem, (ii) transferring the differentiation from the dependent variable c_i to the weighting function and (iii) simplifying the boundary terms using the specified boundary conditions. The test function in the first step can be thought of as a variation in the dependent variable to be solved for. It also must be chosen to satisfy the homogeneous form of any primary boundary conditions. (Primary boundary conditions are those in which the dependent variable is specified exactly at a boundary.) The second step involves using integration by parts, the divergence theorem and the gradient theorem.

The steps for obtaining equations (4-19a-c) along with boundary conditions (4-21)- (4-25) listed in Table 4-2 into the variational formulation over a typical element in the mesh are given below. Since equations (4-19a,b) are in similar form, the variational formulation is applied to them first. Equation (4-19c), due to the extra nonlinear diffusivity term, is treated separately.

Equations (4-19a,b) are repeated below:

$$\frac{1}{\rho^m} \frac{\partial}{\partial \rho} \left\{ \rho^m \frac{\partial c_g}{\partial \rho} \right\} + \varepsilon^2 \frac{\partial^2 c_g}{\partial \zeta^2} - \overline{V} \ (c_g, c_o) = 0 \qquad (4\text{-}19a)$$

$$\frac{1}{\rho^m} \frac{\partial}{\partial \rho} \left\{ \rho^m \frac{\partial c_o}{\partial \rho} \right\} + \varepsilon^2 \frac{\partial^2 c_o}{\partial \zeta^2} - \frac{1}{2} \overline{V} \ (c_g, c_o) = 0 \qquad (4\text{-}19b)$$

The general form of these equations is:

$$\frac{1}{\rho^m} \frac{\partial}{\partial \rho} \left\{ \rho^m \frac{\partial c_i}{\partial \rho} \right\} + \varepsilon^2 \frac{\partial^2 c_i}{\partial \zeta^2} - v_i \overline{V} \ (c_i, c_j) = 0 \qquad (4\text{-}19)$$

where c_i is the concentration for species i, v_i is the stoichiometric coefficient for species i, ($v_g = 1$ for glucose, $v_o = 0.5$ for oxygen) and

the reaction term, $\overline{V}$, is a function of both species. When m=0 the solution is for planar coordinates and when m=1, the solution is for cylindrical coordinates.

In the method of weighted residuals, the residual for equation (4-19) is formed by substituting in an approximate solution of the form $c_i = \Sigma c_{ij}\ \psi_j$ for c_i. As described in the introduction using the Galerkin method, the residual is then multiplied by a weighting function, ψ_k, and the product is integrated over the domain, Ω.

The mathematical formulation is now shown for equation (4-19a); i.e. for glucose.

$$\int_\Omega \psi_i(\rho,\zeta)\Big(\text{left hand side of 19a using approx.}c_g \text{ for } c_g\Big)\ \rho^m\ \partial\rho\partial\zeta =$$

$$\int_\Omega \psi_i(\rho,\zeta)\ \left(\frac{1}{\rho^m}\ \frac{\partial}{\partial\rho}\ \left\{\rho^m\ \frac{\partial c_g}{\partial\rho}\right\} + \varepsilon^2\ \frac{\partial^2 c_g}{\partial\zeta^2}\ -\ \overline{V}\ (c_g,\ c_o)\right)\rho^m\ \partial\rho\partial\zeta = 0$$

(1)

In equation (1), the integral is taken over the domain under consideration, which in the present case is a typical element. Writing this out explicitly generates a double integral over ρ and ζ.

We are now ready to apply step (ii) from above. Equation (1) can be rewritten using vector notation as:

$$\int_\rho \int_\zeta \psi_i(\rho,\zeta) \, (\nabla\bullet(\nabla c_g))\rho^m \, \partial\rho\partial\zeta - \int_\rho \int_\zeta \psi_i(\rho,\zeta) \, \overline{V}\rho^m \, \partial\rho\partial\zeta = 0 \qquad (2)$$

In writing equation (2) the gradient and divergence operators are slightly modified by the aspect ratio, ε. The gradient and divergence operators used in the vector notation are redefined as:

$$\nabla = (\frac{\partial}{\partial\rho}, \varepsilon\frac{\partial}{\partial\zeta}),$$

and

$$\nabla\bullet a = \left(\frac{1}{\rho^m} \frac{\partial}{\partial\rho} (\rho^m \, a) \, n_\rho + \varepsilon \frac{\partial a}{\partial\zeta} n_\zeta \right)$$

respectively. The first term in (2) can be further rewritten using the vector identity:

$$(\nabla\bullet(\nabla F))G = (\nabla^2 F)G = \nabla\bullet[(\nabla F)G] - (\nabla F)\bullet(\nabla G),$$

where F and G are scalar quantities. Applying this identity to the first term in (2) we obtain:

$$\int_{\rho} \int_{\zeta} \psi_i \, (\nabla \cdot (\nabla c_g)) \rho^m \partial \rho \partial \zeta =$$

$$\int_{\rho} \int_{\zeta} \nabla \cdot [(\nabla c_g) \psi_i] \, \rho^m \partial \rho \partial \zeta - \int_{\rho} \int_{\zeta} (\nabla c_g) \cdot (\nabla \psi_i) \rho^m \partial \rho \partial \zeta \qquad (3)$$

Applying the divergence theorem to the first term on the right hand side of equation (3) and expanding yields:

$$\int_{\rho} \int_{\zeta} \nabla \cdot [(\nabla c_g) \psi_i] \, \rho^m \partial \rho \partial \zeta = \oint_{\Gamma} \frac{\partial c_g}{\partial n} \, \psi_i \, d s$$

$$= \oint_{\Gamma} \left(n_\rho \, \psi_i \, \frac{\partial c_g}{\partial \rho} + n_\zeta \, \varepsilon^2 \, \psi_i \, \frac{\partial c_g}{\partial \zeta} \right) d s \qquad (4)$$

In equation (4), the line integral is taken over the surface of the domain, Γ, and n_ρ and n_ζ are the normals in the ρ and ζ directions, respectively. It is noted that the quantity $\frac{\partial c}{\partial n}$ is redefined including the aspect ratio as: $\frac{\partial c}{\partial n} = (n_\rho + \varepsilon \, n_\zeta) \cdot \nabla c$, with ∇ defined as before.

A typical element and the normals are shown in Figure 5-1 . (It is noted that the variational formulation of the problem does not

depend on the exact type of element chosen. At this point, however, using a different shape element such as triangular would change the remainder of this analysis slightly.) Using Figure 5-1, the last term in (4) can be rewritten over the element as shown in equation (5).

Figure 5-1: Applying the boundary terms to each element:
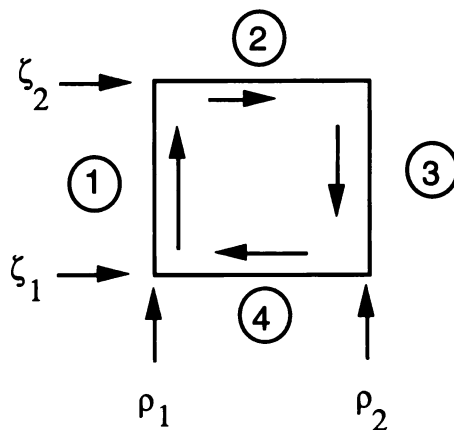
Along side 1: $\rho = \rho_1$, $n_\rho = -1$, $n_\zeta = 0$

side 2: $\zeta = \zeta_2$, $n_\rho = 0$, $n_\zeta = 1$

side 3: $\rho = \rho_2$, $n_\rho = 1$, $n_\zeta = 0$

side 4: $\zeta = \zeta_1$, $n_\rho = 0$, $n_\zeta = -1$

$$\oint_\Gamma \left(n_\rho \, \psi_i \, \frac{\partial c_g}{\partial \rho} + n_\zeta \, \varepsilon^2 \, \psi_i \, \frac{\partial c_g}{\partial \zeta} \right) ds =$$

$$\int_{\zeta=\zeta_1}^{\zeta=\zeta_2} -\left[\psi_i(\rho,\zeta) \, \frac{\partial c_g}{\partial \rho} \rho^m \right]_{\rho=\rho_1} d\zeta + \varepsilon^2 \int_{\rho=\rho_1}^{\rho=\rho_2} \left[\psi_i(\rho,\zeta) \, \frac{\partial c_g}{\partial \zeta} \right]_{\zeta=\zeta_2} \rho^m d\rho +$$

side 1   **side 2**

$$\int_{\zeta=\zeta_1}^{\zeta=\zeta_2} \left[\psi_i(\rho,\zeta) \, \frac{\partial c_g}{\partial \rho} \rho^m \right]_{\rho=\rho_2} d\zeta + \varepsilon^2 \int_{\rho=\rho_1}^{\rho=\rho_2} -\left[\psi_i(\rho,\zeta) \, \frac{\partial c_g}{\partial \zeta} \right]_{\zeta=\zeta_1} \rho^m d\rho$$

side 3   **side 4**

$$= J_{i1}^{(e)} + J_{i2}^{(e)} + J_{i3}^{(e)} + J_{i4}^{(e)} \tag{5}$$

In the last line of equation (5), $J_{i1}^{(e)}$ represents the flux into side 1 of element (e), etc. One aspect of interelement connectivity implies that the convective contribution at any interelement node or side is assumed to be zero. This can be seen more clearly in Figure 5-2, below. This means that if element 1 and 2 share side 3 of element 1 and side 1 of element 2, then $J_{i3}^{(1)} = -J_{i1}^{(2)}$. Thus the interelement conditions work to cancel adjacent fluxes. In addition,

as shown below, the nodal values between the two elements at the adjoining side must be equal.

Figure 5-2 :   Interelement Connectivity
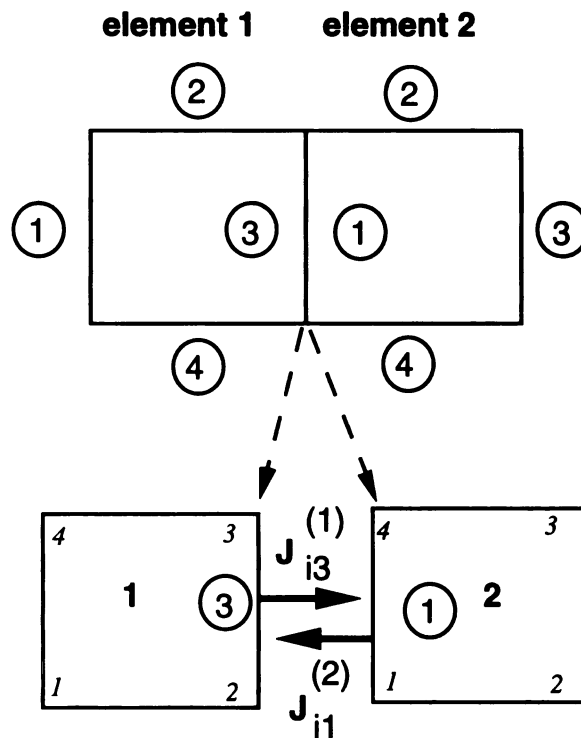
Flux connectivity: $J_{i3}^{(1)} = - J_{i1}^{(2)}$

Nodal connectivity: $n_2^{(1)} = n_1^{(2)}$ (where $n_\#$ = node number)

$n_3^{(1)} = n_4^{(2)}$

Similar relations are derived for vertically adjacent elements whose shared boundaries are not the boundary of the whole domain.

The nondimensional boundary conditions over the entire domain are given by equations (4-21)-(4-25) in Table 4-2.   These boundary

conditions can be applied to equation (5) in a slightly modified form. Over a typical element the boundary conditions for sides 1, 3 and 4 can be applied directly. Since the fluxes on sides 1 and 3 of the entire domain are zero at the boundaries; $J_{i1}^{(e)} = 0$ or $J_{i3}^{(e)} = 0$; and the interelement conditions apply elsewhere; $J_{i1}^{(e+1)} = - J_{i3}^{(e)}$. The boundary condition along side 4, given by equation (4-25) is a primary boundary condition where $c_g = c_{gbottom}$ such that the integrated flux along that side is zero. Since c_g is specified along this edge, the weight function, ψ_i must satisfy the homogenous form of this boundary condition, or $\psi_i = 0$. This eliminates the last term in equation (5).

The boundary condition along side 2 is represented in equations (4-22) and (4-23). These can be generalized over an element to be:

$$\frac{\partial c_g}{\partial \zeta} = Bi_g^{(e)}(c_g^* - c_g)\qquad(6)$$

where $Bi_g^{(e)}$ becomes a parameter which is dependent on the element number; that is the term $Bi_g^{(e)}$ is zero for elements not along the boundary. Generalizing equations (4-22) and (4-23) to this form enables all the elements in the mesh to be represented such that elements which share a boundary with side 2, will have different Biot numbers depending on the species and whether or not that element is under the oxygen permeable membrane. Substituting equation (6) into (5), we obtain equation (7):

$$\oint_{\Gamma} \left(n_\rho \, \psi_i \, \frac{\partial c_g}{\partial \rho} + n_\zeta \, \varepsilon^2 \, \psi_i \, \frac{\partial c_g}{\partial \zeta} \right) ds =$$

$$\varepsilon^2 \int_{\rho=\rho 1}^{\rho=\rho 2} \left[\psi_i(\rho,\zeta_2) Bi_g^{(e)} (c_g{}^* - c_g (\rho,\zeta_2)) \right] \rho^m d\rho \qquad (7)$$

Putting all this together, and substituting equation (7) into (4), then substituting the resulting equation into (3) and then into (2), the final form of the variational approximation for glucose becomes:

$$- \int_{\rho} \int_{\zeta} \left(\frac{\partial c_g}{\partial \rho} \frac{\partial \psi_i}{\partial \rho} + \varepsilon^2 \frac{\partial c_g}{\partial \zeta} \frac{\partial \psi_i}{\partial \zeta} \right) \rho^m \partial\rho \partial\zeta$$

$$+ \varepsilon^2 \int_{\rho=\rho 1}^{\rho=\rho 2} \left[\psi_i(\rho,\zeta_2) Bi_g^{(e)} (c_g{}^* - c_g (\rho,\zeta_2)) \right] \rho^m d\rho$$

$$- \int_{\rho} \int_{\zeta} \psi_i(\rho,\zeta) \, \overline{V} (c_g,c_o) \rho^m \, \partial\rho \partial\zeta = 0 \qquad (8)$$

The derivation of the variational formulation for equation (4-19b) is analogous to (4-19a) with c_g replaced by c_o, and is not repeated. This similarity arises not only from the fact that equations (4-19a) and (4-19b) are analogous, but also that the boundary conditions for

glucose and oxygen are in the same form. Equation (9) is the final form for the variational approximation for oxygen, with ψ_i as the weighting function, $v_o = -0.5$ and $c_o = \Sigma c_{oj} \psi_j$ as the approximate solution to c_o .

$$-\int_\rho \int_\zeta \left(\frac{\partial c_o}{\partial \rho}\frac{\partial \psi_i}{\partial \rho} + \varepsilon^2 \frac{\partial c_o}{\partial \zeta}\frac{\partial \psi_i}{\partial \zeta}\right)\rho^m \partial\rho\partial\zeta$$

$$+ \varepsilon^2 \int_{\rho=\rho1}^{\rho=\rho2} \left[\psi_i(\rho,\zeta_2)Bi_o^{(e)}(1 - c_o (\rho,\zeta_2))\right] \rho^m d\rho$$

$$- \frac{1}{2} \int_\rho \int_\zeta \psi_i(\rho,\zeta) \overline{V} (c_g ,c_o) \rho^m \partial\rho\partial\zeta = 0 \qquad (9)$$

The variational formulation for hydrogen is very similar to the steps taken in forming equations (8) and (9). The major difference comes in with the additional nonlinear diffusion term, D_{app} given in equation (4-20) and the nonlinear boundary condition given in (4-22b). The same steps can be taken from equation (2) on with the exception that the quantity (∇c_g) is replaced by $(D_{app} \nabla c_h)$. Most of the boundary conditions on hydrogen are in the same form as the boundary conditions for glucose except that the term $\frac{\partial c_g}{\partial \zeta}$ is replaced by $(D_{app} \frac{\partial c_h}{\partial \zeta})$. The boundary condition for side 2, given by (4-22b) is in a similar form to (6). In substituting (4-22b) into (5) written for hydrogen, the surface integral becomes:

$$\oint_{\Gamma} \left(n_\rho \, \psi_i \, D_{app} \, \frac{\partial c_h}{\partial \rho} + n_\zeta \, \varepsilon^2 \, \psi_i \, D_{app} \, \frac{\partial c_h}{\partial \zeta} \right) ds \; =$$

$$\varepsilon^2 \int_{\rho=\rho 1}^{\rho=\rho 2} \left\{ \psi_i(\rho,\zeta_2) Bi_{h^*}^{eff} \, c_h^* - \psi_i(\rho,\zeta_2) \left[Bi_h^{eff}(c_h(\rho,\zeta_2)) \right] c_h(\rho,\zeta_2) \right\} \rho^m d\rho$$

where
$$Bi_{h^*}^{eff} = \left[Bi_h + Bi_b \, \frac{\alpha_b \, c_{tb}}{\alpha_h \kappa_h + c_h^*} \right]; \text{ and}$$

$$Bi_h^{eff}(c_h(\rho,\zeta_2)) = \left[Bi_h + Bi_b \, \frac{c_{tb}}{\kappa_h + c_h(\rho,\zeta_2)} \right]. \tag{10}$$

Thus the variational formulation for hydrogen becomes:

$$- \int_{\rho} \int_{\zeta} D_{app} \left(\frac{\partial c_h}{\partial \rho} \frac{\partial \psi_i}{\partial \rho} + \varepsilon^2 \frac{\partial c_h}{\partial \zeta} \frac{\partial \psi_i}{\partial \zeta} \right) \rho^m \partial \rho \partial \zeta$$

$$+ \varepsilon^2 \int_{\rho=\rho 1}^{\rho=\rho 2} \left\{ \psi_i(\rho,\zeta_2) Bi_{h^*}^{eff} c_{h^*} - \psi_i(\rho,\zeta_2) \left[Bi_h^{eff}(c_h(\rho,\zeta_2)) \right] c_h(\rho,\zeta_2) \right\} \rho^m d\rho$$

$$+ \int_{\rho} \int_{\zeta} \psi_i(\rho,\zeta) \overline{V}(c_g,c_o) \rho^m \partial \rho \partial \zeta = 0 \tag{11}$$

Equations (8) and (9) represent the variational formulation for glucose and oxygen, respectively. Equation (11) is the variational formulation for hydrogen, with the effective Biot numbers given by equation (10), and the nondimensional apparent diffusivity given by equation (4-20).

There are two ways to solve these equations. Due to the dependence of the reaction rate on current glucose and oxygen concentrations, equations (8) and (9) either need to be solved simultaneously or decoupled by assuming an approximate form for the reaction rate. A modified Newton-Raphson method can be used and will be described below. Another method to solve these

equations is to decouple them by assuming an approximate reaction term and solving each equation separately for glucose and oxygen first, and then iterating until the reaction term converges to the correct value. Once the reaction term has been determined, equation (11) can be solved for the hydrogen ion concentration. The latter method proved to be more practical for our use.

## 5.2.2   Discretization of the Domain into Elements

The domain of interest shown in Figure 4-3, is discretized into a collection of preselected finite elements.   Due to the flexibility in choosing the mesh, the elements are not required to be the same size.   If desired the elements directly below the holes can be made smaller in both the ρ and ζ dimensions than those under the hydrophobic membrane.   Figure 5-3 shows a sample of the domain in nondimensional space and a sample discretization of the domain.   An element is defined to be a geometrically simple subdomain within the entire domain.   The elements shown below were chosen to be rectangles.   Triangles, however can also be used.   The elements under the hole are shown to be smaller in the ρ direction than those under the area of the membrane.   All the elements in this example have the same dimensions in the ζ - direction.   This too however can be variable.

The nodes of an element are defined as the values of the solution at a finite number of preselected points over the element. These points usually lie on the vertices of the element, but also can be on the boundary and possibly in the interior of the element.   All the elements in Figure 5-3 are shown to contain 4 nodes per element, and each of these nodes lie on the four corners of each element.   The number and the location of the nodes in an element depends on the geometry of the element, and the degree of the polynomial approximation used.   Linear rectangular elements have

four nodes per element, and four terms in a first degree polynomial, whereas linear triangular elements have three nodes per element and three terms in a first degree polynomial. Quadratic rectangular elements have nine nodes per element, and quadratic triangular elements have 6 nodes per element.

Figure 5-3: Discretization of Domain

HOW DO WE SOLVE THIS PROBLEM?
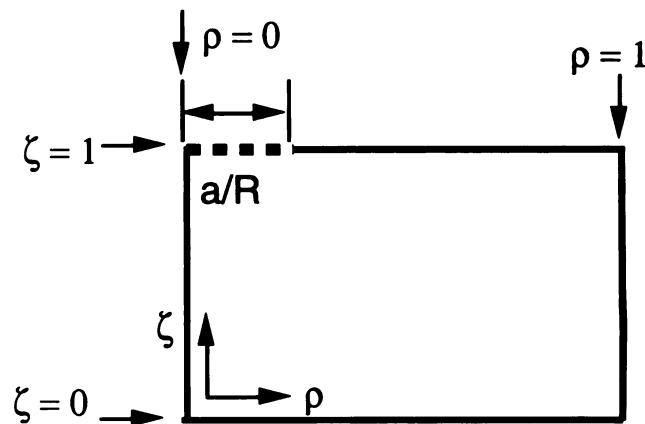
USE FINITE ELEMENT METHOD:
  DIVIDE AREA INTO RECTANGULAR "ELEMENTS" WITH 4
  NODES (OR 9 NODES, NOT SHOWN) PER ELEMENT.
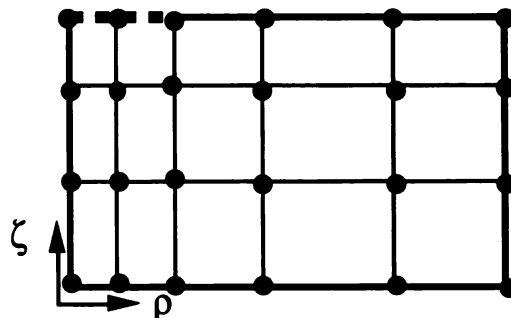
Figure 5-4 shows examples of rectangular and triangular elements which can be used in the program, along with their numbering scheme and the interpolation functions for each type of element. The coordinates used in Figure 5-4 are natural coordinates for each element. This means that these coordinates are the most convenient ones to use in deriving the polynomial approximations and in doing the numerical integration. It is described in Appendix 5-2 how these coordinates are related to the actual coordinates in the problem.

The subroutine MESH generates the finite-element mesh and calculates all the total number of nodes and the corresponding global nodal coordinates, (ρ_i, ζ_i). This program is available upon request. [Note to reader: all referenced computer code is available upon request through Professor R. A. Siegel at UCSF School of Pharmacy.]

Figure 5-4: Two-dimensional Elements and their Interpolation Functions

4-node Linear Rectangular element
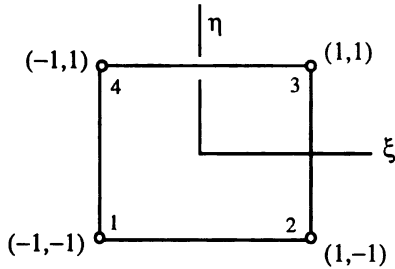
Interpolation Functions

$$\hat{\psi}_1 = \frac{1}{4}(1-\xi)(1-\eta), \quad \hat{\psi}_2 = \frac{1}{4}(1+\xi)(1-\eta),$$

$$\hat{\psi}_3 = \frac{1}{4}(1+\xi)(1+\eta), \quad \hat{\psi}_4 = \frac{1}{4}(1-\xi)(1+\eta)$$

9-node Quadratic Rectangular element
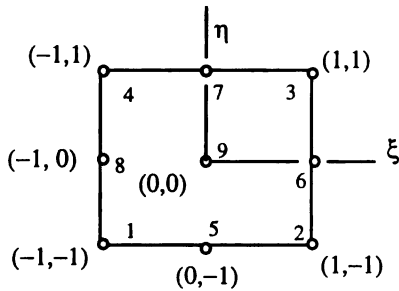
Interpolation Functions

$$\hat{\psi}_1 = \frac{1}{4}(1-\xi)(1-\eta)\xi\eta, \quad \hat{\psi}_2 = \frac{1}{4}(1+\xi)(1-\eta)\xi(-\eta),$$

$$\hat{\psi}_3 = \frac{1}{4}(1+\xi)(1+\eta)\xi\eta, \quad \hat{\psi}_4 = \frac{1}{4}(1-\xi)(1+\eta)(-\xi)\eta,$$

$$\hat{\psi}_5 = \frac{1}{2}(1-\xi^2)(\eta^2-\eta), \quad \hat{\psi}_6 = \frac{1}{2}(\xi^2+\xi)(1-\eta^2),$$

$$\hat{\psi}_7 = \frac{1}{2}(1-\xi^2)(\eta^2+\eta), \quad \hat{\psi}_8 = \frac{1}{2}(\xi^2-\xi)(1-\eta^2),$$

$$\hat{\psi}_9 = (1-\xi^2)(1-\eta^2).$$

3-node Linear Triangular element
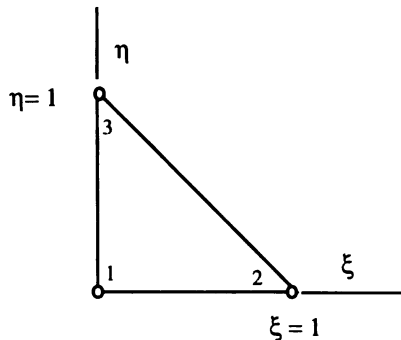
Interpolation Functions

$$\hat{\psi}_i^{(e)} = \frac{1}{2A_e}(\alpha_i + \beta_i\xi + \gamma_i\eta) \qquad i = 1,2,3$$

A_e = area of element

$$\alpha_i = \xi_j\eta_k - \xi_k\eta_j$$
$$\beta_i = \eta_j - \eta_k$$
$$\gamma_i = \xi_k - \xi_j$$

$i \neq j \neq k$, and i,j,and k permute in a natural order

5.2.3   Determination of Polynomial Trial Functions - Interpolation Theory

The degree of the polynomial approximation, ψ_j, over an element as well as the element shape determine the number of nodes each element must have.   The degree of the polynomial approximation, however, is also largely determined by the user's weighting of the desired accuracy of the solution and the computation time involved.   Depending on the formulation of the problem, a higher degree polynomial usually generates a more accurate solution at the cost of more computation.

The number of primary variables per node also plays a role in determining the degree of the polynomial approximation and consequently, the number of nodes in an element. A primary variable is defined to be a variable which is directly specified in the essential boundary conditions; i.e. $u = u_o$ at a boundary. A secondary variable is defined as one which is specified in the natural or flux boundary conditions; i.e. flow from diffusion or convection. For second-order equations, such as those used in heat or mass transfer, the primary variables are either temperature or concentrations, and the secondary variables are flows.   In this case, the species concentrations are all primary variables, and the mass fluxes are secondary variables.   The finite-element interpolation functions are chosen such that the finite-element approximation over an element satisfies the boundary conditions on the primary variable and includes the elementwise continuity condition for the primary variables as well as those for the secondary variables.   The latter

requirement ensures completeness of the set of finite-element interpolation functions and hence convergence.

The variational formulation of the problem also helps to identify the type and the minimum admissible degree of the interpolation functions, and the number of primary variables per node. The correspondence between the number and location of nodal points, the number of primary unknowns per node in a finite element, and the number of terms used in the polynomial approximations of a dependent variable over an element is also determined by the shape of the element for two-dimensional elements. For example, a problem which has more than one primary variable per node may need quadratic or cubic trial functions, corresponding to 9 or 16 nodes for a rectangular element, or corresponding to 6 or 10 nodes for a triangular element. For this particular problem more accuracy was found using quadratic rectangular elements than linear quadratic elements.

The trial functions given in Figure 5-4 were derived using interpolation theory, and are called the Lagrange family of interpolation functions. The construction of the interpolation functions does not depend on the specific differential equation being solved. Rather the construction procedure depends on the geometry, the number and the position of the nodes and the number of primary unknowns identified at the nodes of the element. The reader is referred to Appendix 5-2 and reference 1 for further detail on obtaining the exact formulation for the interpolation functions given for each element in Figure 5-4.

The elements shown in Figure 5-4 are master elements for the problem. Master elements, which all have the same geometry and use identical coordinate systems, facilitate the numerical integration of the element equations derived in the next section. This is not the case for elements in the actual mesh. The mesh elements have global coordinates, and thus each element has slightly different values for the interpolation functions. This problem is overcome by using the Jacobian transformation to convert between the master elements and the actual elements.

In order to perform element calculations required by equations (8), (9), and (11), we must calculate the quantities $\rho^m \partial\rho \partial\zeta$, $\frac{\partial\psi_i}{\partial\rho}$, and $\frac{\partial\psi_i}{\partial\zeta}$. To calculate these quantities in global coordinates we must know the coordinate transformations from natural coordinates to global coordinates, that is: the transformation $\rho = \rho(\xi, \eta)$; $\zeta = \zeta(\xi, \eta)$ and the inverse transformation $\xi = \xi(\rho, \zeta)$; $\eta = \eta(\rho, \zeta)$. These transformations can be described by the Jacobian matrix for each element. The exact nature of these transformations used in this problem are documented in Appendix 5-2.

The subroutine which generates the interpolation functions in global coordinates for each element is SHAPE. For more discussion about interpolation functions, master elements and the Jacobian transformation the reader is referred to any finite element text. [1,2]

5.3 Derivation of Element Equations

In the Galerkin finite-element method, the solution is represented as a linear combination ($c = \Sigma c_j^{(e)} \psi_j$) in terms of the values c_j of c at the j nodal points of element (e), and the trial functions, ψ_j. The trial functions are the polynomials that are derived using interpolation theory over each element discussed above and shown for three different master elements in Figure 5-4. To derive the element equations, the general approximation,

$$c_i = \sum_j^{n_e} c_{ij}^{(e)} \phi_j$$ is substituted into the variational formulations given

in equations (8), (9) and (11) for species i, and the equations are rearranged to obtain the element equations in the form $[K^e]\{c_i^e\} = \{F^e\}$ for each species.

5.3.1   Glucose and Oxygen Element Equations

Again using the glucose equation as the example and using the Galerkin method, with $\phi_j = \psi_j$, the substitution of the approximation

$$c_g = \sum_j^{n_e} c_{gj}^{(e)} \psi_j(\rho,\zeta)$$ in for the actual concentrations c_g transforms

equation (8) into:

$$- \int_\rho \int_\zeta \left(\frac{\partial(\Sigma c_{gj} \psi_j)}{\partial \rho} \frac{\partial \psi_i}{\partial \rho} + \epsilon^2 \frac{\partial(\Sigma c_{gj} \psi_j)}{\partial \zeta} \frac{\partial \psi_i}{\partial \zeta} \right) \rho^m \partial\rho\partial\zeta$$

$$+ \epsilon^2 \int_{\rho=\rho1}^{\rho=\rho2} \left[\psi_i(\rho,\zeta_2) Bi_g^{(e)} (c_g^* - [\Sigma c_{gj} \psi_j(\rho,\zeta_2)]) \right] \rho^m d\rho$$

$$- \int_\rho \int_\zeta \psi_i(\rho,\zeta) \overline{V}(\Sigma c_{gj} \psi_j, \Sigma c_{oj} \psi_j) \rho^m \partial\rho\partial\zeta$$

$$= 0 \qquad\qquad (12)$$

In equation (12) the terms $(\Sigma c_{gj} \psi_j)$ and $(\Sigma c_{oj} \psi_j)$ represent the glucose and oxygen approximations over an element, respectively. It should be understood that the summations are taken over all the n_e nodes of the element.

Continuing the derivation by interchanging the integral and the summation for the linear terms, equation (12) can be rewritten as:

$$\sum_{j=1}^{n_e} \left\{ -\int_\rho \int_\zeta \left(\frac{\partial \psi_j}{\partial \rho} \frac{\partial \psi_i}{\partial \rho} + \varepsilon^2 \frac{\partial \psi_j}{\partial \zeta} \frac{\partial \psi_i}{\partial \zeta} \right) \rho^m \partial \rho \partial \zeta - \varepsilon^2 Bi_g^{(e)} \int_{\rho=\rho_1}^{\rho=\rho_2} \psi_i(\rho,\zeta_2)\psi_j(\rho,\zeta_2)\, \rho^m d\rho \right\} c_{gj}^{(e)}$$

$$- \int_\rho \int_\zeta \psi_i(\rho,\zeta)\, \overline{V} \left(\Sigma c_{gj}\, \psi_j,\ \Sigma c_{oj}\, \psi_j \right) \rho^m\, \partial \rho \partial \zeta$$

$$+ \varepsilon^2 Bi_g^{(e)}\, c_g^* \int_{\rho=\rho_1}^{\rho=\rho_2} \psi_i(\rho,\zeta_2)\, \rho^m d\rho = 0 \qquad (13)$$

Equation (13) can be shortened by defining the matrices, $[s^{(e)}]$, $[b_k^{(e)}]$, and $[R^{(e)}]$ and the vector $\{F_k^{(e)}\}$, where now the subscript k refers to species k as shown below.

$$\left[s_{ij}^{(e)} \right] = -\int_\rho \int_\zeta \left(\frac{\partial \psi_j}{\partial \rho} \frac{\partial \psi_i}{\partial \rho} + \varepsilon^2 \frac{\partial \psi_j}{\partial \zeta} \frac{\partial \psi_i}{\partial \zeta} \right) \rho^m \partial \rho \partial \zeta \qquad (14)$$

$$\left[b_{gij}^{(e)} \right] = -\varepsilon^2 Bi_g^{(e)} \int_{\rho=\rho_1}^{\rho=\rho_2} \psi_i(\rho,\zeta_2)\psi_j(\rho,\zeta_2)\, \rho^m d\rho \qquad (15a)$$

polynomials, ψ_i and ψ_j for that element. The interpolation polynomials are known functions of ρ and ζ, as determined by Figure 5-4 and equations (A2-2) - (A2-4) in appendix 5-2, and thus these integrals can be evaluated separately for each element. (This is done in subroutine STIFF in the program for each element.)

A similar equation to (18) can be written for oxygen using the approximation $c_O = \displaystyle\sum_j^{n_e} c_{Oj}^{(e)} \psi_j$ for c_O , and starting with the variational formulation in equation (9). Using the notation above, the equation for oxygen becomes:

$$\sum_{j=1}^{n_e} \left[s_{ij}^{(e)} + b_{Oij}^{(e)} \right] c_{Oj}^{(e)} - \frac{1}{2} \left[R_{ij}^{(e)} \right] - \left\{ F_{Oi}^{(e)} \right\} = 0 \qquad (19)$$

$$\text{with } \left[b_{Oij}^{(e)} \right] = - \varepsilon^2 \, Bi_O^{(e)} \int_{\rho=\rho 1}^{\rho=\rho 2} \psi_i(\rho,\zeta_2)\psi_j(\rho,\zeta_2) \, \rho^m d\rho \qquad (15b),$$

$$\text{and, } \left\{ F_{Oi}^{(e)} \right\} = - \varepsilon^2 \, Bi_O^{(e)} \int_{\rho=\rho 1}^{\rho=\rho 2} \psi_i(\rho,\zeta_2) \, \rho^m d\rho \qquad (17b).$$

$$\left[R_{ij}^{(e)} \right] = \int_{\rho} \int_{\zeta} \psi_i(\rho,\zeta) \; \overline{V}(\Sigma c_{gj} \psi_j, \Sigma c_{oj} \psi_j) \; \rho^m \, \partial\rho \, \partial\zeta \qquad (16)$$

$$\left\{ F_{gi}^{(e)} \right\} = - \varepsilon^2 \, Bi_g^{(e)} \, c_g^* \int_{\rho=\rho 1}^{\rho=\rho 2} \psi_i(\rho,\zeta_2) \, \rho^m d\rho \qquad (17a)$$

Inserting (14) - (17) into equation (13), the element equation for glucose simplifies to:

$$\sum_{j=1}^{n_e} \left[s_{ij}^{(e)} + b_{gij}^{(e)} \right] c_{gj}^{(e)} - \left[R_{ij}^{(e)} \right] - \left\{ F_{gi}^{(e)} \right\} = 0 \qquad (18)$$

In equation (18), the first term is a linear term consisting of the element stiffness matrix, $\left[s_{ij}^{(e)} \right]$, and the boundary term contribution, $\left[b_{gij}^{(e)} \right]$. The reaction term, $\left[R_{ij}^{(e)} \right]$, is the nonlinear portion of the problem in which the nodal glucose and oxygen values are implicitly involved, and will be considered in more detail below. The load term, $\left\{ F_{gi}^{(e)} \right\}$, is independent of the unknown nodal concentrations and is fully specified. The values c_{gj} are the glucose concentrations at the j nodes of element (e). The integrals in equations (14), (15a) and (17a) are all independent of the concentrations c_{gj} and are only dependent on the interpolation

polynomials, ψ_i and ψ_j for that element. The interpolation polynomials are known functions of ρ and ζ, as determined by Figure 5-4 and equations (A2-2) - (A2-4) in appendix 5-2, and thus these integrals can be evaluated separately for each element. (This is done in subroutine STIFF in the program for each element.)

A similar equation to (18) can be written for oxygen using the approximation $c_O = \sum_j^{n_e} c_{o_j}^{(e)} \psi_j$ for c_O, and starting with the variational formulation in equation (9). Using the notation above, the equation for oxygen becomes:

$$\sum_{j=1}^{n_e} \left[s_{ij}^{(e)} + b_{o_{ij}}^{(e)} \right] c_{o_j}^{(e)} - \frac{1}{2} \left[R_{ij}^{(e)} \right] - \left\{ F_{o_i}^{(e)} \right\} = 0 \qquad (19)$$

with $\left[b_{o_{ij}}^{(e)} \right] = - \varepsilon^2 \, Bi_o^{(e)} \int_{\rho=\rho 1}^{\rho=\rho 2} \psi_i(\rho,\zeta_2)\psi_j(\rho,\zeta_2) \, \rho^m d\rho \qquad (15b),$

and, $\left\{ F_{o_i}^{(e)} \right\} = - \varepsilon^2 \, Bi_o^{(e)} \int_{\rho=\rho 1}^{\rho=\rho 2} \psi_i(\rho,\zeta_2) \, \rho^m d\rho \qquad (17b).$

Equations (18) and (19) are the element equations for glucose and oxygen. These equations are still not in the desired form of $[K^e] \{c_i^e\} = \{F^e\}$, due to the nonlinear reaction term $\left[R_{ij}^{(e)}\right]$, however. There are various methods for handling this nonlinear term which will be discussed before deriving the element equations for hydrogen.

5.3.2 Handling of the Nonlinear Reaction Term

Rewriting equation (16) using equation (4-18) with the assumed approximations for glucose and oxygen, the reaction term is expressed as:

$$\left[R_{ij}^{(e)}\right] = \int_{\rho} \int_{\zeta} \psi_i(\rho,\zeta) \, \frac{\phi^2}{1 + \kappa_g/(\Sigma c_{gj} \, \psi_j) + \kappa_o/(\Sigma c_{oj} \, \psi_j)} \, \rho^m \, \partial\rho\partial\zeta \qquad (20)$$

There are several ways that this term can be handled, each of which involve iterations. The method used for handling the reaction term is discussed below. Other methods which were considered, are discussed in Appendix 5-3. This method decouples the glucose and oxygen equations by assuming an approximate reaction rate. This allows equations (18) and (19) to be solved independently for the glucose and oxygen concentrations. Once the glucose and oxygen concentrations have been calculated the reaction rate is updated and equations (18) and (19) are resolved. These iterations are finished

once the glucose and oxygen concentrations and the reaction rate have converged to within a given tolerance.

Approximate Reaction rate as a function of the Nodal reaction rates. ($\overline{V} = \Sigma\ V_j^{(e)}\ \psi_j$).

In this method the reaction rates are calculated at the nodes of the elements using the approximate nodal values of c_g^o and c_o^o. The reaction rate is then approximated over an element in the same fashion as the concentrations by assuming that the reaction term is a combination of the approximate reaction term calculated at the nodes and the polynomial trail functions. In doing this the reaction rate is expressed as:

$$\overline{V} = \sum_j^{n_e} V_j^{(e)}\ \psi_j = \sum_j^{n_e} \frac{\phi^2}{1\ +\ \kappa_g/c_{gj}^o\ +\ \kappa_o/c_{oj}^o}\ \psi_j. \qquad (21)$$

Using the above expression for the reaction rate, the reaction matrix can be expressed as is shown in equation (22):

$$\left[R^{(e)}_{ij} \right] = \int_{\rho} \int_{\zeta} \psi_i(\rho,\zeta) \left(\sum_{j}^{n_e} V^{(e)}_j \psi_j \right) \rho^m \, \partial\rho \, \partial\zeta$$

$$= \sum_{j}^{n_e} V^{(e)}_j \int_{\rho} \int_{\zeta} \psi_i(\rho,\zeta) \psi_j(\rho,\zeta) \rho^m \, \partial\rho\partial\zeta \Rightarrow \left\{ R_i \right\} \qquad (22)$$

As mentioned above this method decouples equations (18) and (19) by making the reaction rate independent of the current concentrations. This method is more flexible than method (1) considered in Appendix 5-3 in that it allows for changes in the reaction rate within an element. In using this method, the element equations for glucose and oxygen can be rewritten in the desired form $[K^e] \{c^e_i\} = \{F^e\}$. In doing this equations (18) and (19) become:

$$\sum_{j=1}^{n_e} \left[K^{(e)}_{gij} \right] c^{(e)}_{gj} = \left\{ \tilde{F}^{(e)}_{gi} \right\} \qquad (23)$$

$$\sum_{j=1}^{n_e} \left[K^{(e)}_{o\,ij} \right] c^{(e)}_{oj} = \left\{ \tilde{F}^{(e)}_{oi} \right\} \tag{24}$$

where :

$$\left[K^{(e)}_{k\,ij} \right] = \left[s^{(e)}_{ij} + b^{(e)}_{k\,ij} \right] \quad k = g, o \tag{25}$$

$$\left\{ \tilde{F}^{(e)}_{k\,i} \right\} = \nu_k \left\{ R_i \right\} + \left\{ F^{(e)}_{k\,i} \right\} \quad \nu_k = 1 \text{ for glucose and}$$

$$\nu_k = \frac{1}{2} \text{ for oxygen}$$

$$\nu_k = -1 \text{ for hydrogen} \tag{26}$$

In rewriting equations (18) and (19) in the form of (23) and (24), the element stiffness matrix [K], and the load vector $\left\{ \tilde{F} \right\}$, are independent of the unknown concentrations and are only a function of the known polynomial trial functions. Both the element stiffness matrix and the element load vector can now be calculated using the interpolation functions given in Figure 5-4 and using equations (A2-2) through (A2-4). Since equations (23) and (24) are decoupled, they can be solved separately once the elements have been assembled. As mentioned above, the glucose and oxygen solutions are recoupled by iterating until convergence of the concentrations and the reaction

rate. This will be elaborated on in the Numerical Solution section. An important point in this formulation is that the element stiffness matrices given by K_k, k = g,o in equations (23) and (24), are both symmetric matrices. This implies that only the unique values of these matrices need to be saved. This facilitates solving the problem in that the amount of computations are decreased and the problem can be solved more quickly.

5.3.3   Derivation of Element Equations for Hydrogen

At this point we are ready to return to deriving the element equations for hydrogen. Beginning with the variational formulation for hydrogen given by equation (11), substituting the approximation

$$c_h\,(\rho,\zeta) = \sum_{j}^{n_e} c_{h_j}^{(e)}\,\psi_j(\rho,\zeta)$$ for c_h, and rearranging, the element

equation for hydrogen becomes:

$$\sum_{j=1}^{n_e} \left\{ -\int_\rho \int_\zeta D_{app}(\Sigma c_{hj}\,\psi_j)\left(\frac{\partial\psi_j}{\partial\rho}\frac{\partial\psi_i}{\partial\rho} + \varepsilon^2\frac{\partial\psi_j}{\partial\zeta}\frac{\partial\psi_i}{\partial\zeta}\right)\rho^m\partial\rho\partial\zeta \right\} c_{hj}^{(e)}$$

$$+ \sum_{j=1}^{n_e} \left\{ -\varepsilon^2 \int_{\rho=\rho 1}^{\rho=\rho 2} \left[Bi_h^{eff}(\Sigma c_{hj}\,\psi_j(\rho,\zeta_2)) \right] \psi_i(\rho,\zeta_2)\,\psi_j(\rho,\zeta_2)\,\rho^m d\rho \right\} c_{hj}^{(e)}$$

$$+ \int_\rho \int_\zeta \psi_i(\rho,\zeta)\,\overline{V}(\Sigma c_{gj}\,\psi_j,\Sigma c_{oj}\,\psi_j)\,\rho^m\,\partial\rho\partial\zeta$$

$$+ \varepsilon^2 Bi_{h*}^{eff}\,c_h{}^* \int_{\rho=\rho 1}^{\rho=\rho 2} \psi_i(\rho,\zeta_2)\,\rho^m d\rho = 0 \qquad (27)$$

The first two lines of (27) can be separated into a linear and a nonlinear portion by inserting the definitions for D_{app} (eqn 4-20) and Bi_h^{eff} (eqn 10).

Thus, the first two lines can be simplified as:

$$= \sum_{j=1}^{n_e} \left\{ \left[s_{ij}^{(e)} \right] + \left[s_{h_{ij}}^{NL} \right] + \left[b_{h_{ij}}^{(e)} \right] + \left[b_{h_{ij}}^{NL} \right] \right\} c_{hj}^{(e)} \qquad (28)$$

where $\left[s_{ij}^{(e)} \right]$ is given by equation (14) and $\left[b_{h_{ij}}^{(e)} \right]$ is given by equation (15c) shown below. The nonlinear portions, $\left[s_{h_{ij}}^{NL} \right]$ and $\left[b_{h_{ij}}^{NL} \right]$ are given explicitly by equations (29) and (30), respectively.

$$\left[b_{h_{ij}}^{(e)} \right] = - \varepsilon^2 \, Bi_h^{(e)} \int_{\rho=\rho 1}^{\rho=\rho 2} \psi_i(\rho,\zeta_2)\psi_j(\rho,\zeta_2)\, \rho^m d\rho \qquad (15c)$$

$$\left[s_{h_{ij}}^{NL} \right] = - \int_{\rho} \int_{\zeta} \left(\frac{c_{tb} \, \kappa_h}{(\kappa_h + \Sigma c_{hm}\psi_m)^2} \right) \left(\frac{\partial \psi_j}{\partial \rho} \frac{\partial \psi_i}{\partial \rho} + \varepsilon^2 \frac{\partial \psi_j}{\partial \zeta} \frac{\partial \psi_i}{\partial \zeta} \right) \rho^m \partial \rho \partial \zeta \qquad (29)$$

$$\left[b_{h_{ij}}^{NL} \right] = - \varepsilon^2 \, Bi_b^{(e)} \int_{\rho=\rho 1}^{\rho=\rho 2} \left(\frac{c_{tb}}{\kappa_h + \Sigma c_{hm}\psi_m(\rho,\zeta_2)} \right) \psi_i(\rho,\zeta_2)\psi_j(\rho,\zeta_2)\, \rho^m d\rho$$

$$(30)$$

Now with the aid of equations (14), (15c), (16), (17c) and (28) through (30), equation (27) can be simplified with to:

$$\sum_{j=1}^{n_e} \left\{ \left[s_{ij}^{(e)} + b_{h_{ij}}^{(e)} \right] + \left[s_{h_{ij}}^{NL} + b_{h_{ij}}^{NL} \right] \right\} c_{hj}^{(e)} + \left[R_{ij}^{(e)} \right] - \left\{ F_{h_i}^{(e)} \right\} = 0$$

(31)

where

$$\left\{ F_{h_i}^{(e)} \right\} = - \varepsilon^2 \, Bi_{h^*}^{eff} \, c_h^* \int\limits_{\rho=\rho 1}^{\rho=\rho 2} \psi_i(\rho,\zeta_2) \, \rho^m d\rho$$

(17c)

and $Bi_{h^*}^{eff}$ is given in (10).

Equation (31) is analogous to equation (18) for glucose with the exception of the nonlinear terms shown in equations (29) and (30), both of which are dependent on the unknown hydrogen ion concentration, and are included in the integrals.

Since we have chosen to use equation (4-18) to describe the reaction term, the reaction rate is independent of the hydrogen concentration and is known once the glucose and oxygen concentrations are known. Thus the equation which describes the hydrogen concentration is decoupled from the glucose and oxygen equations. Therefore regardless of the method chosen for handling nonlinear reaction term, the hydrogen concentrations at each node

can be solved for once the glucose and oxygen concentrations, and the following reaction rates at each node are determined. Since the reaction rates at each node are known, the reaction term in equation (31) is given exactly by equation (22). Thus the reaction rate matrix is a vector, and equation (31) can be simplified using equations (25) and (26) for hydrogen, to:

$$\sum_{j=1}^{n_e} \left[K_{h_{ij}}^{(e)} \right] c_{h_j}^{(e)} + \sum_{j=1}^{n_e} \left[K_{h_{ij}}^{NL(e)}(c_{h_j}^{(e)}) \right] c_{h_j}^{(e)} = \left\{ \tilde{F}_{h_i}^{(e)} \right\} \tag{32}$$

where,

$$K_{h_{ij}}^{(e)} = s_{ij}^{(e)} + b_{h_{ij}}^{(e)} \tag{25}$$

$$K_{h_{ij}}^{NL(e)}(c_{h_j}^{(e)}) = s_{h_{ij}}^{NL} + b_{h_{ij}}^{NL} \tag{33}$$

$$\tilde{F}_{h_i}^{(e)} = \left\{ F_{h_i}^{(e)} \right\} - \left\{ R_i \right\} \tag{26}$$

The nonlinear terms in equation (32) can be evaluated using either of the methods described in handling the reaction term. The method of assuming an initial value for the hydrogen concentration to calculate the nonlinear matrices $s_{h_{ij}}^{NL}$, and $b_{h_{ij}}^{NL}$ and iterating after assembly and solution using Picard's method (described further in the Numerical Methods Section) can be used. The Newton-Raphson

method can also be used once an initial guess is given. After assembly the values of the nonlinear matrices $s_{h_{ij}}^{NL}$, and $b_{h_{ij}}^{NL}$ can be updated with the next hydrogen concentration approximations and the problem can be resolved.

If the nodal values of the hydrogen concentration are approximated as c_h^0, then the nonlinear portions in equation (32) can be treated as a function of the approximate hydrogen concentrations and the element equation for hydrogen becomes:

$$\sum_{j=1}^{n_e} \left[K_{h_{ij}}^{(e)} + K_{h_{ij}}^{NL^0} \right] c_{h_j}^{(e)} = \left\{ \tilde{F}_{h_i}^{(e)} \right\}$$

where,

$$K_{h_{ij}}^{NL^0}(c_{h_j}^0) = s_{h_{ij}}^{NL}(c_{h_j}^0) + b_{h_{ij}}^{NL}(c_{h_j}^0)$$

or in matrix form:

$$\left[K_{T_h}^{(e)} \right] \left\{ \tilde{c}_h^{(e)} \right\} = \left\{ \tilde{F}_h^{(e)} \right\} \qquad (34)$$

In expressing the element equation for hydrogen in this form, the nonlinear portion of the element stiffness matrix, $[K^{NL^0}]$, is made independent of the current hydrogen concentrations by using the last iteration values of the hydrogen concentration. In writing equation (34), the total element stiffness matrix $[K^T_h]$, and the load vector

$\left\{ \tilde{F_h} \right\}$, are independent of the current unknown concentrations and are only a function of the known polynomial trial functions.

Both the total element stiffness matrix $[K + K^{NL^o}]$, and the element load vector can now be calculated using the interpolation functions given in Figure 5-4, and equations (A2-2) through (A2-4). It should be noted that the total element stiffness matrix given in equation (34) is symmetric and only a portion of the n_e by n_e elements need to be calculated and saved. This decreases computation time and greatly simplifies the problem.

The element equation for hydrogen given by equation (34) is now in the desired form and can be solved by inverting the global stiffness matrix once the elements have been assembled. It will be necessary to iterate on the hydrogen ion concentration until convergence within tolerance, of the approximate $c_{h_j}^o$ used in estimating the nonlinear term, and the current solution for c_{h_j}. This will be elaborated on in the Numerical Solution section.

The subroutines which generate the elemental stiffness matrices, $\left[K^{(e)}_{k_{ij}} \right]$ for all the species are STIFF and CONV. The STIFF subroutine calculates the quantites corresponding to $\left[s^{(e)}_{ij} \right]$, equations (14), or (14) and (29) for hydrogen. The CONV subroutine calculates the convective boundary condition contributions to the stiffness matrix, either $\left[b^{(e)}_{k_{ij}} \right]$ for glucose or oxygen or $\left[b^{(e)}_{h_{ij}} \right] + \left[b^{NL}_{h_{ij}} \right]$ for hydrogen. These subroutines could be adapted for the Newton-

Raphson method of solution given in Appendix 5-3 with a few alterations.

5.4 Assembly

At this point we turn to assembling the element equations. Each element equation given by (23), (24) and (34) for glucose, oxygen and hydrogen respectively for the symmetric case; or by (A3-9), and (A3-17) for the Newton-Raphson case, are derived for an arbitrarily typical element and therefore hold for any element in the finite element mesh. Before these equations can be solved it is necessary to assemble the individual finite elements into the global mesh to obtain the global equations. This is done using the interelement continuity conditions. These conditions give a correspondence between the local nodes and the global nodes by equating the connected nodes. Thus, the assembly part of a finite element program is a matter of book-keeping between element node numbers and global node numbers. It simply involves placing the correct element stiffness matrix value in the correct position in the global equation.

A detailed example of the assembly of a finite element problem is given in Appendix 5-4. The reader is referred to finite element textbooks for further information or specific programs.[1,2]

The computer implementation involves generating a matrix which contains correspondence between the local and global nodes.

This matrix keeps track of how each element stiffness and load value fit into the global equation. It should be noted that when the elemental stiffness matrices are symmetric, so is the global matrix, and only half of the entries need to be saved. This allows the global stiffness matrix to be stored in an upper-half-banded form which makes computer implementation easier and faster. In addition general-purpose equation solvers are available for such banded systems of equations.

The assembly portion of the code is given by the subroutine ASSEM which assembles the element equations into a global equation. The subroutine works for symmetric element stiffness matrices and stores the global equations in an upper-half-banded form.

5.5 Imposition of Numerical Boundary Conditions

Once the finite-elements have been assembled, it remains to impose the specified boundary conditions over the domain. First the boundary conditions on the secondary variables are imposed (the natural boundary conditions). These conditions represent the imposed fluxes at the boundaries. Then the essential boundary conditions are applied. These are the specified values of the primary unknowns at the boundaries. In doing this the assembled matrix is rearranged slightly. The problem is finally solved by inverting the global stiffness matrix.

It should be noted that in many two-dimensional problems like the example above, singular points occur. Singular points are points at which both the primary variables and the secondary variables are specified or those at which two separate primary or secondary conditions are specified. Obviously one cannot impose both boundary conditions at the same point. As a general rule, the essential boundary condition (i.e., the boundary condition on the primary variables) should be imposed at the singular points and the natural boundary conditions (i.e. the boundary condition on the secondary variables) should be disregarded. When either two primary or two secondary boundary conditions are given at one point the user must choose which value is more appropriate, or take an average of the two values.

The reader is again referred to Appendix 5-4 for a detailed example of applying the boundary conditions for a specific problem. The reader is referred to finite element textbooks for further information or specific programs.[1,2]

The boundary conditions for the glucose oxidase sensor are given by equations (4-21) - (4-25) in Table 4-2 and shown in Figure 4-4. The natural boundary conditions occur along sides 1, 2 and 3 and the essential boundary conditions occur along side 4. There are four singular points at the corners of the domain. The two points at the top of the domain (corresponding to points 7 and 9 in figure A4-1) are assigned the natural boundary conditions of side 2. The other two points at the bottom edge (corresponding to points 1 and 3 in Figure A4-1) are assigned the essential boundary conditions along

side 4. In solving this problem the natural boundary conditions along sides 1, 2 and 3 are applied first. Then the essential boundary conditions along side 4 are applied. The global set of equations are rearranged in the same fashion as described above. Once this is completed, the remaining set of equations is solved for the remaining primary and secondary unknowns by inverting the global stiffness matrix.

Imposing the boundary conditions in the code is completed by using the subroutines MAKEBND and BOUND. MAKEBND generates the files used to impose the boundary conditions and BOUND applies these conditions to the correct elements. The subroutine BOUND works for symmetric global equations stored in an upper-half-banded form.

5.6 Numerical Solution - program methods

At this point the we have gone through all the details of setting up the finite-element method. Now it remains to solve the equations for the unknown concentrations. Various solvers exist depending on whether the matrix is banded or not. The subroutine that is used for the symmetric, banded equations given by equations (23), (24) and (34) solves a banded system of equations and returns the solution in the load matrix. The routine performs gaussian elimination and back substitution to obtain the solution.

A variety of equation solvers are available. For the cases of non-symmetric, unbanded systems, i.e. equations (A3-9) and (A3-17) the solution can be obtained by inverting the matrix using the Gauss-Jordan elimination method. This is often time consuming, however due to the fact that the full matrix is used. The global matrices corresponding to equations (A3-9) and (A3-17) are sparse matrices. There are several solvers for sparse matrices which should be used.[10]

Regardless of the numerical method used for inversion of the global stiffness matrix, this problem still requires iteration due to the nonlinear reaction term and the nonlinear hydrogen diffusivity and effective Biot numbers for hydrogen transport. In addition iteration on the boundary condition of side 4 is required for a steady state solution. This latter part is described in more detail below.

The element equations (23) and (24) for glucose and oxygen, respectively generate symmetric element and global matrices. This implies that we are artificially separating the glucose and oxygen equations. In using this method each set of concentrations is solved for separately for the next solution values of glucose and oxygen concentrations. Therefore assembly and applying the boundary conditions are done separately for glucose and oxygen. First the glucose matrix is inverted to obtain the glucose solutions, and then the same is done for oxygen, to obtain the oxygen solutions. At this point the solutions are checked to determine how accurate the initial approximations used to obtain the reaction term at each node were. The problem is recoupled by comparing the initial

approximations to the new solutions. An overall convergence criterion is used to compare the old and new solutions at each node. If the error value is not within the tolerance value, then new values for the glucose, oxygen and the resulting reaction term at each node are obtained using Picard's method shown below. (The error at each node is also determined and used to check how close the solutions are to the original approximations used to obtain reaction term at each node.)

Error calculations are performed for each concentration at each node and for the combined convergence criteria as shown below. The error for a species i at node j is given by:

$$error_{ij} = \sqrt{\frac{\left| c_{ij}^{k} - c_{ij}^{k-1} \right|^2}{\left| c_{ij}^{k} \right|^2}} \qquad (35)$$

where c_{ij}^{k} is the concentration of species i at node j for the current solution and c_{ij}^{k-1} is the concentration of species i at node j for the last iteration. The overall convergence criteria for glucose and oxygen is given by the square root of the sum over all the nodes of the fractional differences between the last and current iterations. This is given explicitly in equation (36) below:

$$\frac{\left[\sum_{i=1}^{N_{tot}}\left(\left|c_{g_i}^k - c_{g_i}^{k-1}\right|^2 + \left|c_{o_i}^k - c_{o_i}^{k-1}\right|^2\right)\right]^{1/2}}{\left[\sum_{i=1}^{N_{tot}}\left(\left|c_{g_i}^k\right|^2 + \left|c_{o_i}^k\right|^2\right)\right]^{1/2}} \leq \text{tolerance} \qquad (36)$$

The tolerance value for the overall convergence criteria is set by the user and can be variable. The tolerance for the convergence criteria was usually set at 0.00001

As mentioned above if the convergence criterion is not within the tolerance value, then new values for the glucose, and the oxygen concentrations and the resulting reaction term at each node need to be determined. At this point Picard's method of iteration is used after each solution step to get new nodal values for glucose and oxygen. Picard's method obtains the next iterative value by combining the new solution obtained using the last iterative value and the old iterative value as shown by equation (37):

$$c_{ij}^{k+1} = x_{pic} * c_{ij}^k + (1 - x_{pic}) * c_{ij}^{k-1} \qquad (37)$$

where x_{pic} is a fraction between 0 and 1. In most cases x_{pic} was set to 0.66. The new solution values at each node are now used to calculate a new reaction term, and the problem is resolved. This

iterative method is represented in the flowchart shown in Figure 5-5 below.

The Newton-Raphson method uses a more direct method to obtain the new solution values by calculating them directly. In using this method, the next values of the glucose and oxygen concentrations are solved for simultaneously by determining the solution of the change in the global $\tilde{q}_{gl}$ vector, $\Delta\tilde{q}_{gl}^{n+1} = \tilde{q}_{gl}^{n+1} - \tilde{q}_{gl}^{n}$. This is accomplished by inverting the assembled modified stiffness matrix, A_{gl}. At this point it was decided not to use this method due to the added computation that was required by assembling and inverting the nonsymmetric matrix A_{gl}. Figure 5-6 shows the iterative procedure which would be used in this case.

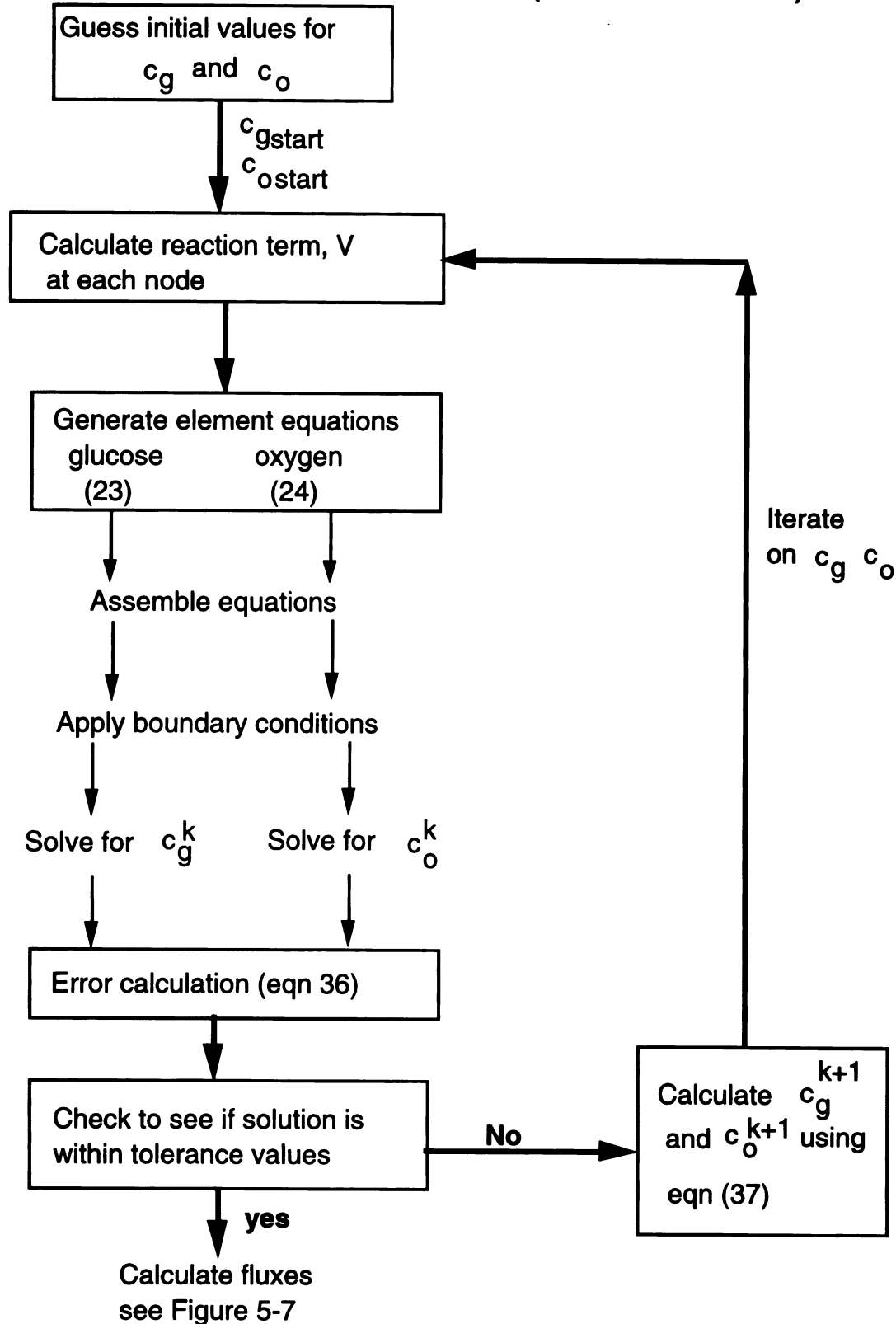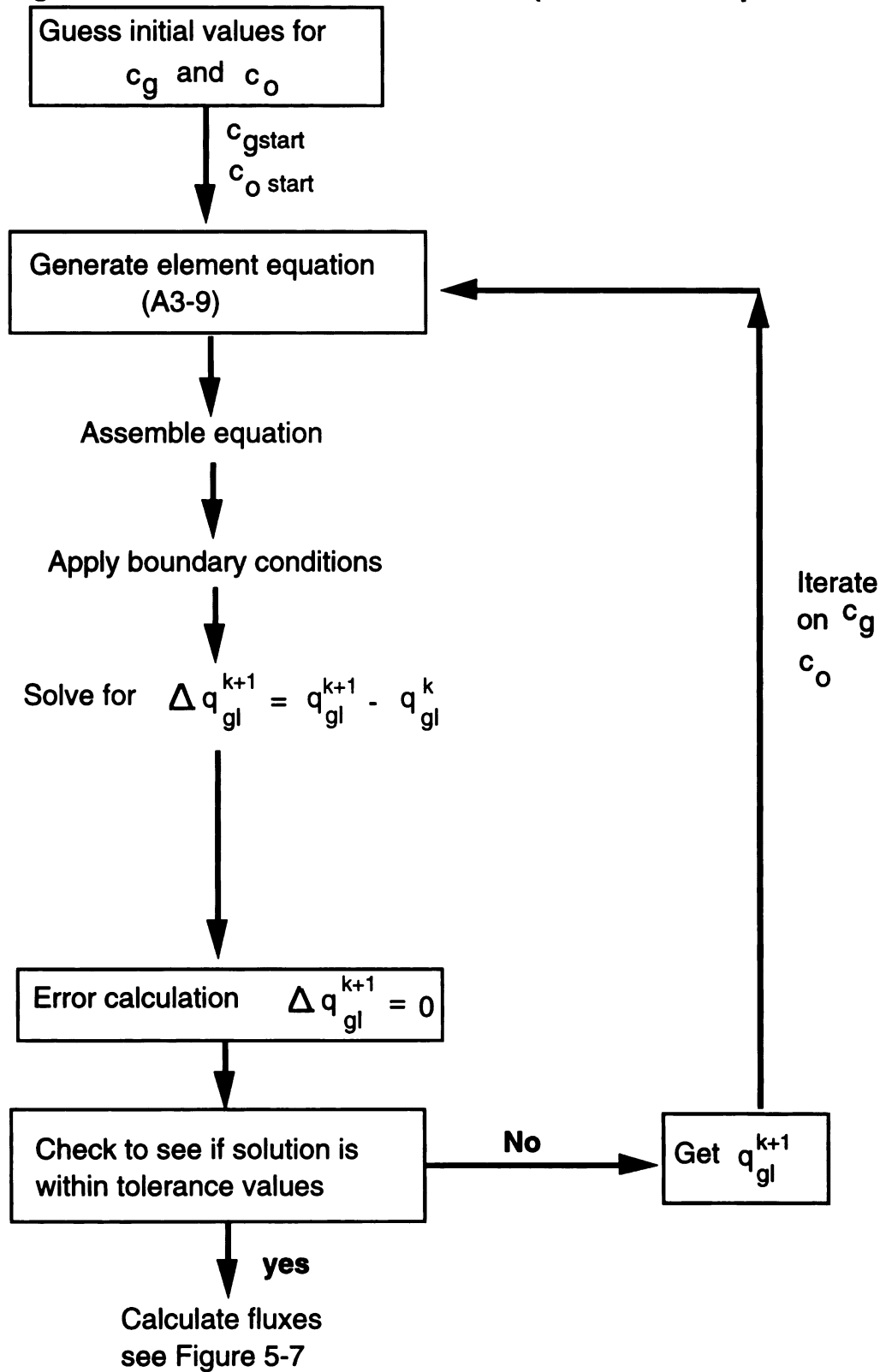**Figure 5-5:   Method of Solution (Picard's solution)**

Guess initial values for c_g and c_o

c_{gstart}
c_{ostart}

Calculate reaction term, V at each node

Generate element equations
glucose   oxygen
(23)   (24)

Assemble equations

Apply boundary conditions

Solve for c_g^k Solve for c_o^k

Error calculation (eqn 36)

Check to see if solution is within tolerance values

Iterate on c_g c_o

No

Calculate c_g^{k+1} and c_o^{k+1} using eqn (37)

yes

Calculate fluxes see Figure 5-7

Figure 5-6:   Method of Solution (Newton- Raphson Scheme)

Guess initial values for
c_g and c_o

c_{gstart}
$c_{o\ start}$

Generate element equation
(A3-9)

Assemble equation

Apply boundary conditions

Solve for $\quad \Delta q_{gl}^{k+1} = q_{gl}^{k+1} - q_{gl}^{k}$

Error calculation $\quad \Delta q_{gl}^{k+1} = 0$

Check to see if solution is
within tolerance values

No

Get q_{gl}^{k+1}

Iterate
on c_g
c_o

yes

Calculate fluxes
see Figure 5-7

Once having a preliminary solution for glucose and oxygen, we now need to check the boundary condition along side 4. This involves calculating the integrated fluxes for both glucose and oxygen. If the integrated fluxes are zero or within a tolerance value then the solution is a steady state solution and the problem is solved. If the fluxes are not zero, then a new boundary condition is guessed along side 4. This is done using a minimization scheme obtained from Numerical Recipes.[10]

The minimization scheme that is used for this problem is a multidimensional scheme based on Powell's Quadratically Convergent Method. This method is used to minimize a function of more than one variable, and involves using successive line minimizations. The choice of successive directions does not involve explicit computation of the function's gradient, which would be very difficult in our case. The idea of this method is to evaluate the function at a number of points, or directions to find the minimum. This is based on the fact that the optimum (or minimum) of an N-dimensional quadratic function can be found by exactly N single-variable searches along each of the N conjugate directions.

Briefly, Powell's method involves calculating the minimum of the N-dimensional function along N mutually conjugate directions, u_i. Initially the set of directions is taken as the basis vectors which span the space. (In our case, initially it is the glucose and oxygen boundary conditions along side 4 which need to be determined. Therefore initially we are attempting a two dimensional search.) A starting position is picked and the function
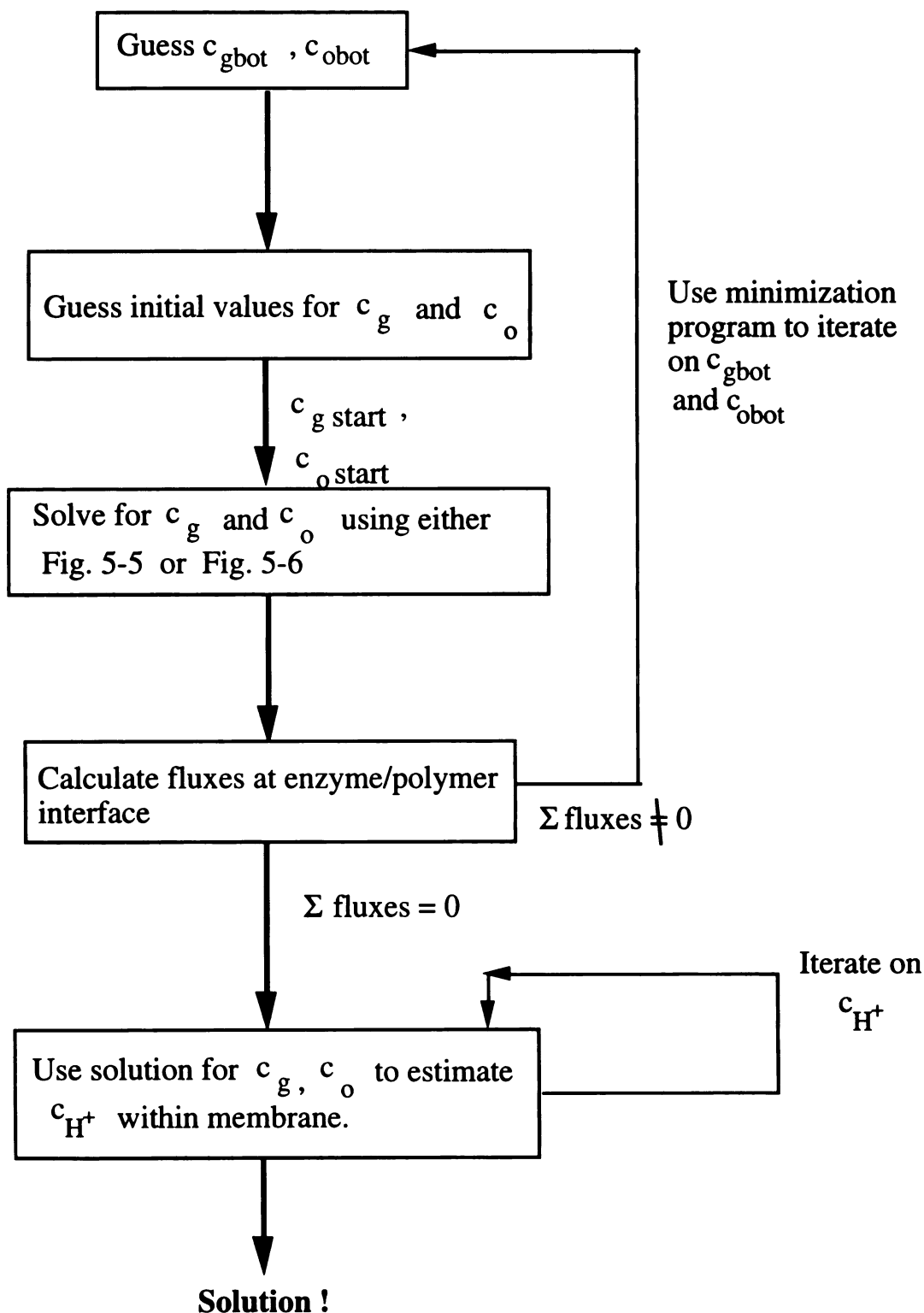
to be minimized is calculated at this position. Then for each dimension, i = 1, . . ., N, along each basis vector, the minimum is found in that direction. That is: move along the first direction to its minimum, then from there along the second direction to its minimum and so on, cycling through the whole set of directions one time. At this point the set of directions are evaluated and a new set of conjugate directions are chosen based on the new minimum found. This basic scheme is repeated until the minimum value of the function is within a set tolerance value.

Several different minimization functions were tried for this problem. The goal is to find the glucose and oxygen concentrations along side 4 which will generate zero integrated fluxes along this side. This boundary condition is given in equation (4-25). It was finally decided to use the minimization function given below:

$$f(c_{gbot}, c_{obot}) = \left(\sum_{i=1}^{Xelem} fluxg_i(c_{gbot}) \right)^2 + \left(\sum_{i=1}^{Xelem} fluxo_i(c_{obot}) \right)^2 \qquad (38)$$

This function minimized the square of the integrated fluxes for both glucose and oxygen. The program calculates the above function given guessed values for the bottom concentrations of glucose and oxygen. For each new value of glucose and/or oxygen concentration along side 4, the entire problem is resolved and the fluxes into the destination layer are recalculated. This is done in order to obtain a new estimate for equation (38). Then the minimization program is used to minimize equation (38) by obtaining new values for the bottom concentrations. This is illustrated in the flowchart in Figure 5-7.

**Figure 5-7: Method to determine boundary conditions**

Guess c_{gbot}, c_{obot}

Guess initial values for c_g and c_o

$c_{g\,start}$, $c_{o\,start}$

Solve for c_g and c_o using either Fig. 5-5 or Fig. 5-6

Calculate fluxes at enzyme/polymer interface

Σ fluxes $\neq 0$

Use minimization program to iterate on c_{gbot} and c_{obot}

Σ fluxes $= 0$

Use solution for c_g, c_o to estimate c_{H^+} within membrane.

Iterate on c_{H^+}

Solution !

When the glucose and oxygen concentrations have been determined, it remains to solve for the hydrogen ion concentrations. This is done using equation (34). At this point the reaction term is known at each node. It is still necessary to iterate on the hydrogen ion concentration until convergence within tolerance due to the nonlinear diffusivity term. In this case Picard's method was used. Picard's method is simpler to implement and was chosen over the Newton-Raphson method which generates asymmetric element and global stiffness matrices. [The Newton-Raphson method can be used with equation (A3-17) if desired.]

In using Picard's method the initial value of the hydrogen ion concentration is approximated as $c_{h_j}^o$ in order to calculate the nonlinear terms in the stiffness matrix given by equations (25) and (33). The problem is solved as shown by the flowchart in Figure 5-8 below. The error calculation for this portion of the solution is given by equation (39) below. Equation (37) is still used to determine the next value used in the next iteration.

$$\frac{\left[\sum_{i=1}^{N_{tot}} \left(\left| c_{h_i}^k - c_{h_i}^{k-1} \right|^2 \right) \right]^{1/2}}{\left[\sum_{i=1}^{N_{tot}} \left(\left| c_{h_i}^k \right|^2 \right) \right]^{1/2}} \leq \text{tolerance} \qquad (39)$$

In this case tolerance was set at 0.0001.

Figure 5-8:   Method of Solution for Hydrogen Ion
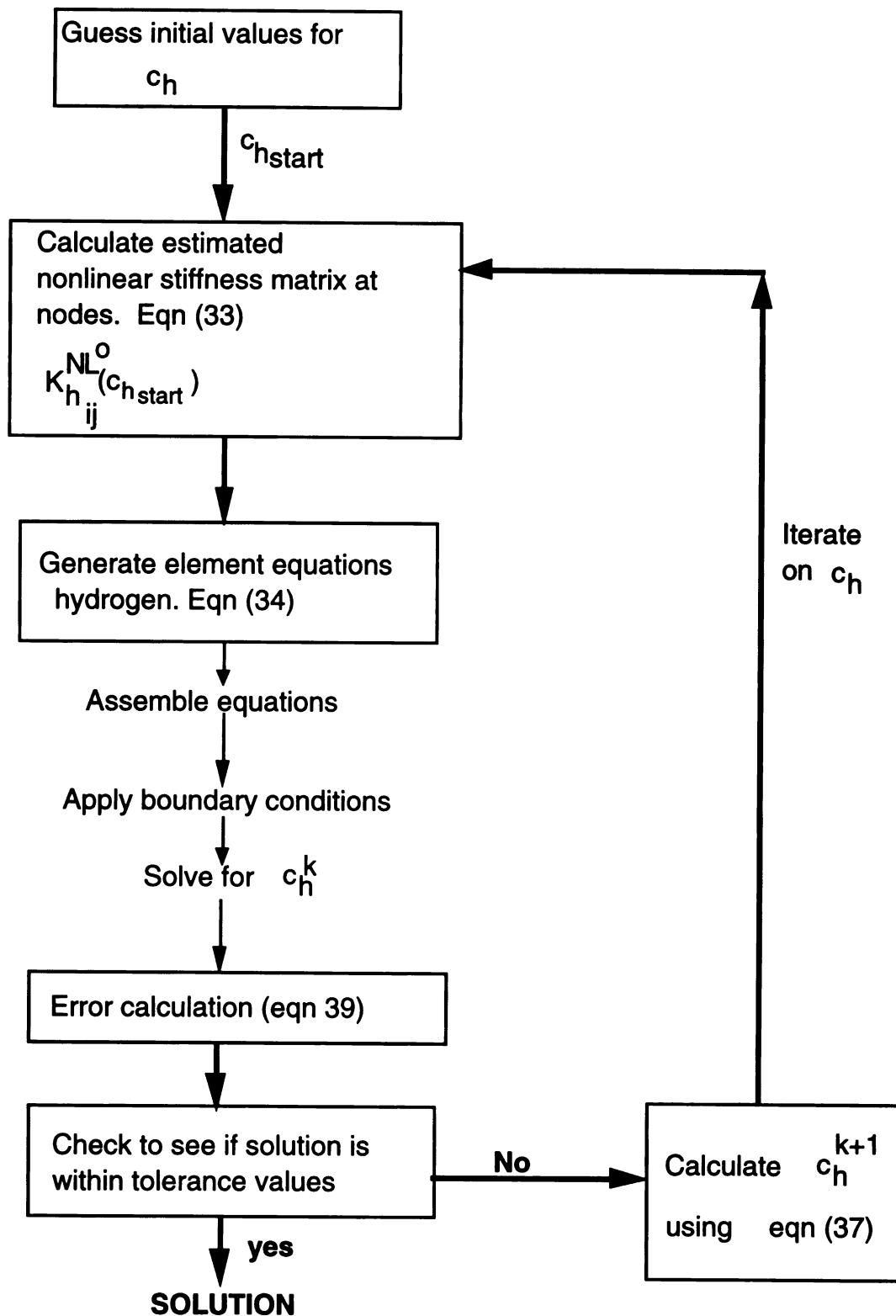
5.7 Postprocessing

Once the final solutions are obtained for a particular geometry, it remains to process the solutions. Postprocessing involves the computation of the gradient of the solution and plotting the solution contours and fluxes. This is done using a subroutine which calculates fluxes at either the center of each element or on the user designated side of each element. Another graphics program is used to plot the fluxes and the concentration contours.

References

1. Reddy, J.N.   An Introduction to the Finite Element Method; McGraw-Hill: New York, 1984

2. Ross, C.T.F., Finite Element Programs for Axisymmetric Problems in Engineering; John Wiley & Sons, New York, 1984

3. Finlayson, B.A.   Nonlinear Analysis in Chemical Engineering; McGraw-Hill: New York, 1980.

4. Carey, G.F. and Finlayson, B.A.   Orthogonal Collocation on Finite Elements. *Chemical Engineering Science*, 1975; **30**, 587-596

5. Leypoldt, JK, Gough DA.   Model of a Two-Substrate Enzyme Electrode for Glucose. *Anal. Chem.* 1984; **56**, 2896-2904

6. Gough DA, Lucisano JY, and Tse, PHS.   Two-dimensional enzyme electrode sensor for glucose. *Anal Chem* 1985; **57**: 2351-7

7. Villadsen, J.; Michelsen, M.L.   Solution of Differential Equation Models by Polynomial Approximation; Prentice-Hall: Englewood Cliffs: NJ, 1978.

8. Klumb L. A. and Horbett T.A., Design of insulin delivery devices based on glucose sensitvie memebranes, *J. Controlled Release*, **18** (1992) 59-80

9. Klumb L.A. and Horbett T.A., The effect of hydronium ion transport on the transient behavior of glucose sensitive membranes, *J. of Controlled Release*, **27**, 1993, 95-114

10. Press, William H.   Numerical Recipes: the art of Scientific Computing. Cambridge University Press: New York (1983)

Chapter 5.

Appendices

Appendix 5-1.

List of Variables:

General

c_j	concentration of species of interest at node j
ϕ_j	approximation function at node j
ψ_i	$= \phi_i$, approximation functions or polynomials derived using interpolation theory
Ω	domain under consideration
$[K^e]$	element stiffness matrix for element # e
$\{u^e\}$	unknown nodal values for element # e, in vector form
$\{F^e\}$	force or reaction vector for element # e, in vector form
$[\mathbf{K_{gl}}]$	global stiffness matrix for the problem
$\{\mathbf{F_{gl}}\}$	global load vector for the problem
V_i	reaction term at node i
c_i	nondimensional concentration for species i
v_i	stoichiometric coefficient for species i, ($v_g = 1$ for glucose, $v_o = 0.5$ for oxygen)
$\overline{V}\ (c_i, c_j)$	nondimensional reaction rate
c_{ij}	nondimensional concentration for species i at node j
n_ρ ; n_ζ	the normals in the ρ and ζ directions, respectively
$J_{ik}^{(e)}$	represents the flux into side k of element (e) corresponding to interpolation function ψ_i

$n_j^{(e)}$ node number j from element e

N_{tot} total number of nodes in the mesh

$Bi_i^{(e)}$ Biot number for species i at a boundary element e

ρ,ζ nondimensional cylindrical coordinates for problem

ξ,η natural coordinates within an element (see Appendix 5-2)

δ_{ij} Dirac Delta function (= 1 when i = j, = 0 for all i ≠ j)

$\hat{\psi}_i$ $= \hat{\psi}_i(\xi,\eta)$ are the element interpolation functions in natural coordinates shown in Figure 5-4

$error_{ij}$ error for a species i at node j from last iteration to current solution

x_{pic} fraction used to reset species concentrations if not within error tolerance

c_{ij}^k concentration of species i at node j for the current solution

c_{ij}^{k-1} concentration of species i at node j for the last iteration

c_{gbot} glucose concentration along side 4

c_{obot} oxygen concentration along side 4

$f(c_{gbot},c_{obot})$ minimization function used to minimize fluxes along destination layer

$fluxg_i$ flux of glucose at element i into the destination layer

$fluxo_i$ flux of oxygen at element i into the destination layer

$Xelem$ number of elements in the r-direction along the side 4

Elemental Matrices and Equations

$$\left[s^{(e)}_{ij}\right] = - \int_{\rho} \int_{\zeta} \left(\frac{\partial \psi_j}{\partial \rho}\frac{\partial \psi_i}{\partial \rho} + \varepsilon^2 \frac{\partial \psi_j}{\partial \zeta}\frac{\partial \psi_i}{\partial \zeta}\right)\rho^m \partial\rho\partial\zeta$$

general element stiffness matrix [eqn (14)]

$$\left[b^{(e)}_{k_{ij}}\right] = - \varepsilon^2 Bi^{(e)}_k \int_{\rho=\rho 1}^{\rho=\rho 2} \psi_i(\rho,\zeta_2)\psi_j(\rho,\zeta_2)\, \rho^m d\rho$$

contribution to element stiffness matrix from convective terms for species k [eqn (15)]

$$\left[R^{(e)}_{ij}\right] = \int_{\rho} \int_{\zeta} \psi_i(\rho,\zeta)\, \overline{V}(\Sigma c_{gj}\,\psi_j, \Sigma c_{oj}\,\psi_j)\, \rho^m\, \partial\rho\partial\zeta$$

Reaction term contribution [eqn (16)]

$$\left\{F^{(e)}_{k_i}\right\} = - \varepsilon^2 Bi^{(e)}_k\, c_g^* \int_{\rho=\rho 1}^{\rho=\rho 2} \psi_i(\rho,\zeta_2)\, \rho^m d\rho$$

convective term contribution to load vector for species k [eqn (17)]

$$\left[K^{(e)}_{k_{ij}} \right] = \left[s^{(e)}_{ij} + b^{(e)}_{k_{ij}} \right] \quad k = g, o, h$$

total elemental stiffness matrix for element # e [eqn (25)]

$$\left\{ \tilde{F}^{(e)}_{k_i} \right\} = \nu_k \left\{ R_i \right\} + \left\{ F^{(e)}_{k_i} \right\} \quad \nu_k = 1 \text{ for glucose; } \nu_k = \frac{1}{2} \text{ for oxygen}$$

$$\nu_k = -1 \text{ for hydrogen}$$

total load vector for element # e

Mathematical Notation

$$\nabla = \left(\frac{\partial}{\partial \rho}, \varepsilon \frac{\partial}{\partial \zeta} \right) \qquad \text{gradient term}$$

$$\nabla \bullet a = \left(\frac{1}{\rho^m} \frac{\partial}{\partial \rho} (\rho^m \ a) \ n_\rho + \varepsilon \frac{\partial a}{\partial \zeta} n_\zeta \right) \qquad \text{divergence term}$$

$$\int_\rho \int_\zeta a \ \rho^m \partial \rho \partial \zeta$$

volume integral for function a over domain Ω, bounded by ρ and ζ

$$\oint_\Gamma a \ d \ s \qquad \text{line integral for function a over a surface } \Gamma \text{ bounded by}$$

ds

$$\frac{\partial c}{\partial n} = (n_\rho + \varepsilon \ n_\zeta) \bullet \nabla c$$

definition of normal vector for concentrations

Appendix 5-2

Interpolation Theory

The trial functions given in Figure 5-4 were derived using interpolation theory, and are called the Lagrange family of interpolation functions. The construction procedure for interpolation functions depends on the geometry, the number and the position of the nodes and the number of primary unknowns identified at the nodes of the element. The interpolation functions given for each element in Figure 5-4 have the following properties,

(i) $\psi_i^{(e)}(\xi_j, \eta_j) = \delta_{ij}$ $i, j = 1, 2, \ldots, n_e$

where n_e = number of nodes per element

(ii) $\sum_{i=1}^{n_e} \psi_i^{(e)} = 1$

(iii) $\psi_i^{(e)} = 0$ outside the element $\Omega^{(e)}$

The Lagrange family of functions are constructed for elements with only one type of unknown per node; e.g. primary variables which are

all concentrations. The Lagrange family of interpolation functions for rectangular elements are derived using equation (A2-1).

$$\psi_i^{(e)}(\xi,\eta) = \prod_{\substack{j=1 \\ i \neq j}}^{n_\xi} \frac{\xi-x_j}{\xi_i-x_j} \prod_{\substack{j=1 \\ i \neq j}}^{n_\eta} \frac{\eta-y_j}{\eta_i-y_j}$$ (A2-1)

where n_ξ = total number of nodes in the ξ-direction,

and n_η = total number of nodes in the η-direction.

x_j = ξ-coordinate of jth point

y_j = η-coordinate of jth point

In using (A2-1), the element is split into the ξ-direction and the η-direction. The total number of nodes in the ξ-direction is given by n_ξ, and the n_ξ ξ-coordinates of those nodes are given by x_1, x_2, ..., x_{n_ξ}. The same terminology is used in the η-direction. The term ξ_i represents the coordinate value of node "i" in the ξ-direction. For example, for the quadratic rectangular element shown in Figure 5-4, n_ξ = 3, x_1= -1, x_2= 0, and x_3 = 1. The individual nodal coordinates for nodes 1, 8 and 4 along line x_1= -1, for example are $\xi_1 = \xi_8 = \xi_4 = -1$; and $\eta_1 = -1$, $\eta_8 = 0$ and $\eta_4 = 1$.

The formulation of the interpolation functions for triangular elements is slightly more complex, and uses area coordinates rather than the actual point coordinates. The linear interpolation functions are shown in Figure 5-4. Higher order functions can be constructed but were not used in this problem.

Master Elements

The elements shown in Figure 5-4 are master elements for the problem. Master elements all have the same geometry and use identical coordinate systems, thus each element has the same interpolation function. As described in the text the elements in the actual mesh have global coordinates, and thus each element has different values for the interpolation functions. This problem is overcome by using the Jacobian transformation to convert between the master elements and the actual isoparametric elements.

Isoparametric elements are those which can be used for the description of both the geometry of the element and the variation of dependent variables as shown below in equation (A2-2):

$$\rho(\xi,\eta) = \sum_{i=1}^{n_e} \rho_i \hat{\psi}_i \qquad \zeta(\xi,\eta) = \sum_{i=1}^{n_e} \zeta_i \hat{\psi}_i \qquad c_k(\xi,\eta) = \sum_{i=1}^{n_e} c_{ki} \hat{\psi}_i$$

$$(A2-2)$$

where k = glucose, oxygen or hydrogen and $\hat{\psi}_i = \hat{\psi}_i(\xi,\eta)$ are the element interpolation functions in natural coordinates shown in

Figure 5-4. The elements used in generating the finite-element mesh are isoparametric. Using isoparametric elements facilitates an accurate representation of irregular domains (curved boundaries). Elements which have irregular domains however create difficulties in computing the element coefficient matrices $[K^e]$ and column vectors, $\{F\}$ directly in terms of global coordinates ρ and ζ. This is overcome by introducing an invertible transformation, between the curvilinear element and the master elements illustrated in Figure 5-4. This transformation is illustrated in Figure A2-1. Figure A2-1 also shows how the actual elements in the finite-element mesh can be related to a master element. Different elements in the finite-element mesh can be generated from one master element simply by assigning the global coordinates of the elements.

Figure A2-1 - Transformation of Isoparametric Elements into Master Elements

η $\eta = 1$

$(-1,1)$ 4 3 $(1,1)$
$d\xi\, d\eta$
$\hat{\Omega}$ ξ
$\xi = 1$
$(-1,-1)$ 1 2 $(1,-1)$

$\rho = \rho\,(\xi, \eta)$
$\zeta = \zeta\,(\xi, \eta)$

$\xi = \xi\,(\rho, \zeta)$
$\eta = \eta\,(\rho, \zeta)$

ζ Ω^e ρ

Ω^1 Ω^2 Ω^3

$\rho = \rho\,(\xi, 1)$
$\zeta = \zeta\,(\xi, 1)$

η
4 3
$d\rho\, d\zeta = J\, d\xi\, d\eta$
ξ
ζ
1 Ω^e 2

$\rho = \rho\,(1, \eta)$
$\zeta = \zeta\,(1, \eta)$

ρ
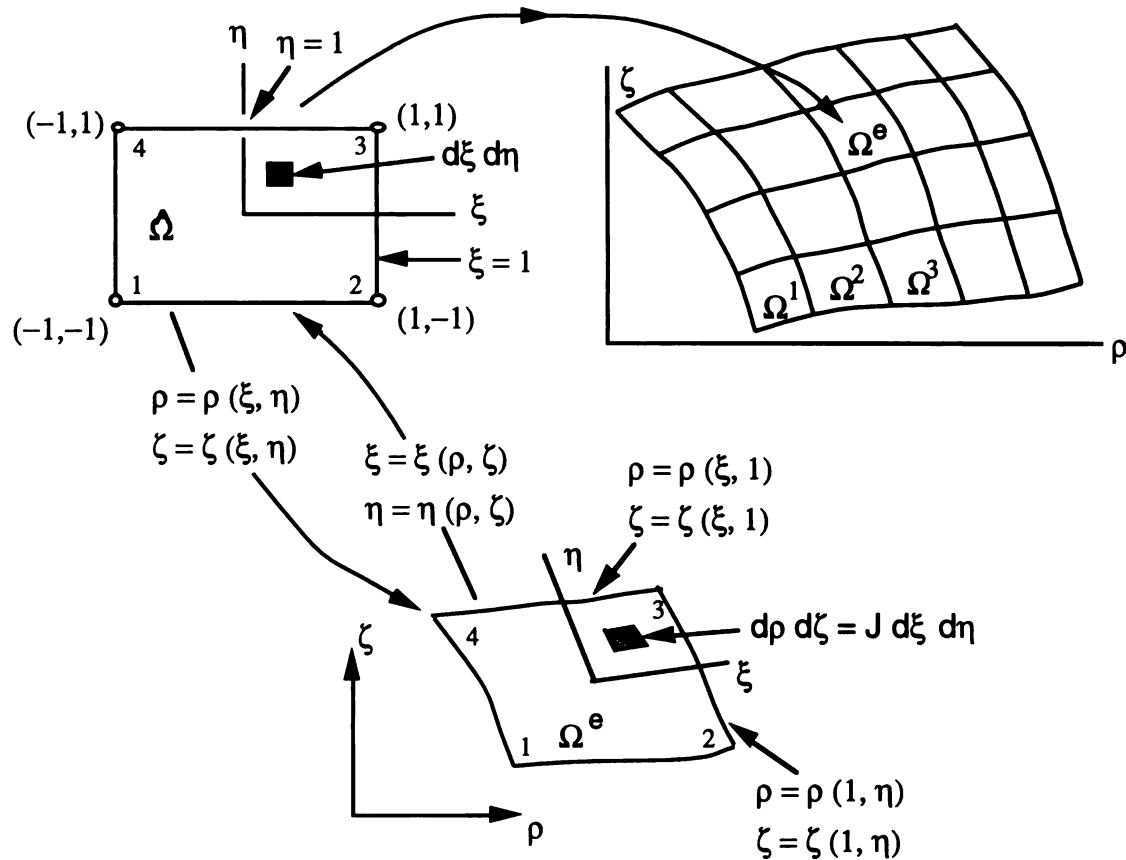
The coordinate transformation, J the Jacobian, which is required to map functions from natural coordinates into global coordinates, is illustrated above. The Jacobian maps the line $\xi = 1$ in the domain $\hat{\Omega}$ of natural coordinates into the curve defined parametrically by $\rho = \rho(1, \eta)$; $\zeta = \zeta(1, \eta)$ in the $\rho\zeta$ plane in the Ω domain. This can be done for each element. For each element (e) in Ω^e, the Jacobian matrix is defined as:

$$[J] = \begin{bmatrix} \dfrac{\partial \rho}{\partial \xi} & \dfrac{\partial \zeta}{\partial \xi} \\[2ex] \dfrac{\partial \rho}{\partial \eta} & \dfrac{\partial \zeta}{\partial \eta} \end{bmatrix} = \begin{bmatrix} \displaystyle\sum_{i=1}^{n_e} \rho_i \dfrac{\partial \hat{\psi}_i}{\partial \xi} & \displaystyle\sum_{i=1}^{n_e} \zeta_i \dfrac{\partial \hat{\psi}_i}{\partial \xi} \\[3ex] \displaystyle\sum_{i=1}^{n_e} \rho_i \dfrac{\partial \hat{\psi}_i}{\partial \eta} & \displaystyle\sum_{i=1}^{n_e} \zeta_i \dfrac{\partial \hat{\psi}_i}{\partial \eta} \end{bmatrix} \qquad \text{(A2-3)}$$

$$= \begin{bmatrix} \dfrac{\partial \hat{\psi}_1}{\partial \xi} & \dfrac{\partial \hat{\psi}_2}{\partial \xi} & \cdots & \dfrac{\partial \hat{\psi}_{n_e}}{\partial \xi} \\[3ex] \dfrac{\partial \hat{\psi}_1}{\partial \eta} & \dfrac{\partial \hat{\psi}_2}{\partial \eta} & \cdots & \dfrac{\partial \hat{\psi}_{n_e}}{\partial \eta} \end{bmatrix} \begin{bmatrix} \rho_1 & \zeta_1 \\ \rho_2 & \zeta_2 \\ \cdot & \cdot \\ \cdot & \cdot \\ \cdot & \cdot \\ \rho_{n_e} & \zeta_{n_e} \end{bmatrix} \qquad \text{(A2-3b)}$$

Equation (A2-2) relates the global coordinates to the natural coordinates, thus calculating ρ^m. Equation (A2-3) gives the coordinate transformation between the two domains, relating $\partial \rho \partial \zeta = [J] \partial \xi \partial \eta$. The terms $\dfrac{\partial \psi_i}{\partial \rho}$, and $\dfrac{\partial \psi_i}{\partial \zeta}$ are calculated by using the inverse Jacobian as shown in (A2-4) below.

$$\left\{ \begin{array}{c} \dfrac{\partial \psi_i}{\partial \rho} \\[2ex] \dfrac{\partial \psi_i}{\partial \zeta} \end{array} \right\} = \begin{bmatrix} \dfrac{\partial \xi}{\partial \rho} & \dfrac{\partial \eta}{\partial \rho} \\[2ex] \dfrac{\partial \xi}{\partial \zeta} & \dfrac{\partial \eta}{\partial \zeta} \end{bmatrix} \left\{ \begin{array}{c} \dfrac{\partial \hat{\psi}_i}{\partial \xi} \\[2ex] \dfrac{\partial \hat{\psi}_i}{\partial \eta} \end{array} \right\} = [J^*] \left\{ \begin{array}{c} \dfrac{\partial \hat{\psi}_i}{\partial \xi} \\[2ex] \dfrac{\partial \hat{\psi}_i}{\partial \eta} \end{array} \right\} \qquad \text{(A2-4)}$$

Using the equations (2), (3) and (4) shown above, the interpolation functions and their derivatives are obtained in global coordinates for each element.

Appendix 5-3.

Handling the Nonlinear Terms

Other Methods for Handling of Nonlinear Reaction Term

Three methods for handling the nonlinear reaction term are listed in this appendix. The first method simplifies the problem by assuming a constant reaction term. Using a constant reaction rate decouples the glucose and oxygen equations and each species can be solved for separately. The second two methods involve solving for the glucose and oxygen concentrations simultaneously. These methods were not used in the program but are mentioned here for completeness.

Method (1) - Approximate Reaction rate as a constant.

The simplest method is to approximate the reaction term as a constant, and update it at each iteration. This would reduce the reaction matrix to a vector which could be included in the load vector.

$$\overline{V} = \frac{\phi^2}{1 + \kappa_g/(\Sigma c^o_{g_j} \psi_j) + \kappa_o/(\Sigma c^o_{o_j} \psi_j)} = V^o \equiv \text{constant}$$

$$\left[R^{(e)}_{ij}\right] = \int_\rho \int_\zeta \psi_i(\rho,\zeta) \, V^o \, \rho^m \, \partial\rho\partial\zeta \Rightarrow \{R_i\} \qquad \text{(A3-1)}$$

Using this method requires having a constant reaction term over the entire area of the problem. Due to this, method (1) was incorporated into the program, but was not used in calculating the results. This method proved useful in checking the accuracy of the program against some analytical problems.

Alternate methods (2) and (3) for evaluating the nonlinear reaction term are simple in concept but quite complicated in application because the element equations become significantly more complicated. A brief outline of each method is given below. Method (2) involves expressing the reaction rate as a function of old values of the concentrations times the actual concentration. Method (3) linearizes the nonlinear reaction rate by representing it in a Taylor series. These methods were not used in the program code but could be implemented if desired. They are discussed here for completeness.

Method (2) - Newton-Raphson method.

This method is the most common method for solving nonlinear sets of equations. Due to the way that this problem is formulated,

however, this method was rejected for use because of the added computation it generates. In using this method, the reaction rate is rewritten as a function of c_g^o and c_o^o, the old values of the concentrations, and the current variable c_{gj} or c_{oj}. This results in a nonlinear symmetric matrix, $[K^{NL}]$, for each species. Rewriting equation (5-20) in this fashion over an element, $\left[R_{ij}^{(e)}\right]$ is expressed as:

$$\left[R_{kij}^{(e)}\right] = \sum_{j=1}^{n_e} c_{kj} \; KNL_{kij}^{(e)}(c_g^o, c_o^o) \qquad (A3\text{-}2);$$

where

$$KNL_{kij}^{(e)}(c_g^o, c_o^o) =$$

$$\int_\rho \int_\zeta \psi_i(\rho,\zeta)\; \psi_j(\rho,\zeta) \; \frac{\phi^2}{(\Sigma c_{kj}^o \; \psi_j)(1 + \dfrac{\kappa_l}{(\Sigma c_{lj}^o \; \psi_j)}) + \kappa_k} \; \rho^m \, \partial\rho\partial\zeta$$

subscript k = glucose or oxygen, and

subscript l = oxygen or glucose, other species than k

c_g^o, c_o^o = estimated concentrations for glucose and oxygen

and $\qquad c_k^o = \Sigma c_{kj}^o \; \psi_j \qquad\qquad\qquad (A3\text{-}3)$

Equations (A3-2) and (A3-3) are written in general and apply to either glucose or oxygen; for example when k = g or glucose, l = o or oxygen, and vice-versa. Unlike the previous two methods where the approximate reaction term is included in the load vector, thereby decoupling element equations (23) and (24), using equation (A3-2) includes the reaction term in the element stiffness matrix. Inserting equation (A3-2) into equations (18) and (19), the element equations become:

$$\sum_{j=1}^{n_e} \left[s^{(e)}_{ij} + b^{(e)}_{g_{ij}} - KNL^{(e)}_{g_{ij}}(c^o_g, c^o_o) \right] c^{(e)}_{gj} = \left\{ F^{(e)}_{gi} \right\} \qquad (A3-4)$$

for glucose and,

$$\sum_{j=1}^{n_e} \left[s^{(e)}_{ij} + b^{(e)}_{o_{ij}} - \frac{1}{2} KNL^{(e)}_{o_{ij}}(c^o_g, c^o_o) \right] c^{(e)}_{oj} = \left\{ F^{(e)}_{oi} \right\} \qquad (A3-5)$$

for oxygen.

In writing equations (A3-4) and (A3-5), the same notation as in equations (5-18) and (5-19) is used; that is the element stiffness matrix $s^{(e)}_{ij}$ is given by (5-14), the boundary term by (5-15), and the load vector by (5-17). The nonlinear portion of the element stiffness matrix, $KNL^{(e)}_{k_{ij}}$, is given by equation (A3-3).

At this point there are two different ways to solve this problem. An analysis similar to the method documented in the text of chapter 5, where the equations are decoupled by using estimated values of $c_{gj} = c^o_{gj}$ and $c_{oj} = c^o_{oj}$ to calculate K^{NL} can be performed. The equations can then be solved separately for the glucose and oxygen concentrations. The glucose and oxygen solutions are recoupled by iterating until the reaction terms given by (A3-2) and (A3-3) converge for both glucose and oxygen. This analysis was tried but lead to slower convergence and more instabilities than the method used. This analysis also involves more calculations than solving equations (5-23) and (5-24) directly and thus was not used.

The other, more conventional method is to solve for the glucose and oxygen concentrations simultaneously by combining the n_e by n_e matrix equations given by (A3-4) and (A3-5), into one matrix equation given by (A3-6) which is $2n_e$ by $2n_e$. This means that we now have two primary variables per node, the glucose and oxygen concentrations. Combining (A3-4) and (A3-5) into one set of matrix equations, we have the complete matrix equations for each element:

$$\begin{bmatrix} s_{ij}^{(e)}+b_{g_{ij}}^{(e)}- KNL_{g_{ij}}^{(e)}(c_g^o,c_o^o) & 0 \\ 0 & s_{ij}^{(e)}+b_{o_{ij}}^{(e)}- \frac{1}{2} KNL_{o_{ij}}^{(e)}(c_g^o,c_o^o) \end{bmatrix} \begin{Bmatrix} c_{g_j}^{(e)} \\ c_{o_j}^{(e)} \end{Bmatrix}$$

$$= \begin{Bmatrix} F_{g_i}^{(e)} \\ F_{o_i}^{(e)} \end{Bmatrix} \qquad \text{(A3-6)}$$

Each of the four terms in the above element matrix is an n_e by n_e term, where n_e is the number of nodes per element. (This includes the zeros which are matrices of n_e by n_e zeros.) The entire matrix given in (A3-6) is thus $2*n_e$ by $2*n_e$. Using a matrix of this size involves twice the amount of computation as does the method in the text. In order to decrease the bandwidth of the matrix, and thereby reduce the computation time, the matrix equations above are rearranged as:

$$
\begin{bmatrix}
K^T_{g_{11}} & 0 & K^T_{g_{12}} & 0 & \cdots & K^T_{g_{1ne}} & 0 \\
0 & K^T_{o_{11}} & 0 & K^T_{o_{12}} & \cdots & 0 & K^T_{o_{1ne}} \\
K^T_{g_{21}} & 0 & K^T_{g_{22}} & 0 & \cdots & K^T_{g_{2ne}} & 0 \\
0 & K^T_{o_{21}} & 0 & K^T_{o_{22}} & \cdots & 0 & K^T_{o_{2ne}} \\
\cdots & \cdots & \cdots & \cdots & \cdots & \cdots & \cdots \\
K^T_{g_{ne1}} & 0 & K^T_{g_{ne2}} & 0 & \cdots & K^T_{g_{nene}} & 0 \\
0 & K^T_{o_{ne1}} & 0 & K^T_{o_{ne2}} & \cdots & 0 & K^T_{o_{nene}}
\end{bmatrix}
\begin{Bmatrix}
c_{g_1} \\ c_{o_1} \\ c_{g_2} \\ c_{o_2} \\ \cdots \\ c_{g_{ne}} \\ c_{o_{ne}}
\end{Bmatrix}
=
\begin{Bmatrix}
F_{g_1} \\ F_{o_1} \\ F_{g_2} \\ F_{o_2} \\ \cdots \\ F_{g_{ne}} \\ F_{o_{ne}}
\end{Bmatrix}
\qquad \text{(A3-7)}
$$

where:

$$
K^T_{k_{ij}} = s_{ij} + b_{k_{ij}} - v_k \, KNL^{(e)}_{k_{ij}}(c^o_g, c^o_o)
$$

$$
k = g, o;
$$

$$
i,j = 1,\dots,n_e.
$$

The element equations are now given by (A3-7). At this point the Newton-Raphson method can be employed to solve (A3-7). To simplify the bookkeeping of the problem the Newton-Raphson method is applied before assembly, and the modified element equations are assembled.

To further simplify applying Newton's method to calculate the

next values of c_{gj}^{n+1} and c_{oj}^{n+1} from the estimated c_{gj}^{n} and c_{oj}^{n}, let the vector of unknowns be designated by $\tilde{q}$. Then in matrix form, equation (A3-7) becomes:

$$\tilde{q} = \begin{Bmatrix} c_{g1} \\ c_{o1} \\ c_{g2} \\ c_{o2} \\ \dots \\ c_{gne} \\ c_{one} \end{Bmatrix}$$

$$[K + C(\tilde{q})] \{\tilde{q}\} = \{F\} \qquad\qquad (A3-8)$$

In equation (A3-8) the matrices K, and C and the vector F are defined in terms of the species stiffness matrices $K_{kij}^{(e)}$ (equation 5-25), the nonlinear reaction matrix $K^{NL}{}_{kij}^{(e)}$ (A3-3), and the species load vector $F_{ki}^{(e)}$ (5-17) as follows:

for $i = 1,...., ne$; $j = 1, ..., ne$

$l = 2*i - 1$; $m = 2*j - 1$

$$\mathbf{K}_{lm} = K_{g_{ij}}, \qquad\qquad \mathbf{K}_{l+1\,m+1} = K_{o_{ij}},$$

(l,m both odd indices) (l,m both even indices)

$$\mathbf{K}_{l+1\,m} = \mathbf{K}_{l\,m+1} = 0$$

and

$$\mathbf{C}_{lm} = - KNL^{(e)}_{g_{ij}}(c^o_g, c^o_o) \qquad\qquad \mathbf{C}_{l+1\,m+1} = -\frac{1}{2} KNL^{(e)}_{o_{ij}}(c^o_g, c^o_o)$$

$$\mathbf{C}_{l+1\,m} = \mathbf{C}_{l\,m+1} = 0$$

and

$$F_l = F_{g_i} \qquad F_{l+1} = F_{o_i}.$$

Now applying the Newton-Raphson method to calculate the change in $\tilde{q}$, where $\Delta\tilde{q}^{n+1} = \tilde{q}^{n+1} - \tilde{q}^n$ such that $\tilde{q}^n$ is known, and $\tilde{q}^o$ is the first guess, the pre-assembled element equations become:

$$\left[\mathbf{K} + \mathbf{C}(\tilde{q}^n) + \left.\frac{\partial \mathbf{C}(\tilde{q}^n)}{\partial \tilde{q}}\right|_{\tilde{q}}^n \tilde{q}^n \right] \{\Delta\tilde{q}^{n+1}\} = \{F\} - [\mathbf{K} + \mathbf{C}(\tilde{q}^n)]\{\tilde{q}^n\}$$

or, more concisely:

$$[\mathbf{A}]^{(e)} \{\Delta\tilde{q}^{n+1}\} = \{\mathbf{B}\}^{(e)} \qquad\qquad \text{(A3-9)}$$

In equation (A3-9), the quantity $\left(\left. \dfrac{\partial C(\tilde{q}^n)}{\partial \tilde{q}} \right|_{\tilde{q}^n} \tilde{q}^n \right)$ is a non-symmetric matrix of size $2 \cdot n_e$ by $2 \cdot n_e$ and is given by,

$$\left[\left. \frac{\partial C(\tilde{q}^n)}{\partial \tilde{q}} \right|_{\tilde{q}^n} \tilde{q}^n \right]_{lm} = \sum_{x=1}^{2 \cdot n_e} \frac{\partial C_{lx}}{\partial \tilde{q}_m} \tilde{q}_x^n \qquad (A3\text{-}10)$$

with C_{lm} and $\tilde{q}^n$ defined by (A3-8). This implies that every entry in the matrix $A^{(e)}$ must be saved, and the complete set of element equations are given by (A3-9).

In using this method, the next values of the glucose and oxygen concentrations are solved for simultaneously by determining the solution of the change in the global $\tilde{q}_{gl}$ vector, $\Delta \tilde{q}_{gl}^{n+1} = \tilde{q}_{gl}^{n+1} - \tilde{q}_{gl}^n$. This is accomplished by inverting the assembled modified stiffness matrix, A_{gl}. At this point it was decided not to use this method due to the added computation that was required by assembling and inverting the nonsymmetric matrix A_{gl}. (The method of assembly for a nonsymmetric matrix of the dimension $2 \cdot n_t$ by $2 \cdot n_t$ where n_t is the total number of nodes can be found in many finite element texts and is not repeated here.)

Method (3) - Linearization of Nonlinear Reaction Term

Method (3) linearizes the nonlinear reaction rate by representing it in a Taylor series in terms of the unknown concentrations, c_{gj} and c_{oj}, and the estimated values c_{gj}^o, and c_{oj}^o. The linearization was considered because of the abrupt discontinuities in the reaction term when it is expressed in the form of equation (4-18). The linearization is shown below in equation (A3-11).

$$\overline{V}\left(\Sigma c_{gj}\,\psi_j,\,\Sigma c_{oj}\,\psi_j\right) = V^o + \left(\Sigma c_{gj}\,\psi_j - c_g^o\right)d_1^o + \left(\Sigma c_{oj}\,\psi_j - c_o^o\right)d_2^o$$

$$(A3\text{-}11)$$

where,

$$V^o = \overline{V}\left(c_g^o, c_o^o\right) = \frac{\phi^2}{1 + \kappa_g/c_g^o + \kappa_o/c_o^o}$$

$$d_1^o = \frac{\partial\,\overline{V}}{\partial c_g} = \frac{\phi^2\,\kappa_g}{(c_g^o)^2\left(1 + \kappa_g/c_g^o + \kappa_o/c_o^o\right)^2}$$

$$d_2^o = \frac{\partial\,\overline{V}}{\partial c_o} = \frac{\phi^2\,\kappa_o}{(c_o^o)^2\left(1 + \kappa_g/c_g^o + \kappa_o/c_o^o\right)^2}$$

and,

$$c_k^o = \sum_{j=1}^{n_e} c_{kj}^o\,\psi_j(\rho,\zeta)$$

Using equation (A3-11) as a definition for the reaction term in equation (5-16), the reaction matrix becomes:

$$\left[R_{ij}^{(e)}\right] =$$

$$\int_{\rho}\int_{\zeta} \psi_i(\rho,\zeta)\,\{V^o + (\Sigma c_{gj}\,\psi_j - c_g^o)d_1^o + (\Sigma c_{oj}\,\psi_j - c_o^o)d_2^o\}\,\rho^m\,\partial\rho\partial\zeta$$

$$= \int_{\rho}\int_{\zeta} \psi_i(\rho,\zeta)\,\{V^o - c_g^o d_1^o - c_o^o d_2^o\}\rho^m\partial\rho\partial\zeta +$$

$$\sum_{j=1}^{n_e}\left[\int_{\rho}\int_{\zeta}\psi_i(\rho,\zeta)\psi_j(\rho,\zeta)d_1^o\rho^m\partial\rho\partial\zeta\right]c_{gj} +$$

$$\sum_{j=1}^{n_e}\left[\int_{\rho}\int_{\zeta}\psi_i(\rho,\zeta)\psi_j(\rho,\zeta)d_2^o\rho^m\partial\rho\partial\zeta\right]c_{oj}$$

$$= F_{R_i}^o + \sum_{j=1}^{n_e}\left[D1_{ij}^o c_{gj} + D2_{ij}^o c_{oj}\right] \qquad (A3\text{-}12)$$

Inserting equation (A3-12) into equations (18) and (19) and rearranging slightly, the element equations become:

$$\sum_{j=1}^{n_e} \left[\left(s_{ij}^{(e)} + b_{g_{ij}}^{(e)} - D1_{ij}^{(e)}(c_g^o, c_o^o) \right) c_{g_j}^{(e)} - \left(D2_{ij}^{(e)}(c_g^o, c_o^o) \right) c_{o_j}^{(e)} \right]$$

$$= \left\{ F_{g_i}^{(e)} + F_{R_i}^{(e)}(c_g^o, c_o^o) \right\} \tag{A3-13}$$

for glucose and,

$$\sum_{j=1}^{n_e} \left[-\frac{1}{2} \left(D1_{ij}^{(e)}(c_g^o, c_o^o) \right) c_{g_j}^{(e)} + \left(s_{ij}^{(e)} + b_{o_{ij}}^{(e)} - \frac{1}{2} D2_{ij}^{(e)}(c_g^o, c_o^o) \right) c_{o_j}^{(e)} \right]$$

$$= \left\{ F_{o_i}^{(e)} + \frac{1}{2} F_{R_i}^{(e)}(c_g^o, c_o^o) \right\} \tag{A3-14}$$

for oxygen.

Combining equations (A3-13) and (A3-14) into one matrix equation, size 2^*n_e by 2^*n_e, the element equations are written as:

$$
\begin{bmatrix}
s_{ij}^{(e)} + b_{gij}^{(e)} - D_{1ij}^{(e)}(c_g^o, c_o^o) & | & -D_{2ij}^{(e)}(c_g^o, c_o^o) \\
-\frac{1}{2} D_{1ij}^{(e)}(c_g^o, c_o^o) & | & s_{ij}^{(e)} + b_{oij}^{(e)} - \frac{1}{2} D_{2ij}^{(e)}(c_g^o, c_o^o)
\end{bmatrix}
\begin{Bmatrix}
c_{gj}^{(e)} \\
c_{oj}^{(e)}
\end{Bmatrix}
$$

$$
= \begin{Bmatrix}
F_{gi}^{(e)} + F_{Ri}^{(e)}(c_g^o, c_o^o) \\
F_{oi}^{(e)} + \frac{1}{2} F_{Ri}^{(e)}(c_g^o, c_o^o)
\end{Bmatrix} \tag{A3-15}
$$

where

$$
D_{1ij}^{(e)}(c_g^o, c_o^o) = \int_\rho \int_\zeta \psi_i(\rho, \zeta) \psi_j(\rho, \zeta) d_1^o \, \rho^m \partial \rho \partial \zeta
$$

$$
D_{2ij}^{(e)}(c_g^o, c_o^o) = \int_\rho \int_\zeta \psi_i(\rho, \zeta) \psi_j(\rho, \zeta) d_2^o \, \rho^m \partial \rho \partial \zeta
$$

$$
F_{Ri}^{(e)}(c_g^o, c_o^o) = \int_\rho \int_\zeta \psi_i(\rho, \zeta) \{V^o - c_g^o d_1^o - c_o^o d_2^o\} \rho^m \partial \rho \partial \zeta
$$

and, $s_{ij}^{(e)}$, $b_{kij}^{(e)}$ and $F_{ki}^{(e)}$ are defined as before.

At this point, the element equations can be rearranged as was outlined in method (2) and the Newton-Raphson method can be applied. The rearrangement of equation (A3-15) generates cross

terms in the final matrix which makes the element matrix analogous to (A3-7) nonsymmetric. This in turn complicates the application of the Newton-Raphson method and requires excessive numerical computations. This method was originally considered due to the some of the numerical problems which occured with the reaction term in the form of (4-18) for large values of the Thiele modulus, ϕ^2. This method proved, however, to add much more computation to the problem and was rejected unless more accuracy was required.

Handling the Nonlinear Hydrogen Terms

If the Newton Raphson method is used to handle the nonlinear diffusivity terms in equation (5-32), then the element equation needs to be reformulated to solve for the change in hydrogen concentration, $\Delta \tilde{c}_h^{n+1}$, at the $(n+1)^{st}$ iteration, given the values for the hydrogen concentration at the nth iteration. The analysis is similar to method (2) used above, equations (A3-8) through (A3-10) using only one variable instead of two. Starting with equation (5-32) for the element equation, and placing it in the same form as (A3-8), the formulation becomes:

$$\left[K + K^{NL}(\tilde{c}_h) \right] \left\{ \tilde{c}_h \right\} = \left\{ \tilde{F}_h \right\} \qquad \text{(A3-16)}$$

Following the same analysis as method (2) above by applying the Newton-Raphson method on each element, equation (A3-16) becomes analogous to (A3-9) where the **A** matrix and the **B** vector are given by:

$$[\mathbf{A}]^{(e)} \{\Delta \tilde{c}_h^{n+1}\} = \{\mathbf{B}\}^{(e)} \qquad (A3\text{-}17)$$

where,

$$[\mathbf{A}] = \left[K + K^{NL}(\tilde{c}_h^n) + \left.\frac{\partial K^{NL}(\tilde{c}_h^n)}{\partial \tilde{c}_h}\right|_{\tilde{c}_h^n} \tilde{c}_h^n \right], \text{ and}$$

$$\{\mathbf{B}\} = \left\{\tilde{F}_h\right\} - [K + K^{NL}(\tilde{c}_h^n)] \{\tilde{c}_h^n\}$$

$$\{\Delta \tilde{c}_h^{n+1}\} = \{\tilde{c}_h^{n+1}\} - \{\tilde{c}_h^n\}$$

In equation (A3-17), the quantity $\left(\left.\dfrac{\partial K^{NL}(\tilde{c}_h^n)}{\partial \tilde{c}_h}\right|_{\tilde{c}_h^n} \tilde{c}_h^n \right)$ is a non-symmetric matrix of size n_e by n_e and is given by,

$$\left[\frac{\partial K^{NL}(\tilde{c}_h{}^n)}{\partial \tilde{c}_h}\bigg|_{\tilde{c}_h{}^n}\tilde{c}_h{}^n\right]_{ij} = \sum_{x=1}^{n_e}\frac{\partial K^{NL}_{ix}}{\partial \tilde{c}_{hj}}\tilde{c}_{hx}{}^n =$$

$$\sum_{x=1}^{n_e}\left[2c_{tb}\kappa_h\int_\rho\int_\zeta\left(\frac{\psi_j}{(\kappa_h+\Sigma c_{hm}\psi_m)^3}\right)\left(\frac{\partial\psi_i}{\partial\rho}\frac{\partial\psi_x}{\partial\rho}+\varepsilon^2\frac{\partial\psi_i}{\partial\zeta}\frac{\partial\psi_x}{\partial\zeta}\right)\rho^m\partial\rho\partial\zeta\right]c_{hx}{}^n$$

$$+ \varepsilon^2 y_b^{(e)}\sum_{x=1}^{n_e}\left[\int_{\rho=\rho1}^{\rho=\rho2}\left(\frac{\psi_i(\rho,\zeta_2)\psi_j(\rho,\zeta_2)}{(\kappa_h+\Sigma c_{hm}\psi_m)^2}\right)\psi_x(\rho,\zeta_2)\,\rho^m d\rho\right]c_{hx}{}^n$$

$$(A3\text{-}18)$$

Due to the asymmetry shown in equation (A3-18), each entry in matrix [A] must be calculated and saved. The global form of matrix [A_g] can be inverted once it is assembled, to solve for $\{\Delta\tilde{c}_{h_{global}}{}^{n+1}\}$. The new values of c_h are calculated from this and the process is repeated until the new and old values of c_h are within tolerance.

As mentioned before, the Newton-Raphson method requires much more computer space and time due to the asymmetry involved. This method was therefore not used and the previous method of guessing c_h and solving was used.

Appendix 5-4.

Assembly and Applying Boundary Conditions: Example

The assembly part of a finite element program is simply a matter of book-keeping between the element node numbers and the global node numbers. This is best shown by example. Figure A4-1 shows a simple two by two element mesh. The four elements are numbered in rows and their numbers are designated by italic type surrounded by circles. The global node numbers are shown by bold type whereas the element node numbers are given in italic type. In this figure, it is assumed that each element has 4 nodes, and that each node has only one primary variable. For a four node element with one unknown per node, the elemental stiffness matrix is four by four and the load and solution vectors are each four by one. In the case of only one primary variable, the global equation $[K_{gl}] \{U\} = \{F_{gl}\}$ has nine unknowns corresponding to the nine nodes in the mesh and consequently the global stiffness matrix is nine by nine. The solution to the problem is to solve for the concentrations at the nine nodes and thus it is necessary to assemble the four element equations into one global equation.

Figure A4-1 : Assembly of a 4 element mesh
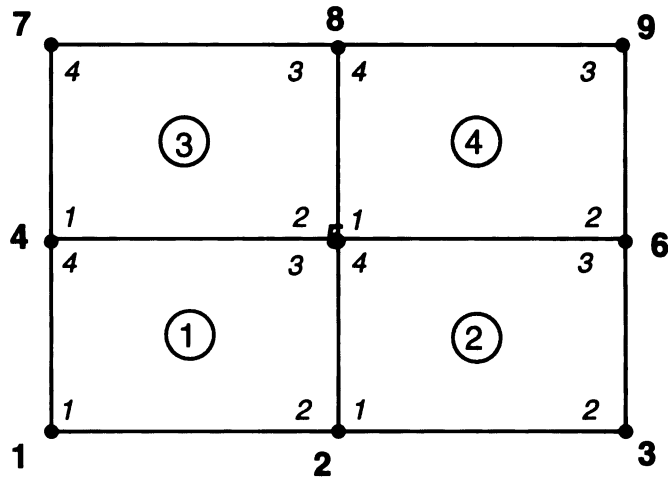
In order to do this the interelement continuity conditions are applied to the element equations and the correct combination of element values are placed in the global equation. The interelement connectivity conditions for this example are shown in the Table A4-1 below. For example at global node 2, there are contributions from element 1, node 2 and element 2, node 1. In order to put this altogether one needs to express each element equation in terms of the global nodal values according to the conditions given in Tables A4-1.

Table A4-1: Correspondence between global and local nodes

global node	local node contribution	primary nodal equality
1	$n_1^{(1)}$	$U_1 = u_1^{(1)}$
2	$n_2^{(1)}, n_1^{(2)}$	$U_2 = u_2^{(1)} = u_1^{(2)}$
3	$n_2^{(2)}$	$U_3 = u_2^{(2)}$
4	$n_4^{(1)}, n_1^{(3)}$	$U_4 = u_4^{(1)} = u_1^{(3)}$
5	$n_3^{(1)}, n_4^{(2)}, n_1^{(4)}, n_2^{(3)}$	$U_5 = u_3^{(1)} = u_4^{(2)} = u_1^{(4)} = u_2^{(3)}$
6	$n_3^{(2)}, n_2^{(4)}$	$U_6 = u_3^{(2)} = u_2^{(4)}$
7	$n_4^{(3)}$	$U_7 = u_4^{(3)}$
8	$n_3^{(3)}, n_4^{(4)}$	$U_8 = u_3^{(3)} = u_4^{(4)}$
9	$n_3^{(4)}$	$U_9 = u_3^{(4)}$

For this simple problem, each element equation is given by

$$\sum_{j=1}^{4} \left[K_{ij}^{(e)} \right] u_j^{(e)} = \left\{ F_i^{(e)} \right\}.$$ The goal is to have a set of equations

in terms of the global nodal values U_i. Using the relations given in

Table A4-1, these equations are expressed in terms of the global nodal values U_i for the first two elements below.

Element 1: (A4-1)

$$
\begin{bmatrix}
K_{11}^{(1)} & K_{12}^{(1)} & 0 & K_{14}^{(1)} & K_{13}^{(1)} & 0 & 0 & 0 & 0 \\
K_{21}^{(1)} & K_{22}^{(1)} & 0 & K_{24}^{(1)} & K_{23}^{(1)} & 0 & 0 & 0 & 0 \\
0 & 0 & 0 & 0 & 0 & 0 & 0 & 0 & 0 \\
K_{41}^{(1)} & K_{42}^{(1)} & 0 & K_{44}^{(1)} & K_{43}^{(1)} & 0 & 0 & 0 & 0 \\
K_{31}^{(1)} & K_{32}^{(1)} & 0 & K_{34}^{(1)} & K_{33}^{(1)} & 0 & 0 & 0 & 0 \\
0 & 0 & 0 & 0 & 0 & 0 & 0 & 0 & 0 \\
0 & 0 & 0 & 0 & 0 & 0 & 0 & 0 & 0 \\
0 & 0 & 0 & 0 & 0 & 0 & 0 & 0 & 0 \\
0 & 0 & 0 & 0 & 0 & 0 & 0 & 0 & 0
\end{bmatrix}
\begin{Bmatrix}
U_1 \\ U_2 \\ U_3 \\ U_4 \\ U_5 \\ U_6 \\ U_7 \\ U_8 \\ U_9
\end{Bmatrix}
=
\begin{Bmatrix}
F_1^{(1)} \\ F_2^{(1)} \\ 0 \\ F_4^{(1)} \\ F_3^{(1)} \\ 0 \\ 0 \\ 0 \\ 0
\end{Bmatrix}
$$

Element 2: (A4-2)

$$
\begin{bmatrix}
0 & 0 & 0 & 0 & 0 & 0 & 0 & 0 & 0 \\
0 & K_{11}^{(2)} & K_{12}^{(2)} & 0 & K_{14}^{(2)} & K_{13}^{(2)} & 0 & 0 & 0 \\
0 & K_{21}^{(2)} & K_{22}^{(2)} & 0 & K_{24}^{(2)} & K_{23}^{(2)} & 0 & 0 & 0 \\
0 & 0 & 0 & 0 & 0 & 0 & 0 & 0 & 0 \\
0 & K_{41}^{(2)} & K_{42}^{(2)} & 0 & K_{44}^{(2)} & K_{43}^{(2)} & 0 & 0 & 0 \\
0 & K_{31}^{(2)} & K_{32}^{(2)} & 0 & K_{34}^{(2)} & K_{33}^{(2)} & 0 & 0 & 0 \\
0 & 0 & 0 & 0 & 0 & 0 & 0 & 0 & 0 \\
0 & 0 & 0 & 0 & 0 & 0 & 0 & 0 & 0 \\
0 & 0 & 0 & 0 & 0 & 0 & 0 & 0 & 0
\end{bmatrix}
\begin{Bmatrix}
U_1 \\ U_2 \\ U_3 \\ U_4 \\ U_5 \\ U_6 \\ U_7 \\ U_8 \\ U_9
\end{Bmatrix}
=
\begin{Bmatrix}
0 \\ F_1^{(2)} \\ F_2^{(2)} \\ 0 \\ F_4^{(2)} \\ F_3^{(2)} \\ 0 \\ 0 \\ 0
\end{Bmatrix}
$$

Elements 3 and 4 each have analogous matrices. Each of the above element equations give the contribution of each element to the overall problem. By adding each of the above element equations the global equation for this system is obtained. The assembled global

stiffness matrix for Figure A4-1 is given by equation (A4-3) and the assembled global load vector is given below.

$$
\{F_{gl}\} = \begin{Bmatrix} F_1^{(1)} \\ F_2^{(1)} + F_1^{(2)} \\ F_2^{(2)} \\ F_4^{(1)} + F_1^{(3)} \\ F_3^{(1)} + F_4^{(2)} + F_2^{(3)} + F_1^{(4)} \\ F_3^{(2)} + F_2^{(4)} \\ F_4^{(3)} \\ F_3^{(3)} + F_4^{(4)} \\ F_3^{(4)} \end{Bmatrix} \tag{A4-4}
$$

Global Stiffness Matrix:

Equation (A4-3)

$$[K_{gl}] =$$

$$\begin{bmatrix}
K_{11}^{(1)} & K_{12}^{(1)} & 0 & K_{14}^{(1)} & K_{13}^{(1)} & 0 & 0 & 0 \\[4pt]
K_{21}^{(1)} & K_{22}^{(1)}+K_{11}^{(2)} & K_{12}^{(2)} & K_{24}^{(1)} & K_{23}^{(1)}+K_{14}^{(2)} & K_{13}^{(2)} & 0 & 0 \\[4pt]
0 & K_{21}^{(2)} & K_{22}^{(2)} & 0 & K_{24}^{(2)} & K_{23}^{(2)} & 0 & 0 \\[4pt]
K_{41}^{(1)} & K_{42}^{(1)} & 0 & K_{44}^{(1)}+K_{11}^{(3)} & K_{43}^{(1)}+K_{12}^{(3)} & 0 & K_{14}^{(3)} & K_{13}^{(3)} \\[4pt]
K_{31}^{(1)} & K_{32}^{(1)}+K_{41}^{(2)} & K_{42}^{(2)} & K_{34}^{(1)}+K_{21}^{(3)} & K_{33}^{(1)}+K_{44}^{(2)}+K_{11}^{(4)}+K_{22}^{(3)} & K_{43}^{(2)}+K_{12}^{(4)} & K_{24}^{(3)}+K_{13}^{(4)} & K_{23}^{(3)}+K_{14}^{(4)} \\[4pt]
0 & K_{31}^{(2)} & K_{32}^{(2)} & 0 & K_{34}^{(2)}+K_{21}^{(4)} & K_{33}^{(2)}+K_{22}^{(4)} & K_{23}^{(4)} & K_{24}^{(4)} \\[4pt]
0 & 0 & 0 & K_{41}^{(3)} & K_{42}^{(3)}+K_{31}^{(4)} & K_{32}^{(4)} & K_{44}^{(3)}+K_{33}^{(4)} & K_{43}^{(3)}+K_{34}^{(4)} \\[4pt]
0 & 0 & 0 & K_{31}^{(3)} & K_{32}^{(3)}+K_{41}^{(4)} & K_{42}^{(4)} & K_{34}^{(3)}+K_{43}^{(4)} & K_{33}^{(3)}+K_{44}^{(4)}
\end{bmatrix}$$

Equations (A4-3) and (A4-4) in the form of $[\mathbf{K_{gl}}]\{U\} = \{\mathbf{F_{gl}}\}$ represent the assembled equations which are to be solved for after applying the boundary conditions for the mesh shown in Figure A4-1. More complicated meshes are assembled similarly to this simple problem.

If there are two or more primary unknowns per node, then assembly of the global stiffness matrix is slightly more complicated. For a two-degree-of-freedom problem (as is the case if equation (A3-9) is used), the assembly of the elements involves two values at each node and thus there are twice as many elemental values to assemble. The assembly is done in much the same manner, however. The asymmetry of the matrices, **A**, given by equations (A3-9) or (A3-17) require however that all the elements in the global stiffness matrix be saved. The method of assembly for nonsymmetric matrices of the dimension $2*N_{tot}$ by $2*N_{tot}$ where N_{tot} is the total number of nodes in the problem can be found in a finite element text.[1,2]

Applying the boundary conditions:

The boundary conditions for the problem are applied after the assembly of each element. To illustrate this let Figure A4-1 be used again, and let the flux be specified to be 0 along the side with nodes 1, 2, and 3 and the flux specified to be 1 along the side with nodes 1, 4, and 7. In addition let the primary boundary conditions be that the

side with nodes 7, 8 and 9 is set to zero concentration (i.e. $U_7 = U_8 = U_9 = 0$), and that the concentration along the side with nodes 3, 6 and 9 is some unspecified value α, (i.e. $U_3 = U_6 = U_9 = \alpha$). The boundary conditions on the secondary variables are imposed by placing the values of the fluxes at the specified nodes directly into the load vector. These conditions would indicate that the global load vector, $\{F_{gl}\}$ be given by:

$$\{F_{gl}\} = \begin{Bmatrix} F_1 = 0 \\ 0 \\ F_3^* \\ 1 \\ F_5 \\ F_6 \\ F_7^* \\ 1 \\ F_8 \\ F_9 \end{Bmatrix} \quad \text{or} \quad \{F_{gl}\} = \begin{Bmatrix} F_1 = 1 \\ 0 \\ F_3^* \\ 1 \\ F_5 \\ F_6 \\ F_7^* \\ 1 \\ F_8 \\ F_9 \end{Bmatrix} \qquad \text{(A4-5)}$$

In this example nodes 1, 3, 7 and 9 are singular points. At node 1 there are effectively two flux conditions specified; i.e. the term F_1 can be either 0 or 1 due to the duplicity of the boundary condition. At node 9 there are two essential conditions specified; i.e. the term U_9 can be either 0 or α due to the duplicity of the boundary condition. Either of these issues can be solved by adding more nodes close to the singular boundary condition, and/or refining the mesh. The user can also use his/her own judgement based on the physics of the problem and decide which boundary condition is more appropriate. At nodes 3 and 7 both primary and secondary boundary

conditions are specified. By the above rule, the primary boundary conditions will be used and thus the fluxes at these points are left unspecified. For this example we will arbitrarily choose $F_1 = 1$ and $U_9 = \alpha$.

Once the secondary boundary conditions are assigned to the load vector, the essential boundary conditions must be applied. This involves modifying the assembled matrix by moving the known products to the right-hand column of the matrix equation, replacing the columns and rows corresponding to the known primary variable by zeros, except on the main diagonal where the variable is set to unity, and replacing the corresponding component of the right-hand column by the specified value of the variable.

To understand this concept, consider the point $U_3 = \alpha$. From equation (A4-3) and (A4-5) the global system of equations can be represented as:

$$\begin{bmatrix} K_{11} & K_{12} & K_{13} & \cdots \\ K_{21} & K_{22} & K_{23} & \cdots \\ K_{31} & K_{32} & K_{33} & \cdots \\ \cdots & \cdots & \cdots & \cdots \end{bmatrix} \begin{Bmatrix} U_1 \\ U_2 \\ U_3 \\ U_4 \\ U_5 \\ U_6 \\ U_7 \\ U_8 \\ U_9 \end{Bmatrix} = \begin{Bmatrix} 1 \\ 0 \\ F_3 \\ 1 \\ F_5 \\ F_6 \\ F_7 \\ 1 \\ F_8 \\ F_9 \end{Bmatrix} \qquad (A4\text{-}6)$$

The boundary condition at U_3 is applied by setting $K_{33} = 1$, and

$F_3 = \alpha$, and setting all the other $K_{3i} = K_{i3} = 0$ for $i \neq 3$ as shown below.

$$
\begin{bmatrix}
K_{11} & K_{12} & 0 & \cdots \\
K_{21} & K_{22} & 0 & \cdots \\
0 & 0 & 1 & 0 \\
\cdots & \cdots & 0 & \cdots
\end{bmatrix}
\begin{Bmatrix}
U_1 \\ U_2 \\ U_3 \\ U_4 \\ U_5 \\ U_6 \\ U_7 \\ U_8 \\ U_9
\end{Bmatrix}
=
\begin{Bmatrix}
1 \\ 0 \\ \alpha \\ 1 \\ \hat{F}_5 \\ \hat{F}_6 \\ \hat{F}_7 \\ 1 \\ \hat{F}_8 \\ \hat{F}_9
\end{Bmatrix}
\qquad \text{(A4-7)}
$$

In equation (A4-7), $\hat{F}_i = F_i - K_{i3}\,\alpha$ for $i = 1, 2, 4, 5, \ldots,9$. Thus in applying the essential boundary conditions, if $U_k = \alpha$ is known then the global equations are rearranged such that:

$$K_{kk} = 1 \qquad F_k = \alpha$$

$$F_i \rightarrow F_i - K_{ik}\,\alpha \qquad\qquad \text{(A4-8)}$$

$$K_{ki} \text{ and } K_{ik} \rightarrow K_{ki} = K_{ik} = 0$$

where $i = 1, 2, \ldots , k\text{-}1, k\text{+}1, \ldots , n,$ $i \neq k$

This procedure enables us to retain the original order of the matrix and the imposed boundary conditions are now printed as part of the solution.

Chapter 6.

Program Testing

6.1 Comparison of Analytical and Numerical Solutions

6.1.1 Constant Reaction Term

The program developed in Chapter 5 was first tested on several analytical problems to ensure the accuracy of the results. Two separate test cases were tested. One case is the constant reaction case, where the reaction term is set at 1. The boundary conditions were varied slightly to complicate the problem. The fully posed problem, in polar coordinates is:

$$\frac{1}{\rho}\frac{\partial}{\partial\rho}\left\{\rho\,\frac{\partial u}{\partial\rho}\right\} + \varepsilon^2\frac{\partial^2 u}{\partial\zeta^2} + 1 = 0 \quad \text{in } \Omega = \{(\rho,\zeta):\ 0 < (\rho,\zeta) < 1\} \tag{1}$$

with boundary conditions given by:

$$\frac{\partial u}{\partial\rho}(0,\zeta) = \frac{\partial u}{\partial\zeta}(\rho,0) = 0 \quad u(1,\zeta) = u(\rho,1) = 0 \tag{2}$$

The analytical solution to this problem with $\varepsilon = 1$, is a series solution given in equation (3) below.

$$u(\rho,\zeta) = \sum_{n=1}^{\infty} \left\{ \frac{2}{I_0(\lambda_n)} \; \frac{1}{\lambda_n{}^3} (-1)^n \cos(\lambda_n \zeta) \; I_0(\lambda_n \rho) \right\} + \frac{1}{2}(1-\zeta^2) \qquad (3)$$

where,

$I_0(\lambda_n \rho)$ is a Bessel function which comes from the solution of the modified Bessel equation of zero order;

and,

$\lambda_n = (2n-1)^* \frac{\pi}{2}$ comes from the homogeneous solution and the boundary condition along $\zeta = 1$.

Figure 6-1 shows the analytical solution in the form of a contour plot. The finite element solutions have similar contours as the analytical solution. Plotting all of these on one contour plot is somewhat meaningless, however. Therefore, the different solutions are compared along lines of constant ρ or ζ.

Figure 6-1:   Contour Plot of Analytical Solution
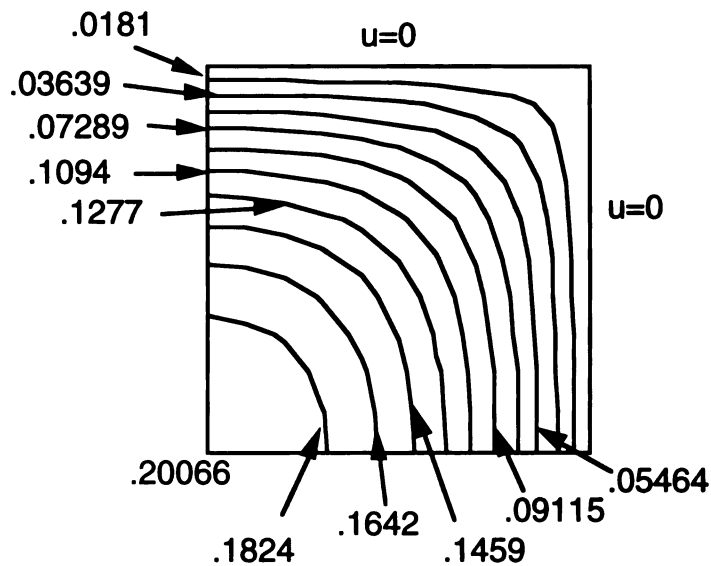
Figures 6-2 through 6-4 show the comparison of the analytical solution with the finite element computer program solution at $\rho=0$, $\zeta=0$, and $\rho=.5$, respectively. The symbols on these Figures represent the finite element solution values for different mesh sizes and different number of nodes per element. The solid line is the analytical solution for the lines $\rho=0$, $\zeta=0$, or $\rho=.5$. Table 6-1 compares the solutions at the point (0,0).

Figure 6-2: Comparison of Analytical Solution and FEM Solution at $\rho = 0$
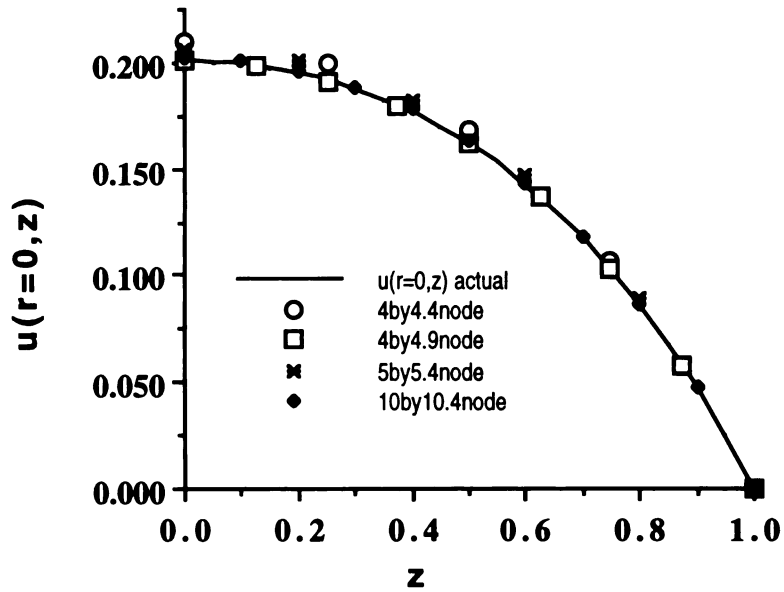
Figure 6-3: Comparison of Analytical Solution and FEM Solution at $\zeta = 0$
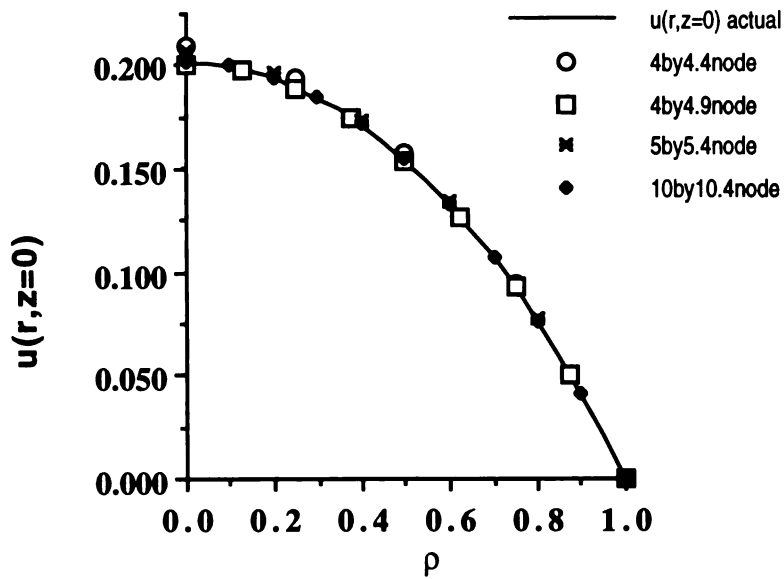
Figure 6-4: Comparison of Analytical Solution and FEM Solution at ρ = 0.5
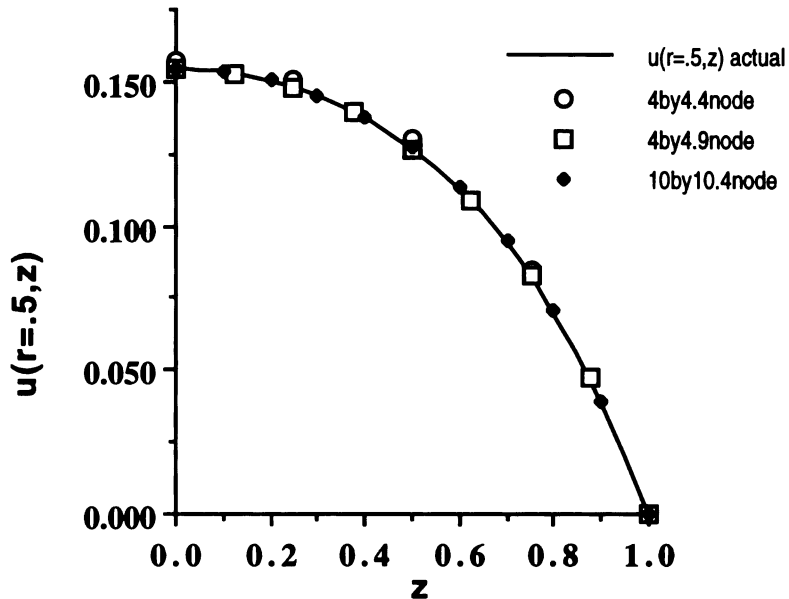
From Figures 6-2 through 6-4 it can be seen that the finite element solutions are very accurate. A more in depth break down can be seen in Table 6-1, which compares the solutions at the point ρ=0, ζ=0.

Table 6-1: Numerical comparison of Solutions at (ρ=0,ζ=0).

actual solution		.2006637
4 by 4 mesh	4 nodes/elem.	.209407
	9 nodes/elem.	.200631
5 by 5 mesh	4 nodes/elem.	.206492
10 by 10 mesh	4 nodes/elem.	.202319

It can be seen that a finer mesh gives a more accurate solution. More refinement on the solution is given by adding more nodes per element. From the above example, it can be seen that the finite element solution is accurate to 4 significant figures if a 4 by 4 mesh is used with 9 nodes per element.

6.1.2 Convective Test Problem

The other test case involves the convective boundary conditions. This problem was posed in rectangular coordinates, and the reaction term is set to zero. The problem is posed by equation (4) and is illustrated in Figure 6-5 below.

$$\frac{\partial^2 u}{\partial x^2} + \frac{\partial^2 u}{\partial y^2} = 0 \quad \text{in } \Omega = \{(x,y): \ 0 < (x,y) < 1\}$$

$$u(x,1) = 4; \qquad \frac{\partial u}{\partial x}(1,y) = 0 \ ; \qquad \frac{\partial u}{\partial y}(x,0) = 0$$

$$\frac{\partial u}{\partial x}(0,y) = \frac{h}{k} u \qquad \text{Convective boundary condition} \qquad (4)$$

Figure 6-5:   Convective Test Problem
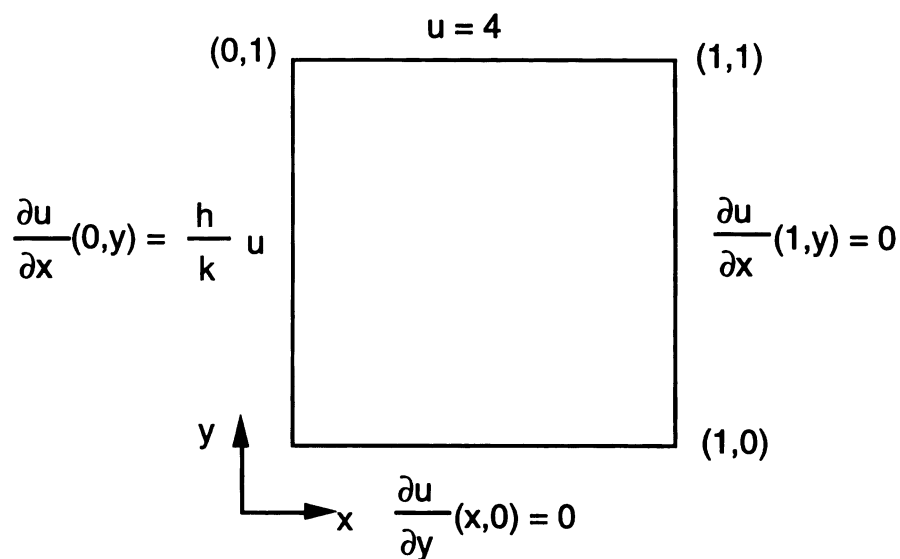
The analytical solution to this problem is given by equation (5).

$u(x,y) =$

$$\sum_{n=1}^{\infty} \frac{4 \sin \lambda_n}{\lambda_n \cosh \lambda_n} \frac{1}{\left(\frac{1}{2} + \frac{\sin 2\lambda_n}{4 \lambda_n}\right)} \cosh \lambda_n y \cos \lambda_n(x-1)$$

(5)

where:

λ_n is the solution of $\tan \lambda_n = \dfrac{Bi}{\lambda_n} = \dfrac{h}{k \lambda_n}$ (6)

comes from boundary condition at x = 0.

Figure 6-6 below shows the analytical solution in the form of a contour plot for Bi = 10.0. Figure 6-7 shows a comparison between the analytical solution and the computer generated solution for this problem for a four by four mesh with four nodes per element and nine nodes per element at x=0. The computer generated solution with nine nodes per element matches the analytical solution with more accuracy than the four node solution. This test case proved that the program was working fairly accurately. For the other cases tried below, nine nodes per element were used.

Figure 6-6: Contour plot of Analytical Solution

u = 4.0

1.692

3.717

3.338

3.042

.6787

2.704

2.367

.3411

1.016

1.354

2.029
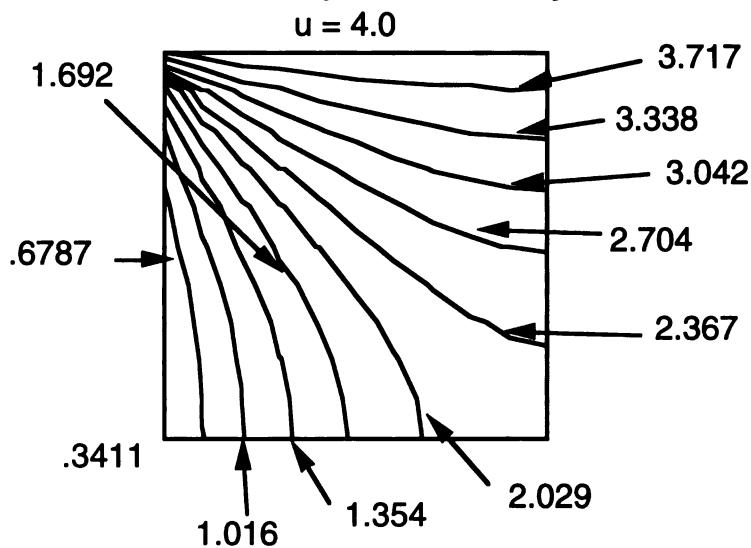
Figure 6-7: Comparison between Analytical and Computer Solutions at x = 0.
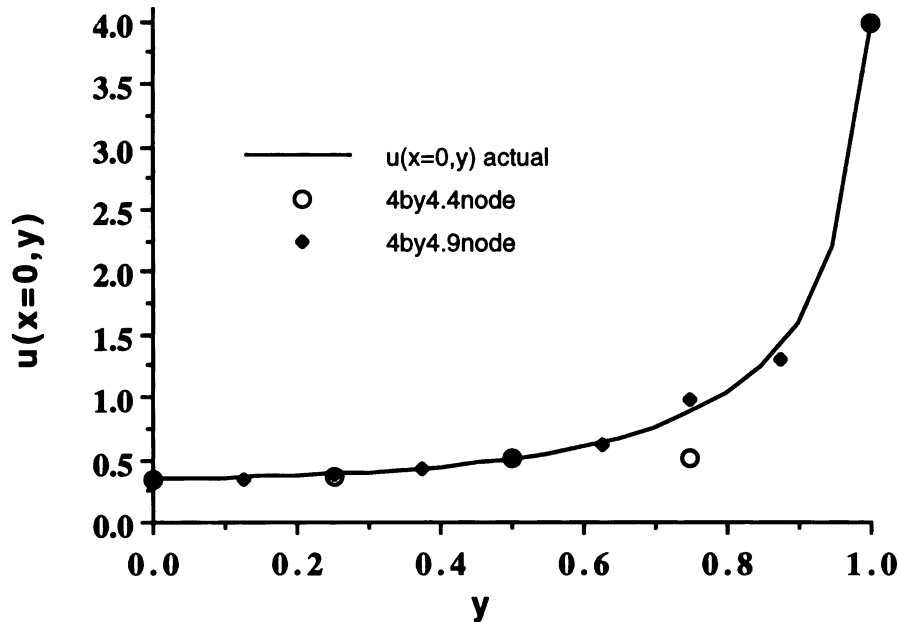
6.2 Comparison for Nonlinear Portion of Code

The next step before trying different geometries was to compare solutions from the finite element code with another author's case. This was done to assure that the nonlinear portion of the finite element code was working correctly. The comparison was done using a design modeled and tested by Albin et.al.[1] The design was a one dimensional membrane containing glucose oxidase. The same parameters were used to compare Albin's one dimensional solution and the one dimensional solution obtained from the finite element code. The parameters which Albin used are given below in Tables 6-2 through 6-4.

Table 6-2:   Albin Parameters

Parameter	Value
k_g	0.000673 cm/sec
k_o	0.00226 cm/sec
k_h	0.00891 cm/sec
k_b	0.000995 cm/sec
D_g	6.75 X 10^{-6} cm^2/sec
D_o	2.29 X 10^{-5} cm^2/sec
D_h	9.3 X 10^{-5} cm^2/sec
$D_b{}^*$	1.0 X 10^{-5} cm^2/sec for bicarb. buffer 6.6 X 10^{-6} cm^2/sec for citrate buffer. SEE TEXT.
α_g	1.0
α_o	1.0
$\alpha_h = \alpha_b$	1.0
K_g	0.06328 M (Weibel ref)[4]
K_o	0.0003729 M (Weibel ref)[4]

k_{cat}	226 sec^{-1} (Weibel ref)[4]
$K_b{}^*$	7.94 X 10^{-7} M (pKa = 6.1) bicarb. 4.07 X 10^{-7} M (pKa = 6.39) citric acid

Table 6-3: Bulk Concentrations used by Albin et. al.[1]

c_{oB}	0.274 mM
c_{qB}	5.56 mM
$c_{bB}{}^*$	26 mM bicarbonate 19.5 mM citric acid
c_{hB}	10$^{-7.4}$ (pH = 7.4)

Table 6-4: Dimensions used by Albin et. al.[1]

R = 0.5 cm
h = 0.02 cm model
h = 0.0129 cm experimental
E_t = 1.0 X 10^{-6} M

In Tables 6-2 through 6-4 the variables have the same meanings as listed in Appendix 4-1. The transport parameters, denoted by k_i correspond to Biot numbers of 2.0 for all species using

a 0.02 cm thick membrane. Two values are listed for the buffer parameters denoted by asterisks. In these cases the first value corresponds to that for bicarbonate buffer which is used in the current model (see Chapter 7 for details) and one value for citric acid buffer. Albin et. al. and Klumb et. al. both use citric acid buffer in their simulations and experiments.[1,2] The reader is reminded however, that the model which Albin uses does not take buffer transport into account. (See Chapter 4, pg 67, and discussion below).

A computer comparison was done for both the calculated and experimental cases listed above. Figure 6-8 compares the glucose and oxygen concentration profiles from Albin's solution and the finite element computer solution for the Albin's base case one-dimensional design.[1] The profiles from Albin's solution are shown as dashed lines. These values were estimated from a graph in reference 1. The destination layer is located at the normalized length equal to 1.0 side of the graph. It can be seen that the glucose, oxygen and reaction rate profiles all match very closely. This validated the method which we were using to solve this problem.

Figure 6-8: Comparison with Albin Solution

One Dimensional Case; No Hydrophobic Membrane; h =0.02 cm
Glucose, Oxygen Concentrations and Reaction Curves
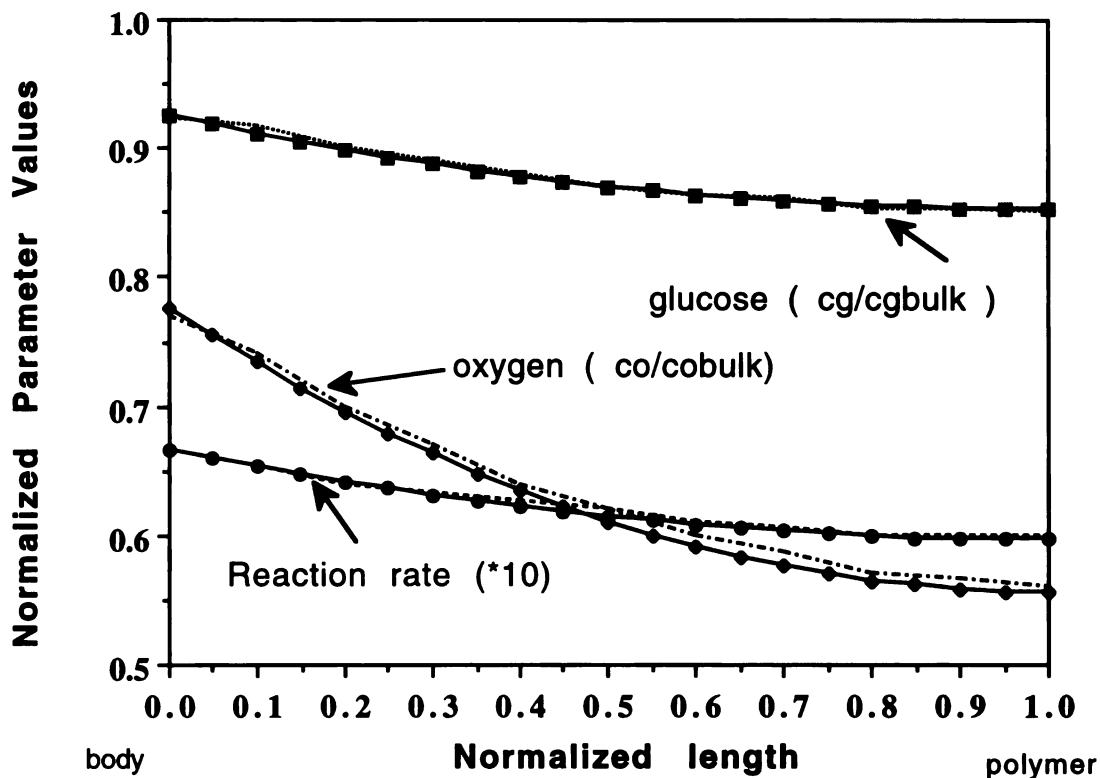
Figure 6-9 shows the comparable hydrogen ion profiles for the exact same case as tried above. Two profiles are shown as well as Albin's solution which is given by a dashed line. The profile which most closely matches Albin's solution was made by modifying the code to solve for the hydrogen ion concentration using the same method which Albin uses. The pH profile which does not match the solution given by Albin was calculated allowing buffer transport using bicarbonate as the buffer. This last pH profile however is not in such good agreement. There are several reasons for this. Albin makes the assumption that the hydrogen ion concentration profile is

identical to its counter ion, gluconate ion. In his model, the pH was calculated using the Henderson-Hasselbach equilibrium expressions from the gluconic acid concentration profiles. In the finite element model used here, the hydrogen ion concentration is calculated directly from the diffusion-reaction equations, equations (4-11) and (4-12). This generates a more accurate concentration profile for the hydrogen concentration and hence for the pH.

Figure 6-9: Comparison of Hydrogen Ion Profiles
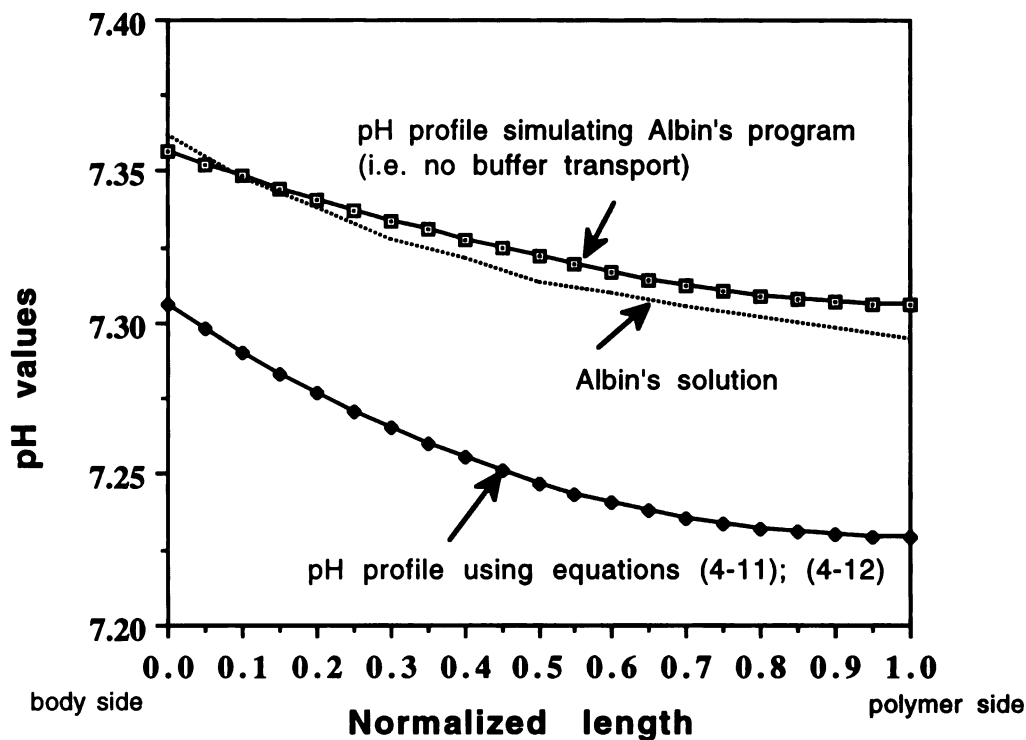
Klumb et. al.[2] (1993) also came up with a solution for this case using this design but a different program code. Klumb et. al.have also incorporated the hydrogen transport equations into their model. Table 6-5 below gives a numerical comparison of the pH

values at the bottom of the membrane calculated and observed experimentally by all three models. The bottom of the membrane refers to the polymer or destination layer. Several values calculated using different diffusion coefficients and buffers are also given.

Table 6-5: **Numerical Comparison of pH values at bottom of membrane**

Author	Calculated h =0.02 cm	Calculated: h = 0.0129 cm	Experimental h=0.0129
Albin soln. no buffer transport	7.295	7.25	7.32
FEM soln bicarbonate buffer	7.23	7.29	not applicable
FEM soln citric acid buffer; Klumb parameters	7.20	not done	not applicable
Klumb soln citric acid as a buffer	7.09	not done	not done

Klumb soln citric acid as a buffer: $D_{citrate} = D_h$	7.37	not done	not done
FEM soln citric acid buffer; Klumb parameters: $D_{citrate} = D_h$	7.38	not done	not applicable

The discrepancy between the calculated pH values at the bottom for the Albin method and the FEM method is again shown in Table 6-5. The predicted values for another membrane are also given. It should be noted that for the experimental membrane, the FEM solution using the bicarbonate buffer predicts a pH value which is very close to the experimental value obtained by Albin. This was very encouraging and showed that incorporating buffer transport in the equations gives a more accurate result.

The next step is to compare the pH values obtained by Klumb et. al. to those obtained using the FEM program. The values which they obtain for the base case for their pH profiles are lower than the values which are obtained by the FEM model however. This initially caused some concern but there are several other differences between the two models. Both Klumb and Albin use citric acid as the buffer in this reaction, and both authors have incorporated titratable amine groups directly into the glucose oxidase membrane model to calculate the pH. The model which we are using contains

bicarbonate buffer and the amine groups are not included in the hydrogen ion equations. The bicarbonate buffer is assumed to be more mobile than the citric acid buffer due to its size and its diffusion coefficient is one order of magnitude larger than that of citric acid.[3] Klumb ran a sensitivity analysis and showed that if the diffusion coefficient of citric acid was increased to that of the hydrogen ion that the bottom pH increases to 7.37.

To check whether the buffer difference would account for the large difference in calculated pH, the FEM model was run using citric acid in the same concentration as used by Klumb. The pH value did decrease but not significantly. This is somewhat puzzling given that when the model is run setting the buffer diffusion coefficient equal to the hydrogen ion diffusion coefficient, the same pH is obtained as Klumb calculated. It is assumed, however that the difference between the bottom pH values between the two models is due to the addition of the amine groups and the dihydrogen monocitrate ion (H_2C^-) which are incorporated into Klumb's model. The sensor we are developing here will not contain amine groups and thus these do not need to be included in the modeling. In addition, the buffer in the body is mainly bicarbonate buffer. It can be seen that due to relatively large concentration of buffer as compared to the other species in the model, the diffusion coefficient for the buffer, and the pKa of the buffer have a much larger affect on the resulting pH. These differences account for the different hydrogen ion concentrations seen for the different models.

6.3 Conclusion

The results of these test cases illustrated that the code was working satisfactorily, and that the results which were obtained were indeed meaningful. Figures 6-8 and 6-9 show the good agreement between Albin's solution and the finite element code solution. This proved that the nonlinear portion of the code was working as well. The next chapter shows the cases which were tried and documents several possible theoretical sensor designs.

References

1. Albin G, Horbett TA, Miller SR and Ricker NL, Theoretical and experimental studies of glucose sensitive membranes, *J. Controlled Release*, **6**: (1987) 267-91

2. Klumb LA and Horbett TA, The effect of hydronium ion transport on the transient behavior of glucose sensitive membranes, *J. of Controlled Release*, **27**: (1993) 95-114

3. Cussler, E. L. <u>Diffusion, Mass Transfer in Fluid Systems.</u> Cambridge University Press: New York. (1984)

4. Weibel, M. K. and Bright, H.J., The glucose oxidase mechanism: interpretation of the pH dependence. *J. Biol. Chem.*, **246**: (1971) 2734-2744

5. CRC Handbook, Standard Mathematical Tables, 27th ed., Beyer, W. H., (editor), CRC Press, Boca Raton, Florida, 1984

Chapter 7.

Results for Model

7.1 Introduction

The model presented in Chapter 4 can now be numerically solved using the code developed in Chapter 5 and tested in Chapter 6. At this point it remains to determine the parameter values required to solve the problem for different geometries. One of the difficulties in ascertaining if experimental observations correspond closely to the predicted response is determining the values of the parameters to be used in the simulations. This chapter documents several cases which were tested and the parameters used to obtain the solutions.

7.2 Parameter Estimation

The dimensional parameters required for the simulations are listed below in Table 7-1. The determination of the mass transfer coefficients, the diffusion coefficients within the membrane and the partition coefficients is discussed in section 7.2.1 below. The reaction parameters were obtained using equation (4-6) and analysis done by Weibel (1971).[8] The exact value of these is discussed in section 7.2.2.

Table 7-1: Dimensional Parameters Needed in Simulation

Mass transfer coefficients from bulk solution to membrane	k_g, k_o, k_h, k_b
Diffusion coefficients in membrane	D_g, D_o, D_h, D_b
partition coefficients	$\alpha_g, \alpha_o, \alpha_h, \alpha_b$
Reaction parameters	K_g, K_o and k_{cat}, K_b

7.2.1 Determination of Transport Parameters

The dimensional mass transfer parameters from the bulk solution to the device have been estimated by Gough et. al. using a membrane-covered, rotated disk electrode system simulating passive diffusion from the bulk solution to a membrane (Reynold numbers less than 5000).[1-4] Using their novel disc electrode system, Gough et. al. determined values for the partition coefficients, diffusion coefficients and the mass transfer coefficients for glucose and oxygen into a hydrophilic membrane.[1-4] The mass transfer properties for each substrate were first determined separately in the absence of the enzyme reaction using Cuprophane PT-150 as the hydrophilic membrane. Cuprophane PT-150 is a regenerated cellulosic membrane containing about 65 vol % water at equilibrium. Then these diffusion and reaction properties were quantitatively characterized for both glucose and oxygen using

membranes containing a glutaraldehyde-crosslinked mixture of purified glucose oxidase, catalase and collagen cast as a thin homogeneous film.[1] Using the estimated parameters obtained from the rotated disk electrode, Gough et. al. showed that their predictions exhibited good agreement with experimental results for their design.[5-7]

Most of the reported values were considered to be accurate enough for our purposes and were used in our simulations. The most recent values were used where possible.[7] Similar theoretical methods were used to estimate the mass transfer coefficients.[2-4] The parameter values for the hydrogen ion and the bicarbonate buffer were estimated using bulk values and similar theoretical methods.

The mass transfer coefficients, k_i, were estimated using the classical rotating disk theory in which the disk surface is uniformly accessible to the reactant and the diffusion boundary layer thickness is known.[9] In the rotating disk theory the hydrodynamic boundary layer for a species i is calculated as,

$$\delta_i = 1.61 \, D_{iB}^{1/3} \, \nu^{1/6} \, \omega^{-1/2} \qquad (1)$$

where ν is the kinematic viscosity of the medium, ω is the angular rotation rate, and D_{iB} is the solute diffusion coefficient in the bulk.

From equation (1) the mass transfer coefficient is calculated as:

$$k_i = \frac{D_{iB}}{\delta_i} = 1.61 \ D_{iB}^{2/3} \ \nu^{-1/6} \ \omega^{1/2} \qquad (2).$$

Equation (2) gives a direct method to calculate the solution mass transfer coefficient for a given species. There are two major assumptions associated with equation (2); that the radius of disk be much greater than the diffusion boundary layer for any species, δ_i, and that the flow be laminar. Since passive diffusion is assumed (i.e. laminar flow), the Reynolds number must be between 100-20,000 for equation (2) to be valid.[10,11] Gough et. al. obtained their values using rotation rates of up to 25 rad/sec.[1-4] Using this value for ω, the Reynolds number can be calculated given the solution's kinematic viscosity, the solution's temperature and the disk radius. The solution is assumed to be similar to water at 37°C. The properties for water at 20 and 37°C and the known bulk diffusion constants of the species considered in this problem in water are given in Table 7-2, below.

Table 7-2:   Known Parameters

Kinematic Viscosity of water/plasma	$\nu_{20^{\circ}C} \cong 0.01$ cm^2 s^{-1}
	$\nu_{37^{\circ}C} \cong 0.0069$ cm^2 s^{-1}
Diffusion coefficients in Bulk Solution	
Glucose	D_{gB} 6.75 X 10^{-6} cm^2 s^{-1}
Oxygen	D_{oB} 2.30 X 10^{-5} cm^2 s^{-1}
Buffer	D_{bB} 1.0 X 10^{-5} cm^2 s^{-1} (assumed bicarbonate buffer)
Hydrogen Ion	D_{hB} 9.3 X 10^{-5} cm^2 s^{-1}

Using these values the diffusion layer thickness and Reynolds numbers can be calculated as shown below.

$$Re_{20^{\circ}C} = \frac{d^2\,\omega}{\nu_{20^{\circ}C}} = 2500\ d^2 \text{ or } Re_{37^{\circ}C} = \frac{d^2\,\omega}{\nu_{37^{\circ}C}} = 3623\ d^2 \qquad (3)$$

where d is the unknown disk radius, and the rotation rate is 25 rad/sec.   The proposed sensor is assumed to be approximately 1 cm in overall diameter (see Chapter 2).   This would give Reynolds numbers well within the required range for use of equation (2).   The

diffusion layer thicknesses for all the species in consideration at 37°C are estimated to be:

$$\delta_g \cong 0.0027 \text{ cm}; \quad \delta_o \cong 0.002 \text{ cm}; \quad \delta_h \cong 0.0064 \text{ cm}; \quad \delta_b \cong 0.003 \text{ cm}.$$

These values are much less than the overall proposed disk dimension of 1 cm and thus equation (2) will be used to estimate the mass transfer coefficients. Therefore using (2), the dimensional mass transfer parameters from the solution to the membrane were estimated at 37°C as shown in Table 7-3.

Table 7-3: Mass Transport Coefficients

Glucose	k_g = 0.00254 cm/sec
Oxygen	k_o = 0.00575 cm/sec
Hydrogen Ion	k_h = 0.0146 cm/sec
Bicarbonate Buffer	k_b = 0.0033 cm/sec

Using these as the mass transfer coefficients the Biot numbers can be estimated once the diffusion coefficients within the membrane and the partition coefficients have been determined. Gough et. al. used their rotating disk electrode to first determine the membrane permeability to a particular species.[1-3] The membrane permeability, P_m, is given by equation (4) below.

$$P_{m_i} = \frac{\alpha_i \, D_{m_i}}{\delta_m} \qquad (4)$$

where the partition coefficient α_i is defined below, D_{m_i} is the diffusion coefficient of species i in the membrane and δ_m is membrane thickness. [In our case δ_m is h.] Once the permeability is known, the quantity $\alpha_i \, D_{m_i}$ can be calculated using equation (4). A transient technique developed by Gough et. al. is then used to obtain separately the partition and diffusion coefficients.[1,4] At this point the most recent values predicted by Gough et. al. for the diffusion coefficients within the membrane, D_{m_i}, were used in this simulation.[7] These values are listed below in Table 7-4.

As mentioned previously (Chapter 4) selective partitioning of species into the enzyme membrane is included in our formulation for completeness and is represented by the partition coefficient for each species. The equilibrium partition coefficient for species i, α_i = c_i/c_{iB}, is defined as the equilibrium ratio at the membrane-solution interface of the solute concentration in the membrane, c_i, divided by the concentration in the bulk solution, c_{iB}. Gough et. al. also estimated values for the membrane partition coefficients for both glucose and oxygen. These values are shown in parenthesis in Table 7-4. For simplicity all the partition coefficients were set to one in the simulations. (This is thought to be a decent assumption, since the exact nature of the glucose oxidase membrane has not been fully determined yet.)

Table 7-4:   Parameter Values used in Simulations

Parameter	Value
D_g	4×10^{-6} cm^2/sec (Gough ref. 7)
D_o	2×10^{-5} cm^2/sec (Gough ref. 7)
D_h	9.3×10^{-5} cm^2/sec (*)
D_b	1.0×10^{-5} cm^2/sec (*)
α_g	1.0 (0.8)
α_o	1.0 (0.8 - 3.0)
$\alpha_h = \alpha_b$	1.0

In Table 7-4, the bulk diffusivities, denoted by the asterisk, were used as the membrane diffusion coefficients for the bicarbonate buffer and the hydrogen ion. The bulk diffusivities were used for both buffer and the hydrogen ion because both species are very mobile and it is assumed that there will be minimal diffusional hindrance to these species due to the proposed hydrophilic nature of the membrane.

The Biot number for each species was calculated using equation (5) below.

$$Bi_i = \frac{k_i \, h}{D_{m_i} \, \alpha_i} = \frac{k_i}{P_{m_i}} \tag{5}$$

The mass transfer coefficients used are given in Table 7-3. The diffusion coefficients within the membrane which were used in this calculation are given in Table 7-4. The partition coefficients were set to 1.0 as mentioned above. Due to some discrepancy in the membrane parameters obtained by Gough et. al.,[5-7] the Biot numbers used in the simulation are slightly different than those calculated using (5). The calculated and the used Biot numbers are listed in Table 7-5.

Table 7-5:   Biot Numbers.
All Values calculated for h = 0.1 cm

Species	Calculated Biot No.	Biot No. used in Simulations
Glucose	$Bi_g \cong 63.5$	Bi_g = used 60
Oxygen	$Bi_o \cong 28.75$	Bi_o = used 27
Hydrogen Ion	$Bi_h \cong 15.68$	Bi_h = used 15
Bicarbonate Buffer	$Bi_b \cong 32.98$	Bi_b = used 31

7.2.2 Determination of Reaction Rate Parameters

As mentioned in Chapter 4 the performance of glucose oxidase is dependent on pH and has an optimum performance at pH 5.5. Weibel and Bright collected data over a range of pH values from 3 to 11.[8] This data led them to generate a minimal mechanism consistent with all the aspects of the high pH experiments.   From

this scheme, a turnover equation for the enzyme of the form of equation (4-5) was determined. From this equation, equations for k_{ox} and k_{cat} as a function of the pH were generated. The parameters that are used in the reaction rate equation (4-6) are K_g and K_o which are ratios of k_{cat} to k_{red} and k_{cat} to k_{ox}, respectively. By expressing the ratios as functions of pH, K_g, K_o and k_{cat} can be expressed as functions of pH. These values were calculated and plotted. The reaction parameters were determined from these plots at pH 7.4. The pH within the sensor is expected to change by less than 0.5 units. Within this range the parameters are relatively constant, and thus were approximated as shown in Table 7-6. Other authors have used similar assumptions.[1-7,13-15]

Table 7-6: Reaction Rate Parameters used in Simulations

K_g	0.07 M (Weibel ref. 8)
K_o	0.0008 M (Weibel ref. 8)
k_{cat}	880 sec^{-1} (Weibel 8)
K_b	7.94 X 10^{-7} M (pKa = 6.1)

7.2.3   Other relevant parameters

It still remains to determine the range of bulk concentrations that are valid for this problem. These are given below in Table 7-7. The total buffer concentration was set at the total concentration of bicarbonate buffer in the body.[16]   The bulk hydrogen ion

concentration was set by the normal body pH since it is known that the body regulates itself quickly. The bulk oxygen concentration was set at 0.1 mM. This value was chosen because it is a reasonable value and Gough et. al. used values similar to this. The maximum saturation of oxygen in water is 0.274 mM at 1 atm. In arterial blood oxygen concentrations can be as high as 0.15 mM. In some peripheral tissues or venous blood, however, oxygen concentrations can be as low as 0.01 mM. The value of 0.1 mM was thought to be conservative enough to give a decent and realistic estimate of the oxygen deficit. Glucose bulk values were varied between 3 mM (54 mg/dl) to 15 mM (270 mg/dl). The value of 10 mM (180 mg/dl) was used to simulate the average value of bulk glucose after a normal meal.

Table 7-7:   Concentration Ranges

c_{oB}	0.1 mM
c_{gB}	3 - 15 mM
c_{bB}	26 mM
c_{hB}	$10^{-7.4}$ (pH = 7.4)

The other important parameters in this problem are the membrane parameters such as the geometry of the membrane, and the total enzyme concentration. Since we are considering only one "cell" of the entire membrane as shown in Figure 4-3, the significant geometric parameters become the overall membrane thickness, h, the radius between holes, R, and the hole radius, a. Realistic values

for the geometries were chosen with some regard for fabrication ease. The values which were considered are listed in Table 7-8, which lists the geometric cases considered.

Table 7-8:   Sensor Dimensions

Case number	Cell Radius, R	Cell thick- ness, h	Hole radius, a	Aspect Ratio, ε	a/R	Thiele modulus, ϕ	E_t (μM)
1 1-d case	0.1 cm	0.1 cm	0.1 cm	1.0	1.0	10.0	0.02273
2 new med hole	0.1 cm	0.1 cm	0.025 cm	1.0	.25	10.0	0.02273
3 small hole	0.1 cm	0.1 cm	0.01 cm	1.0	.1	10.0	0.02273
4 lg hole	0.1 cm	0.1 cm	0.05 cm	1.0	.5	10.0	0.02273
5	0.2 cm	0.1 cm	0.05 cm	2.0	.25	10.0	0.00568
6	0.2 cm	0.1cm	0.1 cm	2.0	.5	10.0	0.00568
7	0.1 cm	0.1 cm	0.025 cm	1.0	.25	*10.0	0.02273
8	0.1 cm	0.1 cm	0.01 cm	1.0	.1	*10.0	0.02273

In Table 7-8, the total enzyme concentration is set by the effective Thiele modulus.   In our formulation the Thiele modulus is

given by $\phi^2 = \dfrac{R^2\ k_{cat}\ E_t}{\alpha_o\ D_o\ c_{oB}}$. This form of the Thiele modulus is used because it is the most convenient when formulating the problem. The Thiele modulus is defined as the ratio between the reaction rate and the diffusion rate, and can be used as a design parameter in membrane designs [Gough, et.al 1982].[1]   It should be noted that in general the Thiele modulus is usually defined with respect to the membrane thickness.   Using this definition, the Thiele modulus is denoted by:

$$\sigma^2 = \dfrac{h^2\ k_{cat}\ E_t}{\alpha_o\ D_o\ c_{oB}} = \phi^2\left(\dfrac{1}{\varepsilon^2}\right) \qquad (6)$$

In our problem, choosing values for the geometry, i.e. the radius or the membrane thickness, gives a direct relationship between the Thiele modulus and the enzyme concentrations.   Due to the numerical expression for the reaction rate (equation (4-18)), for numerical stability with an aspect ratio equal to 1.0 values of no more than 15 can be used for the Thiele modulus.   This has been noted by other authors who were not able to retain numerical stability for values over 10.[5-7,14,15]   A value of 10 for the Thiele modulus corresponds to very low enzyme concentrations as given in Table 7-8.   Gough et. al.[5-7] and Klumb et. al.[14,15] have used values for the Thiele modulus of 10 or lower even though the actual enzyme concentration in their test devices may give a Thiele modulus value as high as 200.   They have justified their use of lower Thiele

modulus values by saying that there is little effect on the concentration profiles by varying the Thiele modulus, σ, above 10.

The assumption of the small effect of the Thiele modulus can be further justified by examining the shape of the reaction curves generated by equation (4-18). The reaction curves generated by equation (4-18) are three dimensional hyperbolas. For a steady state solution the reaction rate must match the diffusion terms. For a given reaction rate, however there is very little numerical difference in concentration values for Thiele modulus values between 15 and 200. [5-7]

In addition it has been noted that as long as the process is diffusion limited, that is for Thiele modulus values greater than five, accurate responses are achieved by this model.[1] Diffusion limited processes require that diffusion is slow compared to any reaction process. The major advantage of the diffusion-controlled design is that even though the intrinsic enzymatic activity may decay during long-term use, enzyme inactivation will have little effect on the signal until the activity becomes sufficiently low that the process is converted to reaction-controlled, and thereafter the sensor response will change dramatically during further use to the point of total failure. Thus the Thiele modulus values for all of the above cases were set at 10.0.

It should be noted that for cases 7 and 8 the effective Thiele modulus value is slightly different. In these cases less enzyme is

packed into a smaller volume to generate the same enzyme concentrations.

Figure 7-1 shows a visual comparison of the geometries of each case listed in Table 7-8.

Figure 7-1: Comparison of Geometries

CASE 1 : NO MEMBRANE

$R = a = 0.1$ cm
$h = 0.1$ cm
$a / R = 1.0$
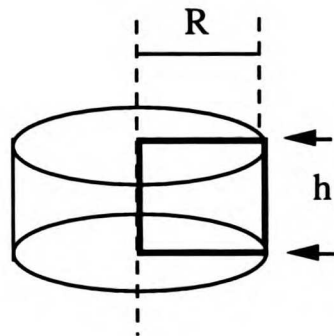
CASE 2 : AVERAGE HOLE
IN MEMBRANE
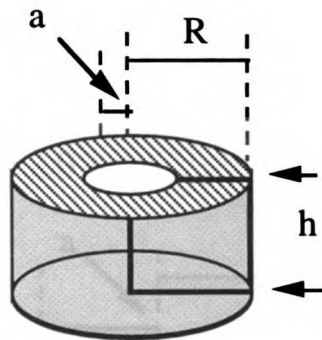
$R = 0.1$ cm
$h = 0.1$ cm
$a / R = .25$

CASE 3 : SMALL HOLE
IN MEMBRANE

$R = 0.1$ cm
$h = 0.1$ cm
$a / R = .1$
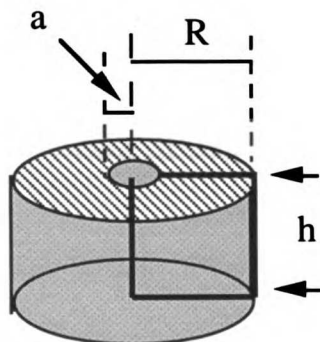
Figure 7-1: cont'd

CASE 4 : LARGE HOLE
IN MEMBRANE
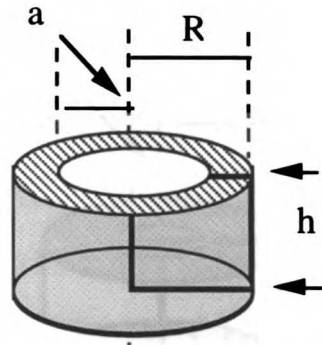
       R = 0.1 cm
       h = 0.1 cm
       a / R = .5

CASE 5 : AVERAGE HOLE IN MEMBRANE, R / h = 2.0
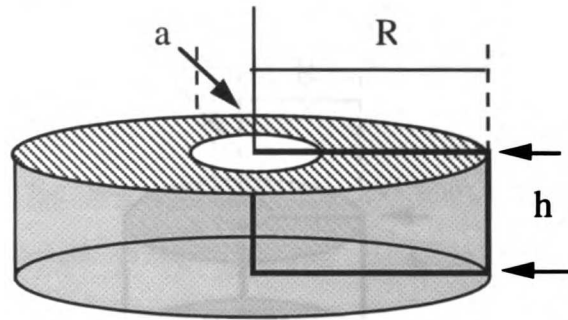
       R = 0.2 cm
       h = 0.1 cm
       a / R = .25

CASE 6 : LARGE HOLE, R / h = 2.0

       R = 0.2 cm
       h = 0.1 cm
       a / R = .5
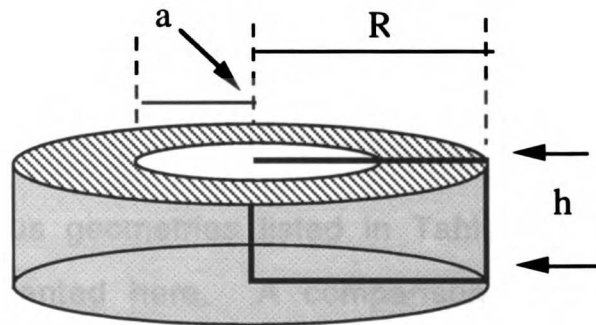
Figure 7-1: cont'd

Variable Enzyme Cases

CASE 7 : AVERAGE HOLE
IN MEMBRANE
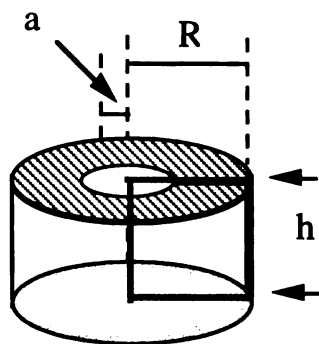
  R = 0.1 cm
  h = 0.1 cm
  a / R = .25

CASE 8 : SMALL HOLE

  R = 0.1 cm
  h = 0.1 cm
  a / R = .10
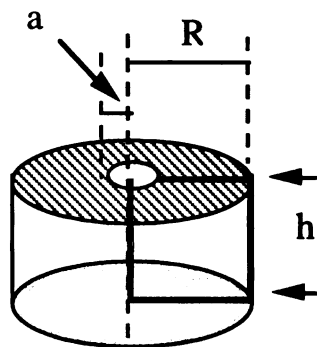
7.3 Results

  The results for the various geometries listed in Table 7-8 and shown in Figure 7-1 are presented here. A comparison of these results determine the set of designs which should be experimentally tested.

  The computer generated solutions for Cases 1-8 listed above in Table 7-8, using the parameters in Tables 7-3 through 7-7 are illustrated in the figures below. A three dimensional visual comparison of the geometries of each case is given in Figure 7-1

above. For each case, the glucose, oxygen and hydrogen concentration contours are given over a cross-section of the unit cell outlined in bold in Figure 7-1.

The first six cases are membranes which contain a uniform distribution of glucose oxidase. The concentration contours for these cases, (excepting case 4) are given in Figures 7-2 through 7-6. Cases where glucose oxidase is distributed uniformly throughout the membrane were the first designs considered for simplicity. The remaining cases contain layers of glucose oxidase combined with layers containing no glucose oxidase. The results for these variable enzyme cases are shown in Figures 7-8 and 7-9. The layers of glucose oxidase are illustrated by the shaded (i.e. dotted) regions in the unit cells in Figure 7-1. Areas of no glucose oxidase are blank. The hydrophobic membrane is illustrated by the striped area at the top of each cell. The results shown below represent the concentration contours at a bulk glucose concentration of 10 mM (180 mg/dl), and a bulk oxygen concentration of 0.1 mM unless otherwise noted.

Case 1 is the one dimensional case where there is no membrane. From Figure 7-2 it can be seen that the concentration contours are flat as expected. There is a significant decrease in oxygen concentration with relatively little decrease in glucose concentration. The overall pH decrease is 0.1 pH units from top to bottom. This decrease in pH is probably not enough to significantly

Figure 7-2:   Case 1 Geometry.   One-Dimensional Design

Glucose Contours

9.94 mM

9.39 mM

9.25 mM

Oxygen Contours

.099 mM

.028 mM

.021 mM

pH Contours

7.397

7.31

7.30
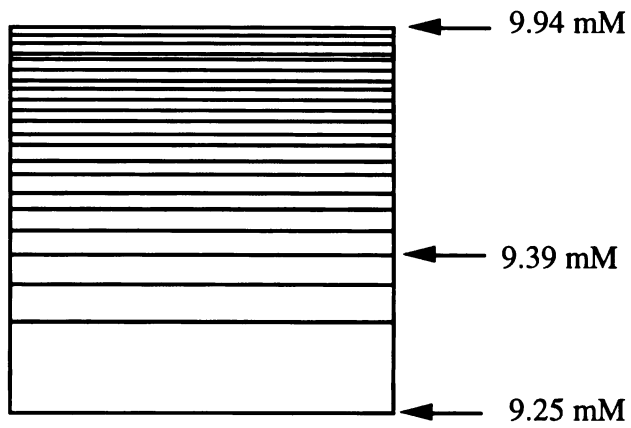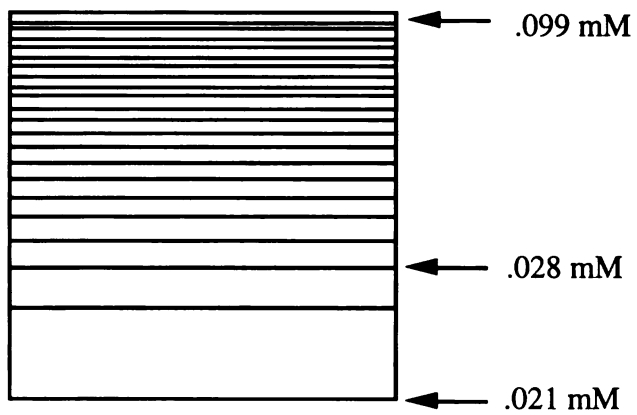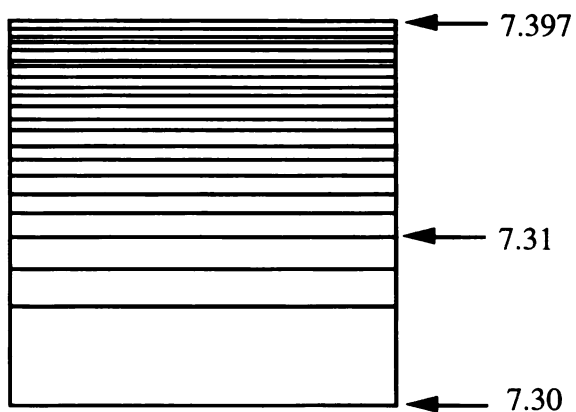
swell the polymer layer at high glucose levels. This design has already been shown to be unsatisfactory in combating the oxygen deficit problem by other authors.[1,5-7,13-15,17,18] It is shown anyway for comparison to the other designs.

The optimal size of the hole in the membrane is partially based on the oxygen to glucose delivery ratio. This ratio is calculated as:

$$\frac{O}{G} = \frac{\text{flux } O_2}{\text{flux glucose}} = \frac{\alpha_o \, D_o \, (c_{oB}-c_{oavg})}{\alpha_g \, D_g \, (c_{gB}-c_{gavg})} * \frac{\text{area } O_2 \text{ flux}}{\text{area gluc. flux}}$$

$$= \frac{\alpha_o \, D_o \, (c_{oB}-c_{oavg})}{\alpha_g \, D_g \, (c_{gB}-c_{gavg})} * \frac{\pi \, R^2}{\pi \, a^2} \tag{7}$$

For an optimal design, at higher bulk glucose concentrations the flux ratio of oxygen to glucose should be greater than or equal to one, if possible. From equation (7) and the parameters given in Tables 7-3 through 7-7, the ratio of the radius of the hole in the hydrophobic membrane to the unit cell radius is given by equation (8):

$$\frac{a^2}{R^2} \leq \frac{(0.1-c_{oavg})}{(c_{gB}-c_{gavg})} * 5.0 \tag{8}$$

In equations (7) and (8), estimated average concentrations of glucose and oxygen are used to estimate fluxes through the membrane. If the one dimensional results are used (a worst case scenario), then a rough average estimate for the glucose and oxygen concentrations in the membrane are 9.5 mM and 0.06 mM, respectively. Now making use of equation (8), for a bulk glucose concentration of 10 mM, a unit cell radius of 0.1 cm, and the average concentrations from the one dimensional case, the radius of the hole in the hydrophobic membrane should be less than or equal to 0.06 cm. The maximum oxygen to glucose delivery parameter is obtained when the maximum fluxes are achieved by setting the average concentrations to zero. For this case the ratio of the hole radius to the unit cell radius becomes: a/R $\leq$ 0.224. These two a/R ratios give a fairly good estimate of how large the hole in the membrane should be. Various values for the hole radius were used. The hole to radius ratio was started at 0.25 for simplicity.

The case 2 design shows the effect of a hydrophobic membrane which covers 93.75% of the area. This corresponds to a hole in the membrane which is a quarter of the radius of the entire unit cell; i.e. an a/R ratio of 0.25. This was taken as the original base case due to the simple calculations on the oxygen to glucose delivery ratio from above. Case 2 results are illustrated in Figure 7-3.

Figure 7-3:   Case 2 Geometry.   Medium Sized Hole: a/R =.25

Glucose Contours
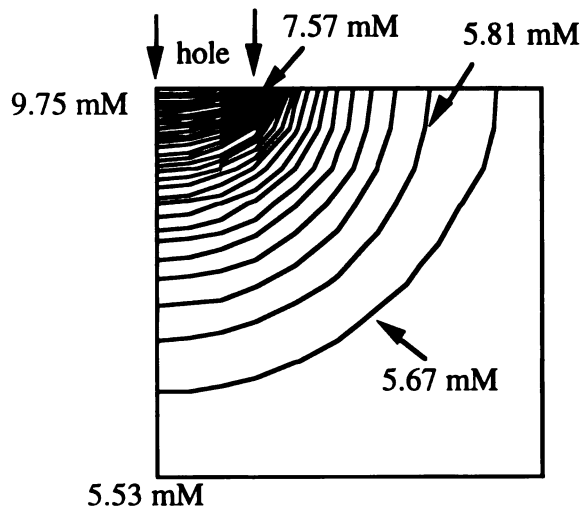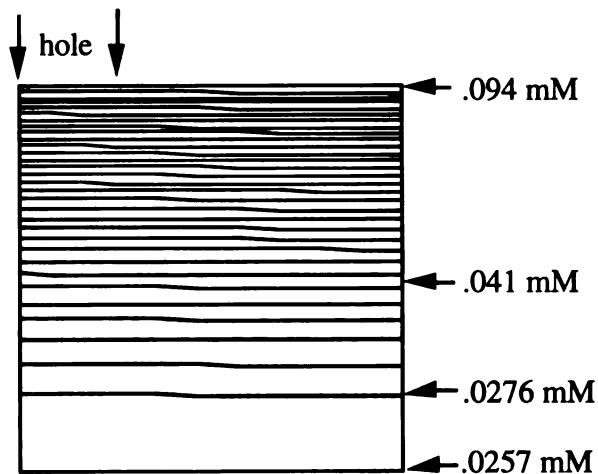
Oxygen Contours
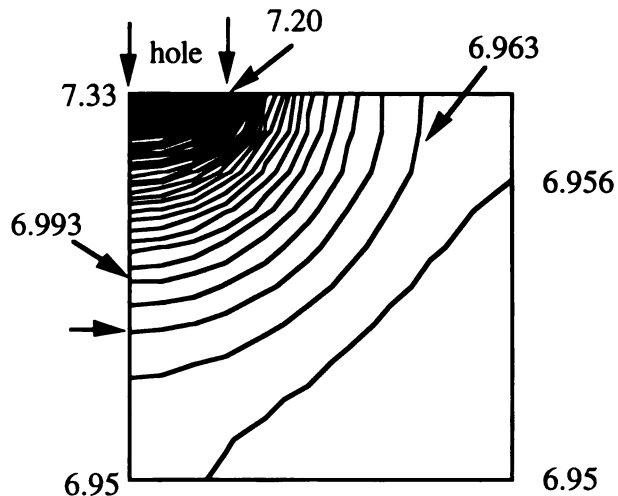
pH Contours

From the concentration contours in Figure 7-3, it can be seen that at the bottom of membrane the glucose concentrations have been reduced by 40% (9.25-5.53/9.25) by adding the hydrophobic membrane. The oxygen concentrations, on the other hand have increased by 22% over the one dimensional design. This is a good improvement over the one dimensional design. Due to the increase in oxygen to glucose ratio at the bottom of the membrane, the pH levels have been decreased to 6.95. This is a significant decrease as compared to the one dimensional design. This result was very encouraging, although we expected to see slightly higher oxygen concentrations within the membrane.

For comparison to the medium sized hole, both a smaller and a larger hole was tried using the same geometry. The smaller hole results are shown in Figure 7-4. For this case the hydrophobic membrane covers 99% of the unit cell.

Figure 7-4:   Case 3 Geometry.   Small Hole: a/R =.1

Glucose Contours

Oxygen Contours

pH Contours

hole

6.75

6.71

7.15

6.703

6.716

6.698
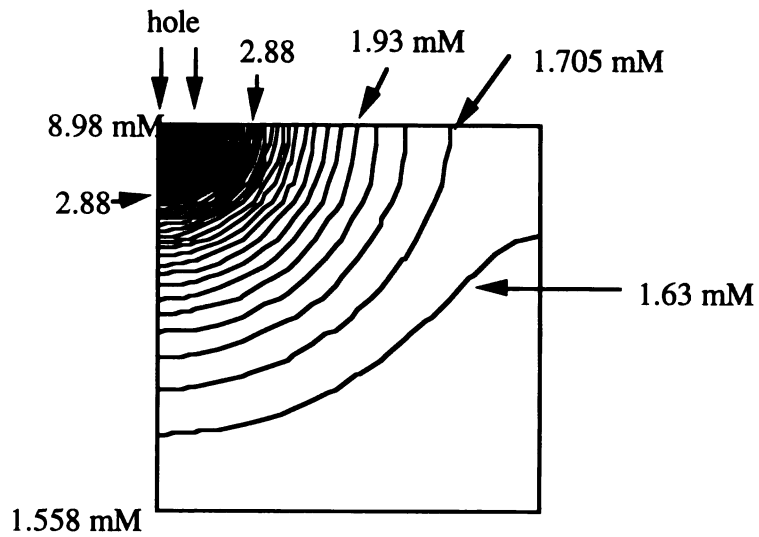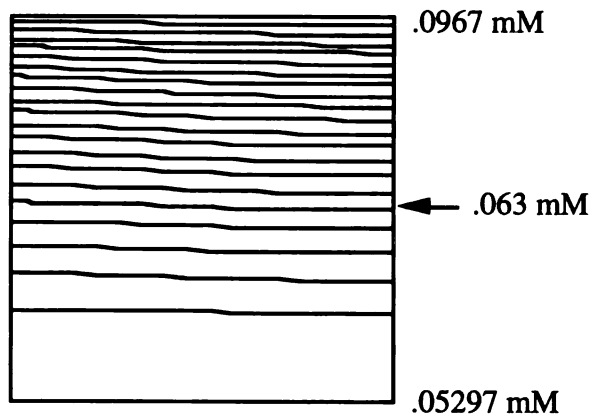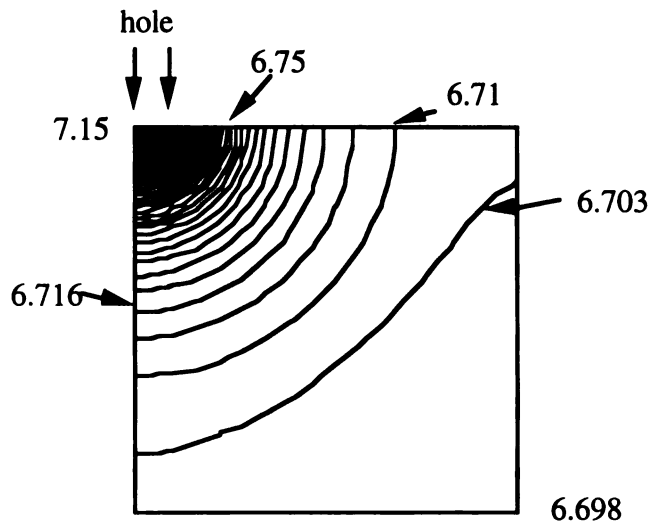
From Figure 7-4 it can be seen that the small hole increases oxygen contours by 150% over the one dimensional case. Both the pH and the glucose concentrations are significantly decreased with this design.

The case 4 geometry was tested as a comparison to cases 2 and 3. Using case 4 geometry, the hydrophobic membrane covers 75% of the unit cell. The larger hole allows the entry of more glucose and hence the oxygen to glucose ratio at the bottom of the membrane is not as favorable as in the previous case. These contours are not shown because they are analogous to the previous two cases. The glucose concentration runs from 8.19 mM at the bottom of the membrane to 9.9 mM at the top. The oxygen contours run from 0.022 mM to 0.094 mM which shows no improvement over the one dimensional case. The larger the hole the more flux of glucose and hydrogen ions into and out of the membrane, thus increasing the

glucose concentration and decreasing the hydrogen ion concentration slightly. The calculated pH at the bottom of this membrane is 7.18 for a bulk glucose value of 10 mM. This value is higher than the bottom pH for case 2, as expected.

Cases 5 and 6 represent trying a larger radius unit cell with the same hole to unit cell ratios as Cases 2 and 4 above. This was done to attempt to increase the oxygen concentration in the membrane. It should be noted that these cases were run using a version of the program which did not attempt to calculate the zero flux condition as given by the boundary condition at side 4, equation (4-17). This boundary condition was implemented after these runs. These runs were not redone using the new boundary conditions because the preliminary results shown below indicate that these cases are unfavorable. In addition, the boundary condition for pH along side 4 is set to 7.2. For these cases the predicted hydrogen fluxes into the polymer layer are also shown.

The results for case 5 are shown in Figure 7-5. Case 5 is similar to case 2 in that the hydrophobic membrane covers 93.75% of the unit cell. This design does increase the oxygen concentrations in the membrane. At the bottom of this membrane, oxygen concentrations are 65% (.73-.257/.73) higher than those in case 2. This increase in oxygen at the destination layer is not, however accompanied by a decrease in the pH due to the thickness of the membrane. The aspect ratio for this membrane is 2.0 which implies that the membrane is thinner compared to the other cases. It has been determined that thinner membranes or those with aspect ratios

greater that one have quicker transport times resulting in increased pH values.[13]   The total hydrogen fluxes are included in this figure. It can be seen that for this design there is some flux into the destination layer which is what is ultimately desired.   When this case is run for lower bulk glucose concentrations, however the flux differences between the two cases are not significant enough to recommend this design. [These results not shown.]

Figure 7-5:   Case 5 Geometry.   Thinner membrane. a/R = .25

Glucose Contours

hole

9.86 mM

8.99 mM

8.2 mM

7.58 mM

7.50 mM

7.89 mM

Oxygen contours

.095 mM

.084

.076 mM

.0734 mM

.073 mM

pH Contours

hole

7.28

7.11

7.15

7.12

7.16   pH = 7.2
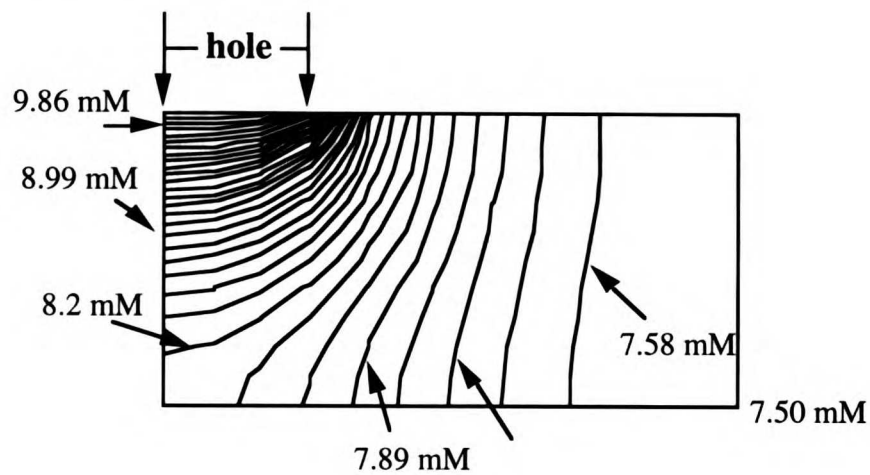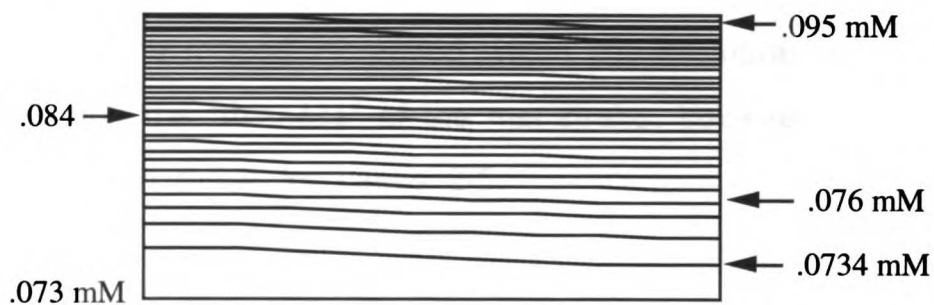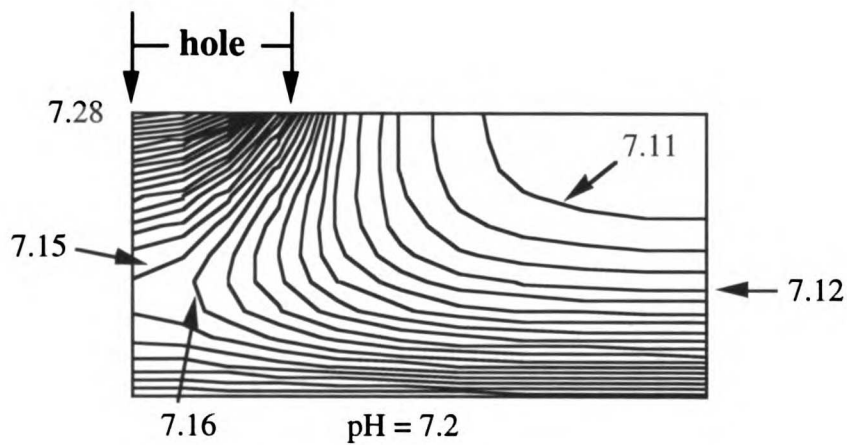
H+ Fluxes
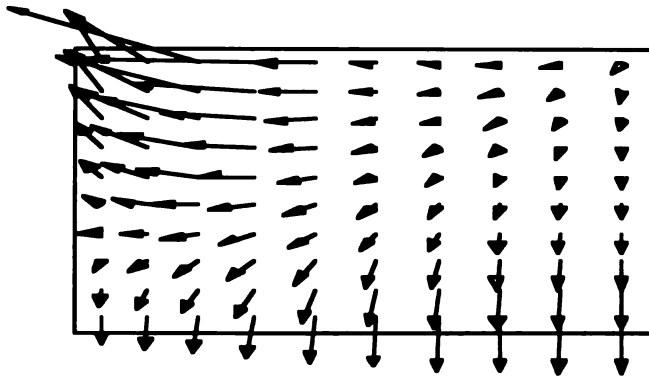
The results for the case 6 design, having an aspect ratio of 2.0 and a hole to radius ratio of 0.5 are shown in Figure 7-6. These results are similar to the results for case 5 in that the oxygen concentration is indeed increased within the membrane. Due to the hole size and the "thinness" of the membrane, however, the pH values are higher than those for cases 2-5.

Figure 7-6:   Case 6 Geometry.   Thinner membrane. a/R = .5

Glucose Contours

9.5mM →

9.08 mM

9.44 mM

9.17 mM

9.05 mM

Oxygen Contours

.095 mM

.078 mM

.072 mM

.0708 mM

pH Contours

7.34

7.30 →

7.25 →

7.16

7.17

7.18

pH = 7.2
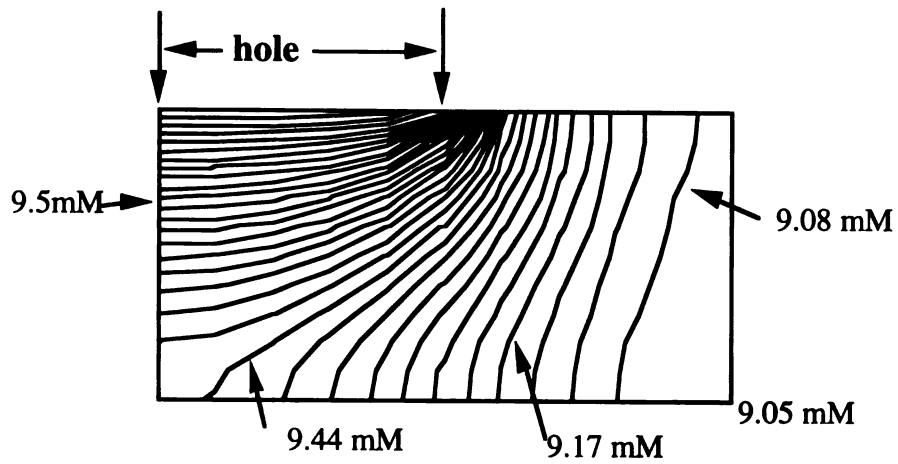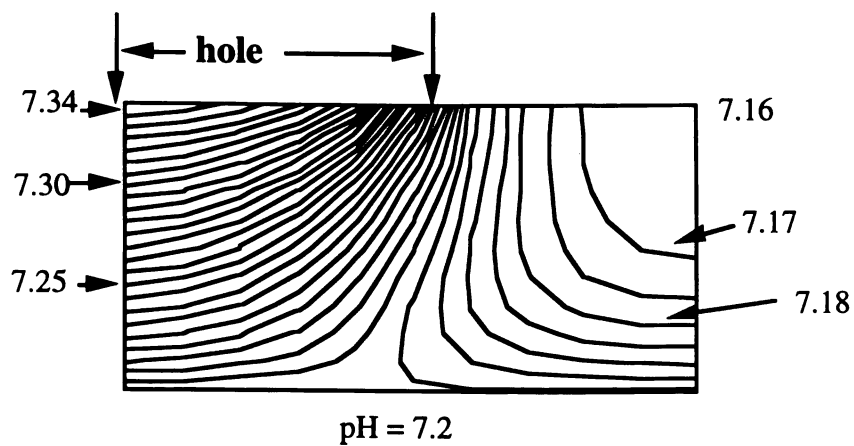
Total H+ fluxes
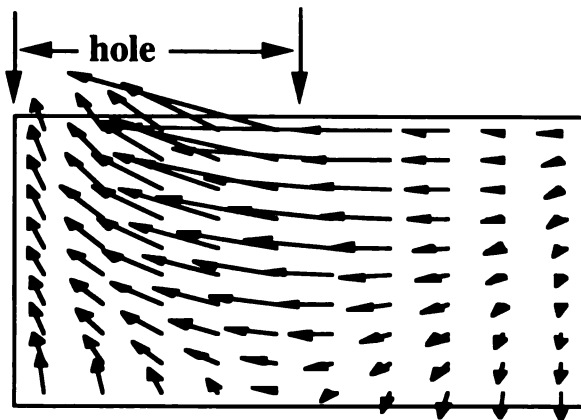
From the results for cases 1-6, it was decided that the reaction to generate hydrogen ions still occurs mainly near the hole in the unit cell. Due to this the oxygen is still depleted first before depleting the glucose sufficiently, thus making the membrane still more sensitive to changes in oxygen concentration rather than changes in glucose concentration. To combat this problem, it was decided to try a different approach. To further enhance the oxygen concentration in the membrane, designs using variable regions of glucose oxidase/catalase were considered. This meant alternating enzyme concentrations in layers, with enzyme rich layers strategically located adjacent to the destination layer and by the hole at the top. The middle layer which contains little or no enzyme, acts like a storage reservoir for oxygen. The perforated hydrophobic silicone membrane which enhances oxygen transport would remain on top. Figure 7-7 below illustrates this solution more clearly.

Figure 7-7: **Membrane Design to Enhance Glucose Sensitivity**
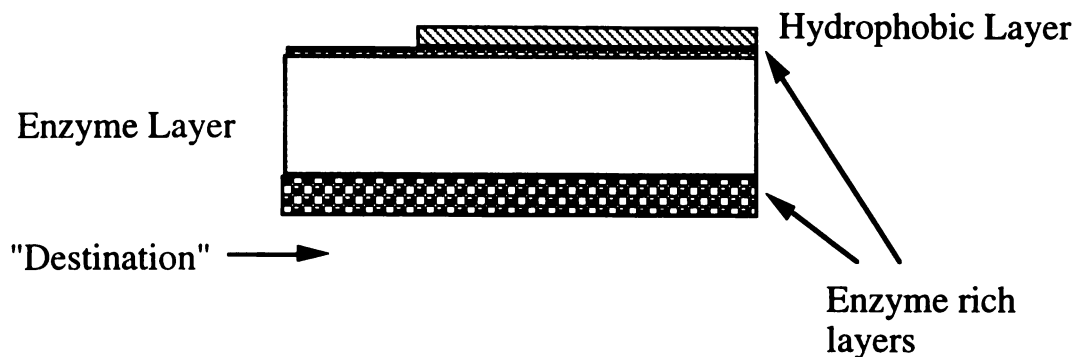
Several different designs were tried using the scheme in Figure 7-7. These are listed as cases 7 and 8 in Table 7-8.

Cases 7 and 8 represent cases with variable enzyme layers and two different hole sizes. For each case the bottom enzyme layer is only 0.03 cm thick. Each case also has an enzyme plug at the hole to filter out excess glucose. The size of the enzyme plug at the hole was arbitrarily set at 0.02 cm. Figures 7-8 and 7-9 show the concentration profiles for these two cases respectively.

Figure 7-8: Case 7 Geometry

Glucose Contours (mM conc)
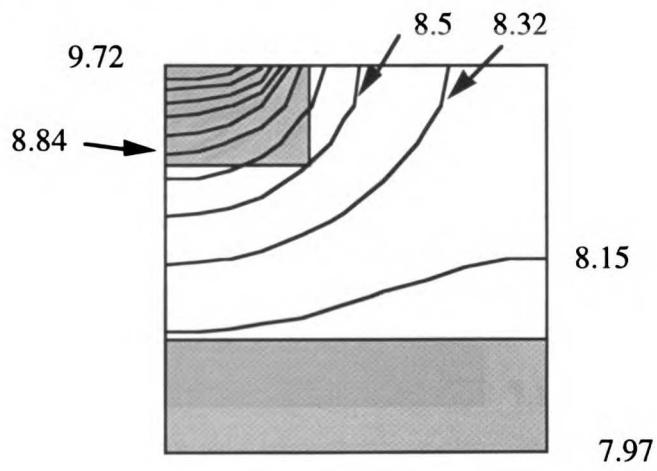
Oxygen Contours (mM Conc)
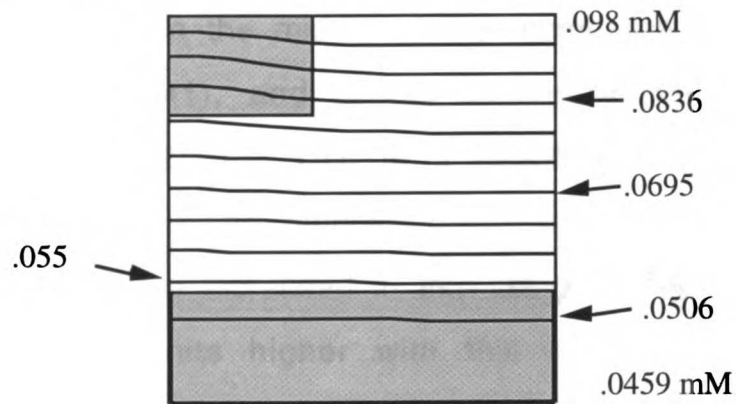
pH Contours
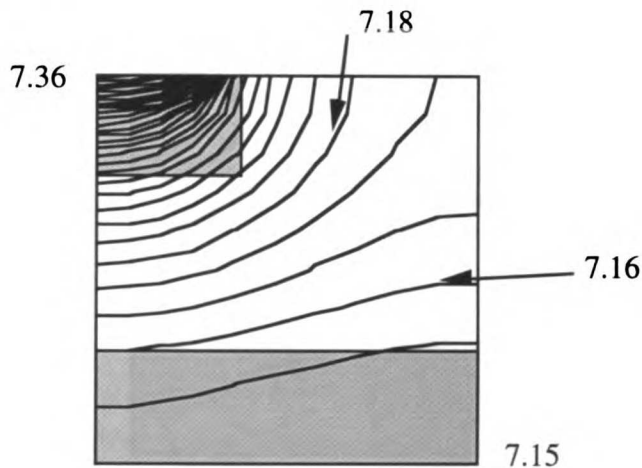
A comparison of case 7 and case 2 gives an idea of how variable enzyme layers change the design. For case 7, oxygen concentrations in the middle of the membrane are enhanced by 54% (.06315-.041/.041), and at the bottom of the membrane by 78% (.0459-.0257/.0257). This is a significant improvement in oxygen concentrations. The glucose concentrations and the corresponding pH, however are increased in this design. The pH at the destination layer is 0.2 units higher with this design than with the case 2 design. In addition the glucose concentrations at the bottom of the membrane are 44% higher with this design.

To combat the problem from case 7, a smaller hole was used. Using a smaller hole, as in Case 8, further magnifies the oxygen enhancement and pH drop. Comparing case 8 to case 2, the pH drop at the destination layer is now 0.07 units below the case 2 design, and oxygen is enhanced by 106% at the bottom of the membrane. Figure 7-9 shows the concentration contours for this case.

Figure 7-9: Case 8 Geometry

Glucose (mM conc)

Oxygen (mM conc)
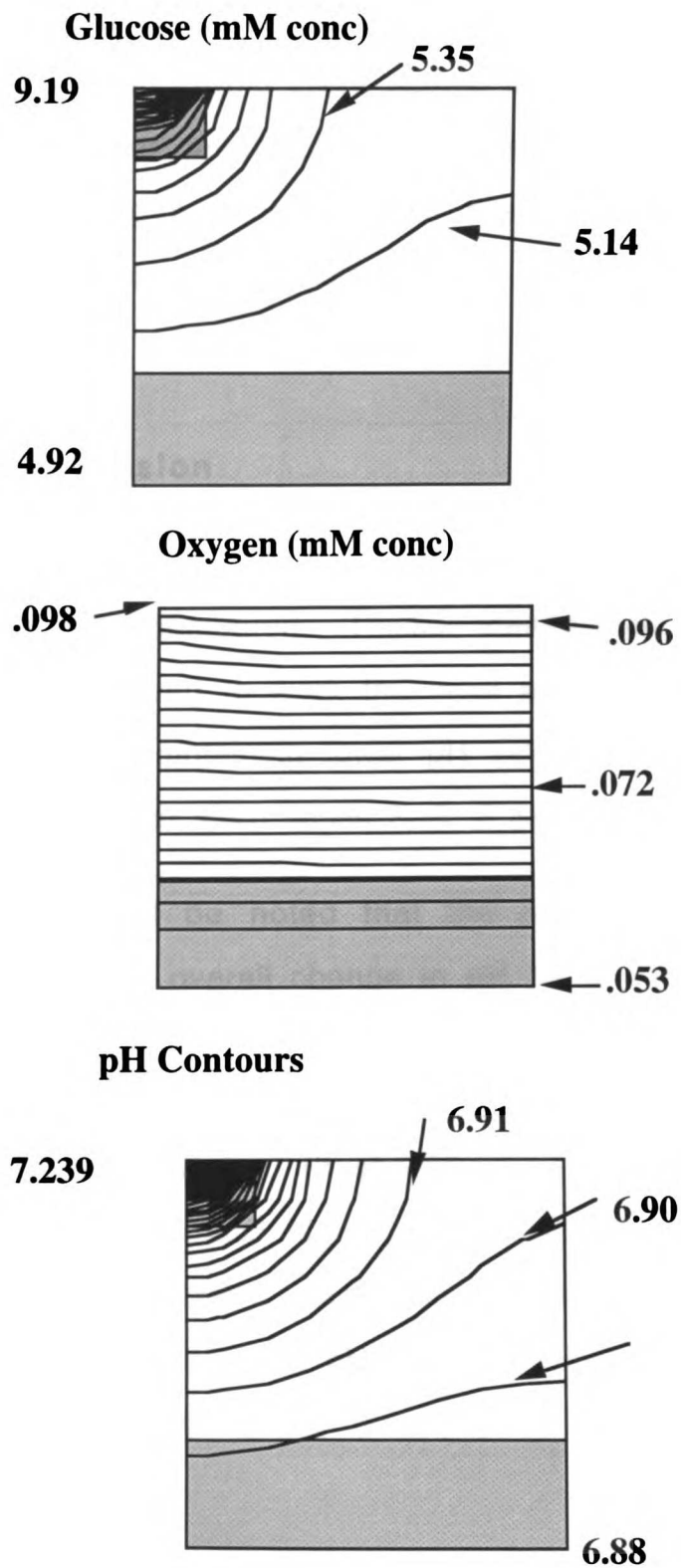
pH Contours

The oxygen contours are essentially identical for Cases 3 and 8. The glucose and pH contours are very different for these two cases however. From these figures it can be seen that the overall pH drop is greater when the entire membrane contains glucose oxidase, but that oxygen concentrations are enhanced for geometries with very small holes or variable enzyme amounts.

7.4 Discussion

At this point in the study designs which showed the most promise were compared. Thicker membranes and small holes in the membrane proved to work the most efficiently to combat the oxygen deficit while maintaining lower pH values. The designs which were compared further were cases 2, 3, 7 and 8.

It should be noted that the important parameters for each design are the overall change in pH for a bulk glucose change from basal level (3 mM) to an average glucose level after a meal (10 mM), and the pH at the destination layer (bottom of the membrane) at basal glucose levels. (It should be noted that glucose levels after meals could go much higher. For design considerations an average glucose concentration was used.) The object of the design is to maximize the change in pH, while maintaining reasonable pH values near 7.4 at the bottom of the membrane during fasting stages or low glucose levels.

Figure 7-10 compares the pH contours for cases 2, 3, 7 and 8 at fasting glucose levels and after a meal. The corresponding overall pH drops at the destination layer for several cases are listed in Table 7-9. It can be seen that the cases 3 and 8 designs give the largest pH drops over the range considered.

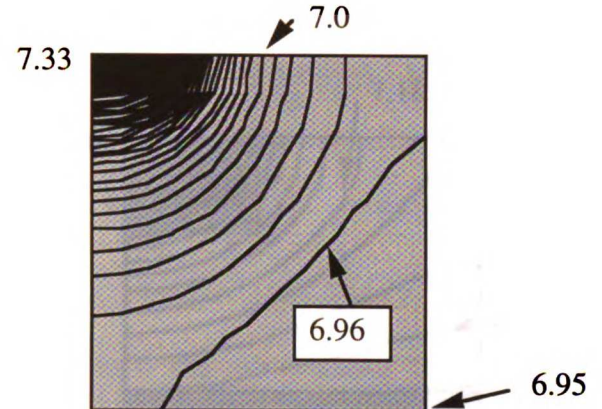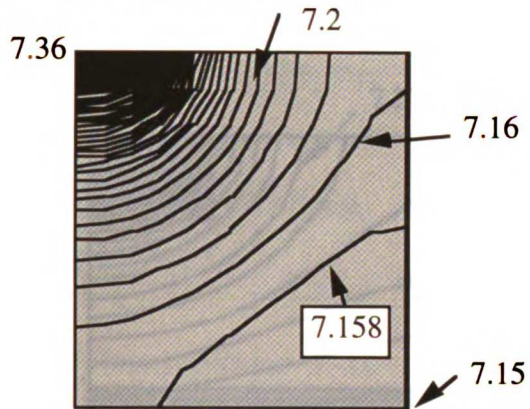**Table 7-9: pH Drops at Bottom of Sensor**

Case #	Δc_{gB} (mM)	Δ pH (bottom)
2	7 (3-10)	0.2
3	7 (3-10)	0.372
7	7 (3-10)	0.1
8	7 (3-10)	0.26

Figure 7-10: pH Contour plots for 4 Cases

C_{gbulk} = 3 mM (54 mg/dl)

C_{gbulk} = 10 mM (180 mg/dl)

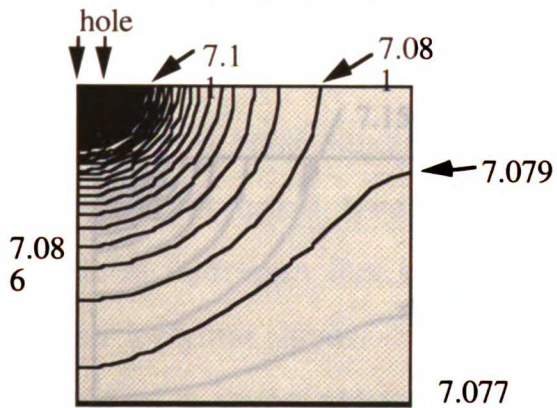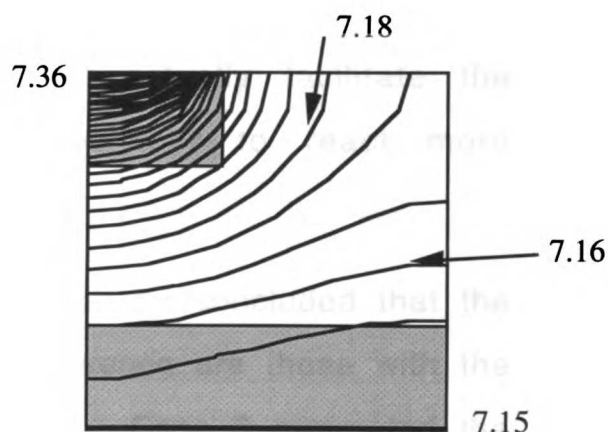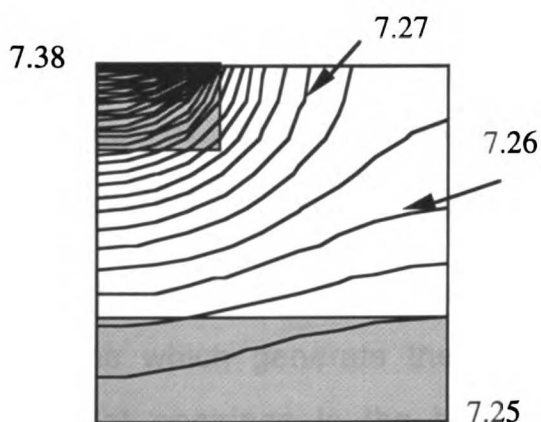Case 2: R/h = 1; hole/R = .25

Case 3 : R/h = 1.; hole/R = .1
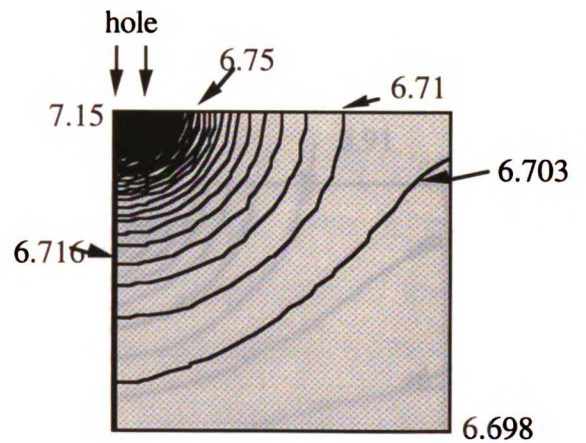
Figure 7-10: cont'd:

C_{gbulk} = 3 mM (54 mg/dl) C_{gbulk} = 10 mM (180 mg/dl)

Case 7 : R/h = 1. ; hole/R = .25

Case 8 : R/h = 1.; hole/R = .1
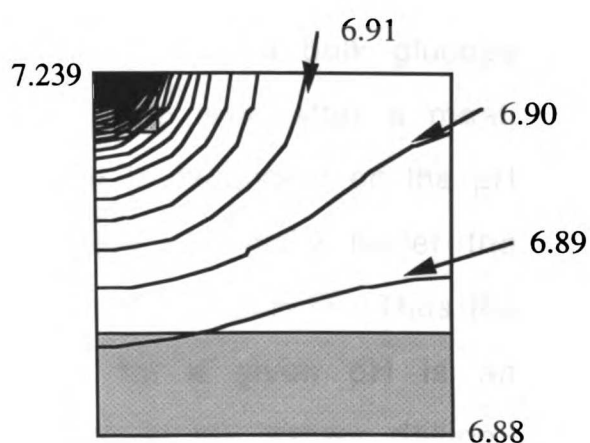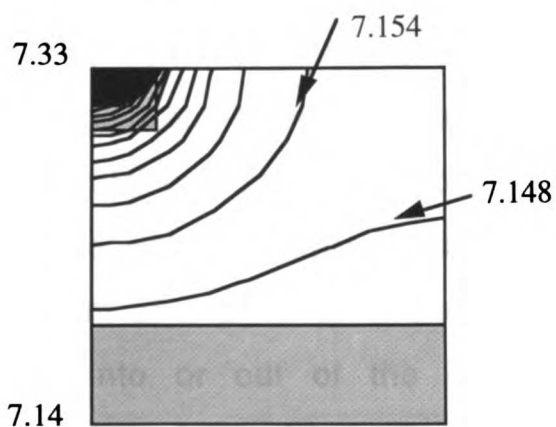
From Figure 7-10, the pH values at the bottom of the membrane during fasting for cases 2, 3 and 8 designs are rather low however. Initially this was cause for concern, since the titratable polymer should be in its "off" or unswollen position or osmotically inactive at basal glucose levels. Depending on the polymer used, the

system may be already swollen or osmotically active at a pH of 7.2 or lower.[19-21] Due to the overall design of the pump, however, it is feasible that the "off" position for the polymer gel or solution, is an already slightly swollen state. The pump could be designed in such a way that the polymer goes from one slightly swollen state to another more swollen state. This will actually facilitate the kinetics of swelling, and allow the polymer to react more quickly.[20-23]

From Figure 7-10 and Table 7-9 it can be concluded that the designs which generate the largest pH difference are those with the smallest openings in the hydrophobic layer. Case 3 generated the largest pH drop at the bottom of the sensor. Another method to determine whether a design is feasible is to maximize the difference in total fluxes into the polymer layer for a bulk glucose change from basal level to an average glucose level after a meal. The total hydrogen flux into the polymer layer is dependent on the pH of the polymer layer. Polymers which could potentially buffer the system at a given pH were synthesized in our laboratory.[20] Thus the flux into or out of the destination layer for a given pH is an important factor in determining the feasibility of the sensor design.

The total hydrogen flow into or out of the polymer layer at a set pH was calculated for the Case 3 design at two bulk glucose levels. The results given in Figure 7-10 show pH contours for the situation of no flow of hydrogen ions into or out of the polymer layer. In Figure 7-10 the bottom pH values shown represent the steady state which the system will eventually come to. If the

polymer, however buffers the system at a given pH then this value will initially override the steady state value and there will be flow into or out of this layer. Figure 7-11 shows the total flow of hydrogen ions into or out of the polymer layer for the Case 3 geometry as a function of the pH of the polymer layer for two different bulk glucose values, basal level 3.0 mM and average glucose level 10.0 mM.

Figure 7-11: Total H+ Delivery Rate vs. polymer pH for Case 3 Design
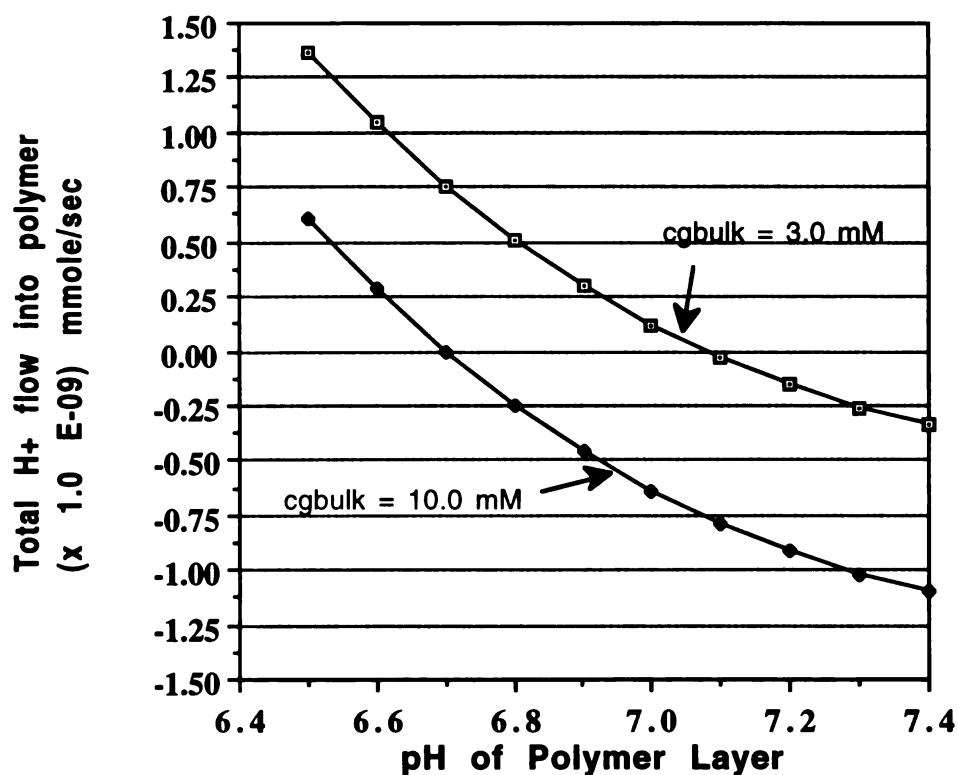
In the above figure, the negative flow values imply that the hydrogen flux is into the polymer layer, whereas positive flow values indicate that the hydrogen ion is moving out of the polymer and the sensor. This graph enables the designer to couple the polymer system and

the sensor. The zero flow conditions are those given in Figure 7-10 under Case 3.

From the above figure, it can be seen that if the polymer for use in the pump buffers the system at pH 7.0, at basal glucose levels the integrated hydrogen flow is positive implying that there is a small flow of protons out of this layer. As the bulk glucose level rises as in the case after a meal, the hydrogen flow is initially negative, and hydrogen ions flow into the destination layer (denoted by dl) protonating it. The pH of the destination layer decreases at a rate that depends on the total hydrogen flow and the buffer capacity of the polymer in the destination layer as given in Equation (9). Equation (9) below is valid for a homogeneous, well-stirred destination layer.

$$\frac{dpH}{dt} = \frac{Q_{ch+}}{V_{dl} (2.303 \times 10^{-pH} - c_M \frac{d\beta}{dpH})} \tag{9}$$

where:

Q_{ch+} is the flow of hydrogen ions into or out of the polymer layer (mmole/sec) from Figure 7-11.

V_{dl} is the volume of the destination layer (cm^3)

c_M is the total number of ionizable amine groups in the destination layer

pH is the pH in the destination layer

β is the fraction of ionized amine groups ($= \frac{c_{hbdl}}{c_M}$), where c_{hbdl} is the concentration of bound hydrogen ions to amine groups

The pH of the polymer layer will decrease until the steady state value of no integrated flow is reached causing the pH at the sensor bottom to decrease to its steady state value. With the above design this is predicted to occur at pH 6.7. Decreasing the pH within the polymer layer acts to increase the osmotic pressure which in turn pumps the insulin out of the pump. Once the glucose level is reduced by the insulin pumped out of the pump, the sensor and polymer will return to their pre-meal states.

These calculations show which designs appear more feasible in enhancing the oxygen concentrations while decreasing pH values. It remains to be experimentally tested whether these designs will actually produce the predicted pH drop. From these calculations it is recommended that the designs to be tested should be cases 2, 3 and 8. Case 1 should also be made and tested to determine if the model predicts accurately the pH drop, for the given chosen parameters. It is expected that cases 3 and 8 will give the best results.

7.5 Conclusion

The equations have been solved for the system of the glucose oxidase membrane covered by a perforated silicone membrane. A finite element model has been used to solve the coupled nonlinear differential equations in cylindrical coordinates. Using this computer model, it has been determined that having a hydrophobic membrane cover most of the unit cell does help to enhance the

oxygen concentration within the enzyme membrane. Several designs have been tested using this computer model and the results have shown that membrane designs with very small holes, a/R < .25, work best in obtaining the largest pH differences and making the "sensor" more sensitive to changes in glucose concentration.

The majority of the oxygen gets consumed at the hole for membranes containing uniform amounts of glucose oxidase. Variations on the design can be accomplished by alternating enzyme rich and enzyme vacant layers within the membrane. By placing glucose oxidase in the hole and at the bottom layer, significant improvements are made in the oxygen enhancement. The pH drop, however is greater for those designs which contain uniform amounts of glucose oxidase.

This program provides an effective means to estimate which designs will produce the most desired results. It has been determined that cases 3 and 8 will most likely give favorable results and these two sensor designs should be tested. The program does have some numerical limitations, however. Increasing the glucose oxidase concentrations above a certain amount results in numerical instabilities which would not occur in practice. In addition, testing extremely small hole sizes, a/R < 0.1 results in excessive computation. Further improvements on the designs for cases 3 and 8 can be made by physically increasing the glucose oxidase content within the membrane, or having a hydrophobic membrane with smaller holes. These improvements can be made if necessary once the base case designs have been tested.

The overall design will depend on polymer solution or gel chosen as well as the sensor. It is necessary to couple the sensor design to a polymer such that the polymer will be able to turn "on" and "off" for the given pH changes. This can be done in part by utilizing the program as was done above in Figure 7-11. Whether or not this idea will work is dependent on all components involved. This program estimates one part of the design.

References

1. Gough, D.A., Leypoldt, J.K., and Armour, J. C. Progress Toward a Potentially Implantable, Enzyme-Based Glucose Sensor. *Diabetes Care*, **5**; (1982) 190-198

2. Gough, D.A. and Leypoldt, J. K. Membrane-Covered, Rotated Disc Electrode. *Anal. Chem.*, **51**(3); (1979) 439-444

3. Gough, D.A. and Leypoldt, J. K. Rotated, Membrane-Covered Oxygen Electrode. *Anal. Chem.*, **52**; (1980) 1126-1130

4. Gough, D.A. and Leypoldt, J. K. A Novel Rotated Disc Electrode and Time Lag Method for Characterizing Mass Transport in Liquid-Membrane Systems. *AIChE Journal*, **26**(6); (1980) 1013-1019

5. Gough DA, Lucisano JY, Tse PHS. Two-dimensional enzyme electrode sensor for glucose. *Anal Chem* ; **57**: (1985) 2351-7

6. Leypoldt, J. K. and Gough, D.A. Model of a Two-Subtrate Enzyme Electrode for Glucose *Anal. Chem.*, **56**(3); (1984) 2896-2904

7. Lucisano J.Y. and Gough D. A. Transient Response of the Two-dimensional glucose sensor. *Anal Chem* ; **60**: (1988) 1272-1281

8. Weibel, M. K. and Bright, H.J., The glucose oxidase mechanism: interpretation of the pH dependence. *J. Biol. Chem.*, **246**: (1971) 2734-2744

9. Levich, V. G., <u>Physicochemical Hydrodynamics</u>, Prentic-Hall, Englewood Cliffs, N.J., 1962.

10. Bird RB, Stewart WE and Lightfoot EN, <u>Transport Phenomena</u>, John Wiley and Sons, New York, 1960.

11. Crank, J. <u>Mathematics of Diffusion.</u> Clarendon Press: Oxford. (1975)

12. Cussler, E. L. <u>Diffusion, Mass Transfer in Fluid Systems.</u> Cambridge University Press: New York. (1984)

13. Albin G, Horbett TA, Miller SR and Ricker NL, Theoretical and experimental studies of glucose sensitive membranes, *J. Controlled Release* , **6**: (1987) 267-91

14. Klumb LA and Horbett TA, Design of insulin delivery devices based on glucose sensitvie memebranes, *J. Controlled Release*, **18:** (1992) 59-80

15. Klumb LA and Horbett TA, The effect of hydronium ion transport on the transient behavior of glucose sensitive membranes, *J. of Controlled Release*, **27**: (1993) 95-114

16. Vander, A. J., <u>Renal Physiology, 3rd ed.,</u> McGraw-Hill Book Company, New York, 1985

17. Fischer U, Abel P, Muller A, Freyse EJ. *J Eur Soc Artif Organs*; **1**: (1983) 45-8

18. Abel P, Muller A, Fischer U. Experience with an implantable glucose sensor as a prerequisite of an artificial beta cell. *Biomed Biochem Acta* ; **43**: (1984) 577-84

19. De Moor, C. P., Doh, L., and Siegel, R. A., Long Term Structural Changes in pH Sensitive Hydrogels, *Biomaterials*, **12**, (1991) 836-840.

20. Cornejo, J., Ph. D. Dissertation, University of California, San Francisco, 1992

21. Firestone, B. A., Ph. D. Dissertation, University of California, San Francisco, 1990

22. Firestone, B. A. and Siegel R. A., Dynamic pH-Dependent Swelling Properties of a Hydrophobic Polyelectrolyte Gel, *Polym. Commun.*, **29**, (1988) 204-208.

23. Siegel, R. A. and Firestone, B.A., pH-Dependent Equilibrium Swelling Properties of Hydrophobic Polyelectrolyte Copolymer Gels, *Macromolecules*, **21** (1988) 3254-3259.

Chapter 8.

Summary and Future Work

In this chapter a summary of the analytical modeling completed on the pump to date is presented. Conclusions and recommendations for fabricating the device and future work are also presented here. There is much future experimentation which must be completed to verify this model. The author feels that the computer model has aided in determining which designs should be tested.

From the results and conclusions given in Chapter 7 we recommend a sensor which would be fairly thick with very small pores in the hydrophobic membrane. There is some concern, however that thick membranes have slower kinetics as noted by Albin, Klumb and Gough.[1-3] Sensor response time will be very important in the design of the pump. This was not one of the major design considerations in this thesis, but should be considered in the overall project. It is also very important to couple the sensor behavior and the polymer layer response as was attempted in Figure 7-11.

In an ideal system the sensor response would be instantaneous as it is in the body. In this case instantaneous response would imply that a rise in glucose concentration be accompanied by an immediate production of hydrogen ions, followed by an immediate increase in the osmotic pressure of the polymer layer. In practicality, however,

this type of response does not occur as it takes time for the glucose to diffuse into the sensor and react to produce hydrogen ions. It then takes time for these ions to diffuse into and protonate the polymer layer to create the increase in osmotic pressure. To this effect, thinner membranes will produce faster response times. From the results found in this thesis, thinner membranes however are not as effective in producing large pH drops and consequently large changes in hydrogen fluxes for different glucose concentrations.

To combat these issues several designs have been recommended, Cases 2, 3, 7 and 8. Cases 7 and 8 use variable amounts of enzyme within the unit cell. These designs which contain glucose oxidase/catalase only in thin layer at bottom of membrane should be tried due to the fact that these membranes may exhibit faster responses since the area of fast change is small in comparison to the rest of the membrane.

It is the author's opinion that each design be tested separately as a unit cell first and then as an entire sensor. For all the recommended designs the cells are 0.1 cm in thickness, and 0.1 cm in radius. According to the model given in Figures 4-1 through 4-3, if the sensor will fit into a pump of 1 cm in diameter, then the sensor will be 1 cm in diameter and 0.1 cm thick, and will contain approximately 19 cells. It will be fascinating to determine experimental differences between the the unit cell designs and the larger sensor.

The experimental testing of the sensors can be done in diffusion cells. The author recommends minimal stirring in each of the diffusion cell compartments, since the proposed implant site in the body will not be well mixed and there will be no flow conditions. Initial experiments should be done with the one dimensional membrane design, Case 1 geometry, to obtain the experimental conditions which most closely mimic the analytical results. These conditions can then be used to test the rest of the designs.

Fabrication of the sensors should be done as close to the recommended design cases as possible. Since Gough et. al. obtained excellent agreement with their electrodes, it is recommended to use the glutaraldehyde-crosslinked mixture of purified glucose oxidase, catalase and collagen cast as a thin homogeneous film for use in the experimental sensors.[3] It will be necessary to have the hydrophobic membranes fabricated using a laser to precisely place the perforations. The hydrophobic membrane covering should be made as thin as possible since in the model it is not considered to have any dimension.

Since the proposed pump is driven by a the change in polymer swelling or osmotic pressure, it will be necessary to couple the sensor response to the polymer or polyelectrolyte chosen to power the pump. Initially the pH change which occurs at the sensor end will be determined for a given glucose change. Transient pH responses and hydrogen ion flux changes from one glucose value to another will be most valuable in determining which polymer system will respond best. Eventually the sensor will be coupled directly to

the polymer system and the pressure change will be determined for a given glucose concentration change. Cornejo began some of the pressure generation analysis using polyelectrolyte gels.[4] Much work is still required in determining a feasible and biocompatible polymer system. It is expected that these results will aid in determining which system will function well within a pump.

In the overall proposed mechanochemical pump there are two valves. It will be necessary to couple the sensor/polymer system design to the valve designs. One of the main questions is will a change in 0.4 pH units be enough to generate enough pressure within the polymer system to open and close valves? The valves are a crucial component of the proposed pump. Preliminary analysis has been started but much more work is needed in this area.[5] The author feels that it would be more beneficial to first design a pressure sensor using Chamber 1 of the pump shown in Figure 2-1. This pressure sensor would include and couple the glucose oxidase sensor, the polymer system and the diaphragm. The valves would be omitted until further pressure data is obtained. The pressure calculations of the polymer/diaphragm system have been completed using a simplified model for obtaining the pressure inside a polymer gel.[6] This model will need to be updated somewhat, but the diaphragm analysis is still valid. Once a feasible polymer system which responds well to the sensor has been determined, the diaphragm analysis dictates the type and material required for the diaphragm.

As mentioned in the Introduction the project can be divided into several inter-related areas of modeling. This thesis represents the analytical modeling of one portion of the mechanochemical pump presented in Chapter 2, the sensor modeling. The other areas which have been studied but are not discussed in this thesis are the pressure calculations of the polymer/diaphragm system, the control dynamics of the pump and the valve design. At this point experimental results are required to couple the individual pump components.

References

1. Albin G, Horbett TA, Miller SR and Ricker NL, Theoretical and experimental studies of glucose sensitive membranes, *J. Controlled Release*, **6**: (1987) 267-91

2. Klumb LA and Horbett TA, The effect of hydronium ion transport on the transient behavior of glucose sensitive membranes, *J. of Controlled Release*, **27**: (1993) 95-114

3. Lucisano J.Y. and Gough D. A. Transient Response of the Two-dimensional glucose sensor. *Anal Chem* ; **60**: (1988) 1272-1281

4. Cornejo, J., Ph. D. Dissertation, University of California, San Francisco, 1992

5. Naghizadeh, J. unpublished work.

6. DeMoor, C. P. and Siegel, R.A., Glucose Sensitive Mechanochemical Insulin Pump, *Proc. Intern. Symp. Control. Rel. Bioact. Mater.* **16**, (1989) 157-158